2022

FINE SCALE MAPPING OF LAURENTIAN MIXED FOREST NATURAL HABITAT COMMUNITIES USING MULTISPECTRAL NAIP AND UAV DATASETS COMBINED WITH MACHINE LEARNING METHODS

Parth P. Bhatt
Michigan Technological University, ppbhatt@mtu.edu

FINE SCALE MAPPING OF LAURENTIAN MIXED FOREST NATURAL HABITAT COMMUNITIES USING MULTISPECTRAL NAIP AND UAV DATASETS COMBINED WITH MACHINE LEARNING METHODS

By

Parth P. Bhatt

A DISSERTATION

Submitted in partial fulfillment of the requirements for the degree of

DOCTOR OF PHILOSOPHY

In Forest Science

MICHIGAN TECHNOLOGICAL UNIVERSITY

2022

This dissertation has been approved in partial fulfillment of the requirements for the Degree of DOCTOR OF PHILOSOPHY in Forest Science.

College of Forest Resources and Environmental Science

Dissertation Advisor:	*Dr. Ann L Maclean*
Committee Member:	*Dr. Tao Liu*
Committee Member:	*Dr. Yvette Dickinson*
Committee Member:	*Dr. Thomas Oommen*
College Dean:	*Dr. David Flaspohler*

Contents

List of Figures

No table of figures entries found.

Author Contribution Statement

Chapters 2, 3 and 4 are comprised of published/under-review research articles and white paper. All of the published articles are accessible through peer-reviewed journal. Chapter 2 contains the white paper or applications paper which was peer-reviewed by experts in the field and was published under the "Forest Commons"-Digital Commons under Michigan Tech Publications. Chapter 3 is composed of a published research article under "Remote Sensing" journal. Chapter 4 is currently under-review in the journal of "GIScience and Remote Sensing".

Chapter 2: **Bhatt, P.**, Edson, C., & Maclean, A. (2022). Image Processing in Dense Forest Areas using Unmanned Aerial System (UAS). http://doi.org/10.37099/mtu.dc.michigantech-p/16366 Retrieved from: https://digitalcommons.mtu.edu/michigantech-p/16366

> **Author contributions**: A.M. and C.E wrote the original project proposal; C.E. and P.B. collected the data; P.B. processed and analyzed the data, did field work, wrote the original draft of the white paper; A.M. advised on methodology improvements and revised the manuscript, did field work.

Chapter 3: **Bhatt P**, Maclean A, Dickinson Y, Kumar C. Fine-Scale Mapping of Natural Ecological Communities Using Machine Learning Approaches. *Remote Sensing*. 2022; 14(3):563. https://doi.org/10.3390/rs14030563. Article belongs to the Special Issue "Advanced Earth Observations of Forest and Wetland Environment".

> **Author contributions**: P.B. analyzed the data, designed the study approach, performed the experiments, did field work and wrote the manuscript draft; A.M. wrote the original project proposal, did field work, advised on methodology improvements and revised the manuscript; Y.D. provided comments and revised the manuscript; C.K. helped with methods, and provided comments on methodology and interpreting the results. All authors have read and agreed to the published version of the manuscript.

Chapter 4: **Bhatt P,** Maclean A (2022). Comparison of High-Resolution NAIP and Unmanned Aerial Vehicle (UAV) Imagery for Natural Vegetation Communities Classification Using Machine Learning Approaches. GIScience & Remote Sensing, (Submission ID: 226232668), UNDER REVIEW. Article submitted under the Special Issue "Remote sensing for sustainable forest and wetland management under climate change".

> **Author contributions**: PB collected and analyzed the data, designed the study approach, performed the experiments, did field work and wrote the original manuscript draft; AM wrote the original project proposal, did field work, advised on methodology improvements, revised and edited the manuscript.

Acknowledgements

"It is good to have an end to journey toward; but it is the journey that matters, in the end." ~ Ursula K. Le Guin

4 years have passed in this exciting journey and the caravan of Ph.D. would not have reached its destination without number of great people in my life. First of all, I would like to express my gratitude towards the most important people, my family, without their invaluable support and faith I cannot imagine this journey. My father (Parimal Bhatt), my mother (Sima Bhatt), my elder brother (Karan Bhatt) and my fiancé (Vaishali) who have always loved and trusted me unconditionally.

Secondly, I would like to express my sincere thankfulness to my advisor Dr. Ann L Maclean, towards whom I am immensely grateful for having the faith in me. It was a blessing to work with you. I would like to thank my committee members Dr. Yvette Dickinson, Dr. Tao Liu, and Dr. Thomas Oommen for their constant support and constructive feedbacks. Along the lines, I would like to express my gratitude towards Dr. Andrew Storer, Dr. David Flaspohler, Dr. Curtis Edson, Dr. Gordon Maclean, Mike Hyslop, and Dr. Mickey Jarvi for their help and support with many enriching and significant things.

I am grateful towards my wonderful colleagues at the College of Forest Resources and Environmental Science for making my day to day life easy here at the CFRES community. In particular, I would like to express my thankfulness to Marjorie Banovetz, Phyllis Williamson, Cindy Kela and Lori Crane, you guys are awesome.

I would like to thank many of my good friends/lab mates that I have had a chance to share the journey. Zhongming (Paul), Olivia, Emma, Joel, Ian, Maeve, Heidi, Tony, Alex, Chris, Robbie, Maria, Chandan and Dhavan these are the people who have made the journey fun and smooth since 2016.

Overall, I would like to thank The U.S. Forest Service, College of Forest Resources and Environmental Science, Graduate School, Michigan Technological University and The Nature Conservancy for their support.

Thank you immensely, this journey would not have been this beautiful and memorable without you all!

List of Abbreviations

AGL - Above Ground Level

avNNet - Averaged Neural Network

CIR – Color Infrared

CRM - Carp River Mouth

DEM – Digital Elevation Model

GCPs - Ground Control Points

GNSS - Global Navigation Satellite System

GPS – Global Positioning System

GLCM - Grey-Level Co-Occurrence Matrix

FGDC - Federal Geographic Data Committee

HNF – Hiawatha National Forest

HUC - Hydrologic Units

ICA - Independent Components Analysis

IUCN - International Union for Conservation of Nature

JMIM - Joint Mutual Information Maximization

k - Kappa

LiDAR - Light Detection and Ranging

LMF - Laurentian Mixed Forest

MNFI - Michigan Natural Features Inventory

MLAs - Machine Learning Algorithms

NAIP - National Agriculture Imagery Program

NIR – Near Infrared

NDVI - Normalized Difference Vegetation Index

NLCD - National Land Cover Database

OA - Over all Accuracy

PAC - Pointe aux Chenes Bay

PCA - Principal Component Analysis

PA - producer's Accuracy

RE - Red Edge

RF - Random Forest

RGB – Red, Green, Blue

SRD - Sturgeon River Delta

SVM - Support Vector Machine

UAS - Unmanned Aerial Systems

UAV - Unmanned Aerial Vehicle

UA - User's Accuracy

USGS - United States Geological Survey

varImp - Variable Importance

WINAIP - Modified Water Index for NAIP

Abstract

Natural habitat communities are an important element of any forest ecosystem. Mapping and monitoring Laurentian Mixed Forest natural communities using high spatial resolution imagery is vital for management and conservation purposes. This study developed integrated spatial, spectral and Machine Learning (ML) approaches for mapping complex vegetation communities. The study utilized ultra-high and high spatial resolution National Agriculture Imagery Program (NAIP) and Unmanned Aerial Vehicle (UAV) datasets, and Digital Elevation Model (DEM). Complex natural vegetation community habitats in the Laurentian Mixed Forest of the Upper Midwest. A detailed workflow is presented to effectively process UAV imageries in a dense forest environment where acquisition of ground control points (GCPs) is extremely difficult. Statistical feature selection methods such as Joint Mutual Information Maximization (JMIM) which is not that widely used in the natural resource field and variable importance (varImp) were used to discriminate spectrally similar habitat communities. A comprehensive approach to training set delineation was implemented including the use of Principal Components Analysis (PCA), Independent Components Analysis (ICA), soils data and expert image interpretation. The developed approach resulted in robust training sets to delineate and accurately map natural community habitats. Three ML algorithms were implemented Random Forest (RF), Support Vector Machine (SVM) and Averaged Neural Network (avNNet). RF outperformed SVM and avNNet. Overall RF accuracies across three study sites ranged from 79.45-87.74% for NAIP and 87.31-93.74% for the UAV datasets. Different ancillary datasets including spectral enhancement and image

transformation techniques (PCA and ICA), GLCM-Texture, spectral indices and topography features (elevation, slope and aspect) were evaluated using the JMIM and varImp feature selection methods, overall accuracy assessment and kappa calculations. The robustness of the workflow was evaluated with three study sites which are geomorphologically unique and contain different natural habitat communities. This integrated approach is recommended for accurate natural habitat community classification in ecologically complex landscapes.

1 Introduction

Ecosystems are defined as “a community of organisms and their physical environment interacting as an ecological unit” [1]. To protect and manage these communities, it is crucial to understand them at multiple scales, from the organism to landscape level. Many different factors (vegetation, soils, spatial and temporal scales, landform and bedrock geology) are utilized to classify these systems, and numerous ecological classification schemes exist in the literature. King [2] discussed ecosystem integrity with respect to scale and hierarchical structure. Jensen et al., [3] explained importance of ecological units in managing the existing homogenous land conditions which have similarities in structure, function, and ecosystem composition. Bailey [4] talked extensively about different ecological classification approaches and importance of ecological units. According to Bailey [5] these ecological unit maps can be useful for assessment of permanent landscape components (i.e., climate, soils, geology, landform) and can evaluate existing status of landscape components (i.e., vegetation). Having a hierarchical classification scheme allows ecosystems to be presented at different spatial scales [6, 7]. Rowe and Barnes [7, 8] introduced the landscape ecosystem, or geo-ecosystems approach which incorporates factors like climate, landforms, soil, water, and biota, and provide a holistic ecological framework. Cowardin [9] developed a classification scheme for wetlands and deep-water habitats organizing the classes having certain homogeneity and uniformity throughout the landscape.

The market for remotely sensed data has grown exponentially in the past four decades. Remote sensing data can be classified in two categories: data collected from passive

sensors and data collected from active sensors [10]. Passive sensors are dependent on the reflection of natural light (solar energy) from objects or targets [10]. Whereas active sensors transmit electromagnetic energy and measure the returned quantity [10]. There are many different types of instruments available to collect the remotely sensed imagery like multispectral (Landsat, Sentinel, WorldView, MODIS), hyperspectral, radar and LiDAR [10]. These imagery datasets are acquired using satellites, manned aircraft and drones. There are wide variety of applications (i.e., natural resources, geology, hydrology, urban, renewable energy) where remotely sensed imagery has aided in monitoring and mapping [10].

Choosing an appropriate classification scheme is important but can be confusing due to the complex interactions of the components. To classify any landscape whether on the ground or using remotely sensed data it is important to have a classification scheme which reduces confusion between various landscape features and makes it relatively easy for the user to make distinction [11]. For this study, the hierarchical classification framework of Cohen et al. [12] is being utilized. Their publication, "Natural Communities of Michigan: Classification and Description", published by the Michigan Natural Features Inventory (MNFI) provides detailed information on dividing Michigan's complex landscape into easily understood and describable components labeled natural communities. The foundation of this classification is based on the work completed by Kim A. Chapman [13], and first published by Kost et al. [14]. The MNFI natural communities scheme is easy to understand and helps describe the complex natural landscape across the State of Michigan. It mainly focuses on the diversity of native ecosystem types that are unchanged by human activities [12]. For activities such has

agriculture, impervious surfaces, and residential development, classes were developed as needed for the study.

For this study widely, available multispectral high-resolution National Agriculture Imagery Program (NAIP) imagery was used. NAIP is collected every 2 years across the continental United States during the summer months and is often referred to as "leaf-on" imagery. NAIP imagery was first collected in 2003 with a 5-year cycle at 2-meter ground sampling distance (GSD) [15]. Starting in 2011 NAIP is now collected every other year at 0.60-meter GSD [15].Along with NAIP, multispectral ultra-high spatial resolution Unmanned Aerial Vehicle (UAV) imagery was used. Both types were used to map natural community habitats. Unmanned Aerial Vehicle (UAV) remotely sensed imagery and processing techniques have rapidly grown over the past decade. It offers low-cost, affordable data, and has been used by researchers to map coastal wetlands, vegetation and individual plant species [16-19]. Both NAIP and UAV imagery have been used by various fields like forestry, geology, education, emergency responses, watershed planning, transportation, recreation, urban development and land use/cover analysis [15, 20].

Along with the classification scheme it is important to choose an appropriate classification method. Commonly used field methods for data collection (e.g. collecting location points using Global Positioning System (GPS), vegetation sampling, field surveys and map interpretation) in wetlands, particularly forested wetlands, are labor intensive, costly, time consuming and confined to small areas due to limited access [21]. With technical advances in the fields of remote sensing and geographic information

science (GIS), an alternative and/or complimentary approach to traditional field data collection techniques is available. Remotely sensed imagery provide a more practical, economical approach to monitor and measure various biological and physical factors; making it more efficient for large area monitoring [22],

In order to classify any remotely sensed imagery it is important to use an appropriate classifying technique. Parametric and non-parametric classifiers have been used within the remote sensing community for years to classify imagery for various applications [23-25]. Bhatt [17] discussed different classification methods which have been used by the remote sensing community. The use of Machine Learning (ML) based classification techniques has increased greatly over the last two decades by the remote sensing community [26-31]. ML algorithms and techniques use a nonparametric approach to model and classify data. Numerous studies have shown ML advantages over traditional parametric classification techniques [28, 32-35]. Large-scale landcover mapping approaches using decision trees (DTs) were utilized in the classification of the 2001 National Land Cover Database (NLCD) [36]. Use of publicly available NAIP and Landsat imagery to map wetlands in particular, *Phragmites spp.,* with high accuracies using ML and support vector machine (SVM) classification techniques has been shown by Xie et al. [37]. Kulkarni and Lowe [29] showed the use of non-parametric methods such as Random Forest (RF) and SVM for landcover classification using Landsat imagery. Their results showed that RF works efficiently with large homogenous datasets and was sensitive to outliers compared to other classifiers.

Multispectral imagery is often not sufficient to accurately classify target features. The addition of ancillary datasets or variables can improve outcomes. Researchers have used variables such as spectral indices (i.e., NDVI, WI, SAVI, LAI) [38], topographic data (i.e., elevation, slope, aspect) [38, 39], first- and second-order textures (i.e., contrast, homogeneity, variance, entropy) [40, 41], soils data, and climate data (i.e., temperature, rainfall) [42]. In cases of multiple geomorphological variables, it is crucial to identify which variable contributes most to the classification process and reduces data complexity (Hughes phenomenon) [43]. In order to test the importance there are available feature selection methods such as Joint Mutual Information Maximisation (JMIM) which can be implemented [44, 45] before executing the actual classification.

Despite the availability of a wide range of data and advanced classification techniques, not many researchers have attempted to classify the complex Laurentian Mixed Forest (LMF) at an individual community level. Vegetation communities are composed of multiple fine scale systems, and these finer scale systems can appear in more than one community. By contrast, land use/ land cover classification schemes use a more generalized scheme with nonoverlapping classes.

This research contains three chapters which evaluate the complexity and challenges of UAV image preprocessing and classification of densely forested areas, using NAIP imagery coupled with geomorphological ancillary datasets to developa robust methodology using Machine Learning algorithms (MLAs), comparing NAIP to UAV imagery understand the advantages and disadvantages of each for delineating and mapping natural habitat communities.

Chapter 2 discusses collection of UAV imagery in a dense forested area and how to efficiently process it using the best settings in photogrammetry software. This published chapter is **titled as "Image Processing in Dense Forest Areas using Unmanned Aerial System (UAS)" [46].**

Chapter 3 discusses the workflow, methodology, and classification results using NAIP imagery and ancillary data with MLAs. The published manuscript goes over the importance of an appropriate classification scheme, the effectiveness of the hybrid classification approach using geomorphological variables, and comparison of two machine learning algorithms (RF and SVM). **Title: Fine-Scale Mapping of Natural Ecological Communities Using Machine Learning Approaches [38].**

Chapter 4 presents a comparison between NAIP and UAV imagery classification using MLAs. It discusses the advantages and disadvantages between the two types imagery, classification of natural community habitats with both types of imagery and accuracy results. **Title: Comparison of High-Resolution NAIP and Unmanned Aerial Vehicle (UAV) Imagery for Natural Vegetation Communities Classification Using Machine Learning Approaches.** This chapter is currently under review as a research manuscript in the GIScience & Remote Sensing journal.

2 Image Processing in Dense Forest Areas Using Unmanned Aerial System (UAS)

Authors: Parth Bhatt[1], Curtis Edson[2], Ann Maclean[1]

Affiliations: [1]College of Forest Resources and Environmental Science, Michigan Technological University, [2]Department of Economics and Geosciences, United States Air Force Academy

(This work is published as an applications paper in Digital Commons: Bhatt, P., Edson, C., & Maclean, A. (2022). Image Processing in Dense Forest Areas using Unmanned Aerial System (UAS). http://doi.org/10.37099/mtu.dc.michigantech-p/16366)

Description

A detailed workflow using Structure from Motion (SfM) techniques for processing high-resolution Unmanned Aerial System (UAS) NIR and RGB imagery in a dense forest environment where obtaining control points is difficult due to limited access and safety issues.

Abstract

Imagery collected via Unmanned Aerial System (UAS) platforms has become popular in recent years due to improvements in a Digital Single-Lens Reflex (DSLR) camera (centimeter and sub-centimeter), lower operation costs as compared to human piloted aircraft, and the ability to collect data over areas with limited ground access. Many different application (e.g., forestry, agriculture, geology, archaeology) are already using and utilizing the advantages of UAS data. Although, there are numerous UAS image processing workflows, for each application the approach can be different. In this study, we developed a processing workflow of UAS imagery collected in a dense forest (e.g., coniferous/deciduous forest and contiguous wetlands) area allowing users to process

large datasets with acceptable mosaicking and georeferencing errors. Imagery was acquired with near-infrared (NIR) and red, green, blue (RGB) cameras with no ground control points. Image quality of two different UAS collection platforms were observed. Agisoft Metashape, a photogrammetric suite, which uses SfM (Structure from Motion) techniques, was used to process the imagery. The results showed that an UAS having a consumer grade Global Navigation Satellite System (GNSS) onboard had better image alignment than an UAS with lower quality GNSS.

2.1 Introduction

Unmanned Aircraft Systems (UAS), or Unmanned Aerial Vehicle (UAV), are a rapidly emerging image acquisition technology. The US Department of Defense (DoD, 2019) and Civil Aviation Authority (CAA, 2015) of the UK adopted the term UAS. The term Remotely Piloted Aerial System (RPAS,) a particular type of UAS, was introduced by the International Civil Aviation Authority (ICAO) in ICAO Circular 328 (ICAO, 2011). According to a recent market research study (Markets, 2018) the global UAS market was $18.14 billion in 2017 and is projected to reach $52.30 billion by 2025. High spatial and temporal resolutions are two important characteristics of UAS. Other factors such as low-cost, smaller components size, longer battery life, improved launching capabilities, and ease of transport and operation make this a preferable choice over other remote sensing platforms for various applications.

The Federal Aviation Administration (FAA) categorizes a UAS as weighing under <=23 kg (55 lbs) as small Unmanned Aircraft Systems (sUAS) (FAA, 2018). Rango et al. [47]

states how small (55 lbs or <50 kg) and micro (11 lbs or <5 kg) UAS platforms provide many benefits for remote sensing applications over larger sized UASs. UASs were used initially for various military purposes from data collection to strategic planning [48]. The US National Aeronautics and Space Administration (NASA), under the "Mini-Sniffer" program, developed unmanned aircraft for atmospheric sampling during the 1970 - 80 (NASA, 2017). In the 1990s, NASA's Environmental Research Aircraft and Sensor Technology (ERAST) program highlighted the development and capabilities of UAS for various scientific research areas (NASA, 2008). UAS provides multiple civil applications including, but not limited to, long-term scientific research, high-spatial resolution aerial imagery, agricultural monitoring, pipeline surveillance, border protection, disaster management, weather monitoring and airborne communications [49-51]. The United States Geological Survey (USGS) has used UAS since 2010 for various research applications, ranging from monitoring shoreline erosion and rapid response volcano monitoring [47]. Two types of UAS are widely available- fixed-wing and multi-rotor. Multi-rotors allow vertical take-off and landing with less open space, are easier to maneuverer, and cost less. However, they have smaller areal coverage, shorter flying times, and are less durable in high winds [52, 53]. Fixed-wing vehicles, are larger in size and more stable, cover larger areas and have a longer battery life. However, they require larger take-off and landing areas and are more expensive [52-54].

Recently, using UAS imagery for mapping and classifying forest vegetation, wetlands delineation and invasive species monitoring has increased. Husson et al. [55] used Personal Aerial Mapping System (PAMS) UAS imagery to interpret and delineate aquatic vegetation and *Phragmites* stands. Precision forestry practices have also

increased the use of UAS for mapping forest cover types and stand conditions [56, 57]. Dunford et al. [58] used UAS image mosaics to characterize Mediterranean riparian forest. Dandois and Ellis [59] illustrated the use of a lightweight, hobby grade UAS to map and observe 3D canopy phenology in temperate deciduous forest sites and incorporated structure from motion (SfM) algorithms in the image processing. Using a fixed wing UAS system to acquire high spatial resolution imagery (~7 cm) Getzin et al. [60] assessed biodiversity by identifying canopy gaps in deciduous and deciduous-coniferous mixed forests in Germany; while Koh and Wich [61] utilized lightweight fixed-wing drone in conservation efforts to survey and map forests and biodiversity. Carbonneau and Dietrich [62] evaluated UAS data and utilized SfM (Structure from Motion) techniques for high-quality topography mapping.

Use of fixed-wing UAS with an on-board survey grade GPS operating in a ground control point (GCP) free environment was demonstrated by Chiang et al. [63]. Direct georeferencing using the SfM technique has been used successfully to process high spatial resolution imagery for agricultural areas requiring high locational accuracy [53, 64]. Others have shown the use of direct georeferencing without ground control points to process UAS imagery with survey grade GPS on-board [65-67]. Samiappan et al. [68] mapped invasive *Phragmites australis* in coastal wetlands adjacent to the Gulf of Mexico using an Altavian Nova UAS platform with image spatial resolution as fine as 5 cm. In another study by Samiappan et al. [16] in the Gulf of Mexico coastal wetlands, they used a hand launched Precision Hawk Lancaster UAS platform to acquire five band multispectral imagery with a high spatial resolution (~ 8 cm) to map *Phragmites* (common reed).

2.2 **Study Area**

The Hiawatha National Forest (HNF) is located in the central and eastern parts of Michigan's Upper Peninsula on the north coast of Lake Michigan (Figure 1), and manages the largest area of coastal wetlands in the Great Lakes Basin. HNF manages the greatest acreage of coastal wetlands in the Great Lakes Basin, encompassing 363,599 ha (898,472 ac) and over 161 km (100 miles) of Great Lakes shoreline, with jurisdiction along Lakes Michigan, Superior and Huron shorelines [69]. The study sites were selected for their diverse land-water vegetation communities including large tracts of forested, submergent, emergent, and shrub-scrub wetlands.

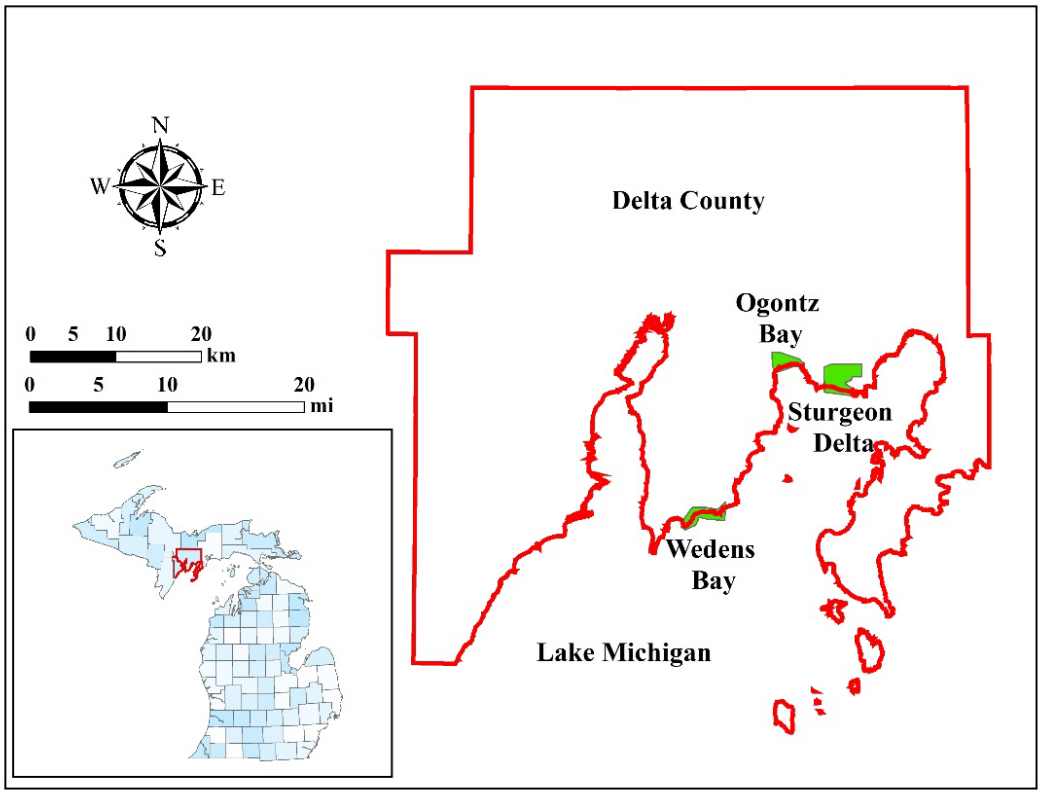

Figure 1. Location of the three UAS study sites in the Hiawatha National Forest in the central part of Michigan's Upper Peninsula along the Lake Michigan shoreline.

2.2.1 Objectives

There are few published UAS studies involving such a large 2,315 ha (5720.49 ac) study area. Most published studies deal with smaller areas focused on a particular plant species or agricultural crop. Dense forest stands, commonly found in the Upper Midwest, have limited accessibility due to remoteness and lack of roads/trails which severely curtails collecting GCPs. Hence, the objectives of this feasibility study were: to develop a rigorous processing workflow for a large UAS imagery dataset with few or no GCPs; and evaluate the capabilities of the fixed-wing UAS platform and data collection components.

2.3 Materials and Methods

Two UAS fixed wing platforms were utilized for the study. A Trimble (Trimble Inc., Sunnyvale, CA) UX5 and a UX5-HP. Both have an expanded polypropylene (EPP) foam fuselage, internal carbon frame, and a pusher propeller driven by an electric motor powered by lithium polymer (LiPo) battery. The Trimble UX5 was mounted with a low-cost mapping grade GNSS receiver located in the electronic control box (eBox), and a Sony a5100, 24-megapixel mirrorless camera with fixed 15mm lens capable of a ground sample distance (GSD) as fine as 2.0 cm and collected RGB imagery. The Trimble UX5-HP payload included a consumer grade GNSS receiver with dual frequency, eBox, and a Sony A7R, 36-megapixel mirrorless DSLR camera with a fixed 35mm lens and GSD capability of 1.0 cm and collected NIR imagery. A comparison of the UASs is compiled in Figure 2 (Trimble, 2019b).

Three areas (Figures 1 and 3) of coastal wetlands and adjacent interior wetlands were flown in August, 2017 with varying flying heights between 75 and 121 m (246-400 ft). Approximately 2,315 ha (5,720 ac) of imagery (~40,000 images) were acquired and collected over 52 flight blocks (Figure 3). The overlap and sidelap for all imagery were set to 80%. Project locations were on the Lake Michigan coastline, and taking off over water was relatively easy. However, both UASs require adequately sized, non-forested, dry, open space to land. Because the study sites were predominantly wetlands, lake levels high and few roads or trails, landing locations were limited.

There were two batteries for the UX5 and four batteries for the UX5-HP, that were used singly, which is important for quick turn-around times for getting the UAS back in the air and collecting images. Manufacturer's estimated flight time capabilities were 50 and 35

Features	**UX5 HP**	**UX5**
Type	Fixed Wing, 100 cm (3.28 ft.) wingspan	Fixed Wing, 100 cm (3.28 ft.) wingspan
GNSS receiver	Dual-frequency L1/L2 GNSS (GPS, Glonass, Beidou, Galileo)	Lower grade GNSS
Camera type	Sony a7R, 36-megapixel, full frame, 35 mm lens, NIR camera	Sony a5100, 24-megapixel, 15 mm lens, RGB camera
Resolution	1.0 cm with 35 mm lens	2.0 cm with 15 mm lens
Weight	2.9 kg (6.4 lb)	2.5 kg (5.5 lb)
Battery	14.8 V, 6,600 mAh	6,600 mAh
Maximum flying speed	88 km/h (55 mph)	80 km/h (50 mph)
Maximum flying time	35 min	50 min

Figure 2. Comparison of UAS devices used in the study (Trimble, 2019b).

minutes for the UX5 and UX5-HP respectively. This fell short when flying in the field, as preflight setup consumes ~ 10% of the battery life, and 10-15% battery life is required for

safe landing. These reduced flight times necessitated careful consideration in flight planning and selecting landing sites.

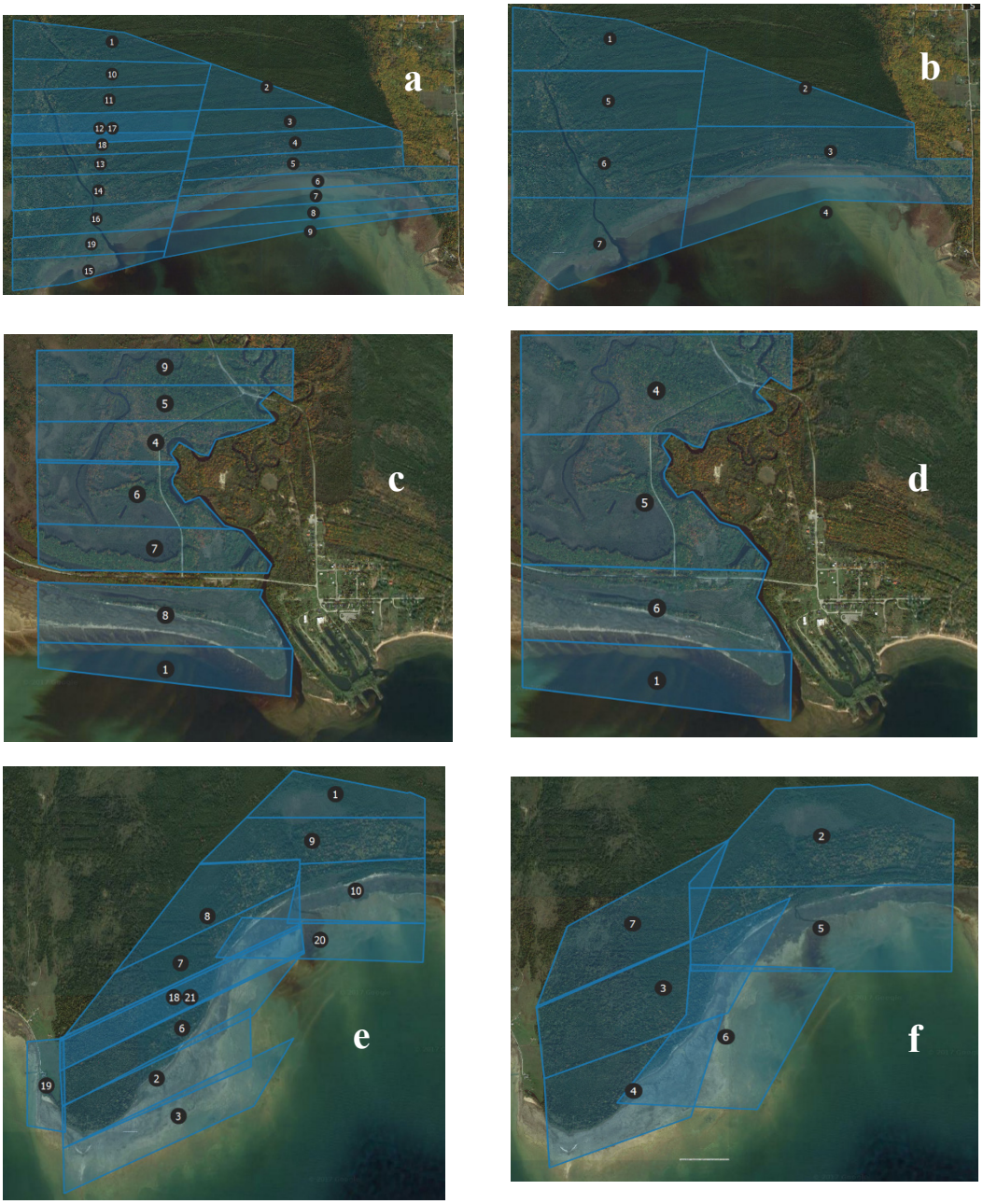

Figure 3. Number of blocks flown for collecting NIR and RGB data with Trimble UX5 HP and UX5 over the three study sites, Ogontz Bay-NIR (a), RGB (b), Sturgeon River Delta-NIR (c), RGB (d) and Wedens Bay-NIR (e), RGB (f). (Source: Google Earth, Aerial Imaging, Trimble)

A bungee cord catapult launched the aircraft to takeoff speed. Takeoff and landing locations were confirmed via the control tablet's internal GNSS receiver before takeoff. Most of the data collection was automated based on the programmed flight plan, which was communicated to the aircraft eBox via a FM modem. For flight mission planning and flight operations, Trimble's Aerial Imaging proprietary software designed for the Trimble UX5 series, was utilized. The software interfaces with Google Earth to download planning imagery for the study sites as shown in Figure 3.

Four flights per day were planned based on factors such as battery life, data download time for each flight, and preliminary office processing. Six was the maximum number of flights achieved in a day. Flight block planning size was based on actual battery life expectancy, with actual times of 45 minutes for the UX5 and 30 minutes for the UX5-HP. In many cases, acquisition of complete blocks was not possible due to strong winds coming off of Lake Michigan, which reduced flying times due to increased power and battery usage. Use of ground control targets for ground control points (GCPs) locations were not used due to inaccessibility caused by dense forest cover and lack of roads and trails.

2.3.1 Photogrammetric Processing

Initially, Trimble Business Center (TBC) and Trimble Inpho UASMaster (Trimble, 2019a) were used to process the data. However, large tracts of the coastal wetlands consisted of dense forest cover where accessibility and easily identifiable ground features did not exist (Figure 4). This precluded the software's automatic tie-point (ATP) algorithm from finding tie-points on overlapping photos; which in turn prevented or

attenuated photo-mosaic creation and posed a serious image mosaicking issue (Hexagon, 2016). Manual tie-point location, often cited as an alternative approach, was not feasible due to the homogeneity of high-density forest cover and the large number of images (700 to 1,500 images) per block. Oblique views of different sides of the same trees make it very difficult and inordinately time consuming to identify the same feature (group of pixels).

Figure 4. Snapshot showing high-density forest cover across Sturgeon River Delta area. (RGB bands – UAS Imagery).

Deep-water areas of Lake Michigan also contributed to the problem, as the water was either relatively monochromatic with insufficient differentiation between pixels, or wind-driven wave action created different spectral reflectance in adjacent imagery for the same geographic location. To help troubleshoot alignment issues, the data were sent to Trimble Germany GmbH (Branch office Stuttgart; Rotebühlstraße 81; 70178 Stuttgart) and a team leader (Inpho Support - Imaging Division) assisted in the tie-point processing. After approximately three months of adjusting inputs and using various processing options, TBC and UASMaster were unable to adequately process the data, and it was concluded the software algorithms were not sufficient to process such highly dense forested areas (Figure 4).

Evaluation of the Agisoft Metashape (previously PhotoScan) Professional Edition Version 1.3, 2017 (Agisoft, 2017a) photogrammetry software package was initiated at the suggestion of USGS, National UAS Project Office [70]. Agisoft uses SfM algorithms (Agisoft, 2017b), and in a forested environment, achieved a higher percentage of success in photo alignment, generation of georeferenced point clouds, mesh creation and the resulting orthomosaic (Figure 5). SfM solves scene geometry, camera positions and internal and external orientation parameters using a bundle adjustment procedure, and automatically extracts features (matching points) from overlapping images.

Metashape aligns photos without the use of GCPs. Input parameters used are based on software recommendations (Agisoft, 2017b), or if needed, by trial and error experimentation, to achieve acceptable results. The amount of processing time for each step, shown in Figure 6, and the number of images processed during that time were based on the trial and error approach. The aircraft trajectory csv file, which contained photo station GNSS locations and image orientation parameters, as well as the imagery were imported imported into the software. Image quality was evaluated and assigned a value with 1 being the best. Values

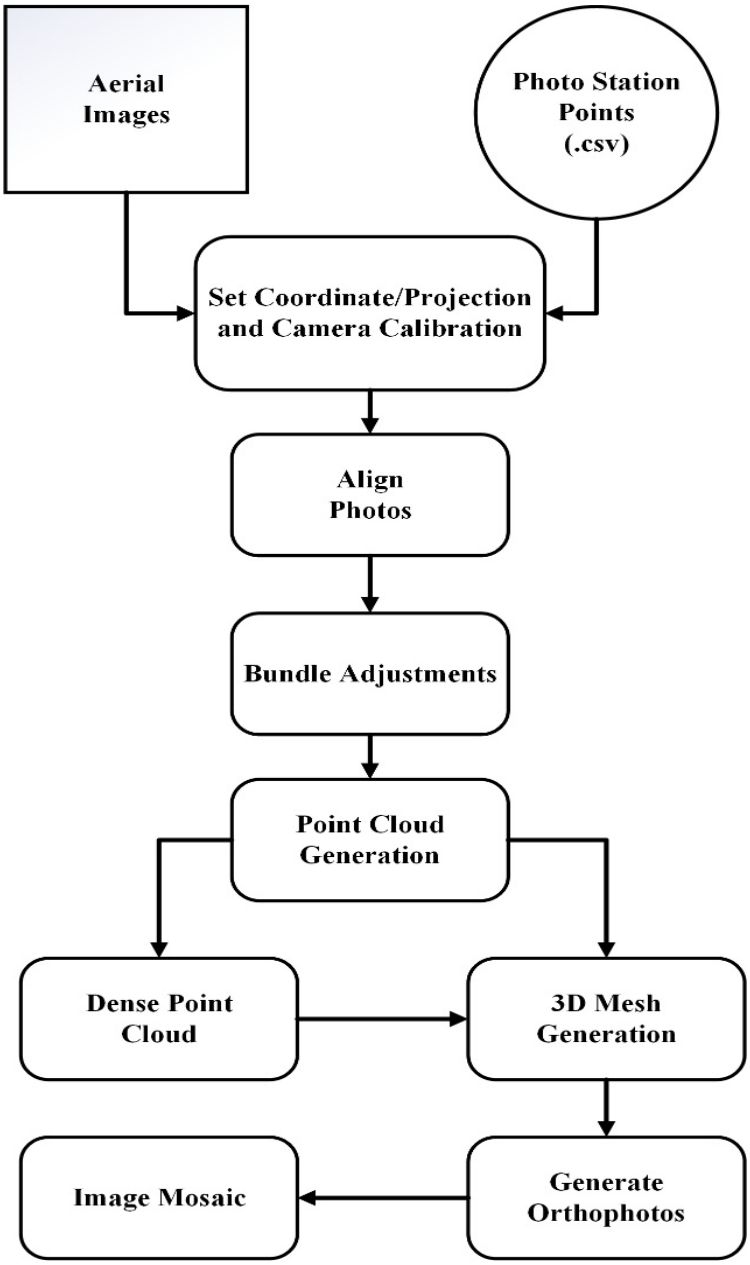

Figure 5. SfM workflow to process the UAS imagery.

below 0.7 indicated the images had low contrast or vignetting effects and were discarded if area coverage was maintained by adjoining photos.

Task	**Parameter (NIR/RGB)**
Align photos (Processing time for approximately 900 to 1400 images: 8 to 12 hrs)	Accuracy: Highest [2]/Medium [2] Pair selection: Reference [1] Key point limit: 60,000 [2] Tie point limit: 0 [2]
Optimize photo alignment (Adaptive camera model fit) (2 to 5 min)	Projection accuracy (pix): 0.1 [1] Tie point accuracy (pix): 0.3 [2] Fit: f, cx, cy, k1-4, p1-4 [1]
Build dense cloud (8 to 12 hrs)	Quality: Medium [2] Depth filtering: Aggressive [2]
Build mesh (1 to 2 hrs)	Surface type: Height field [1] Source data: Dense cloud [1] Face count: Medium [2] Interpolation: Enabled (default) [1]
Color calibration (varies as per number of images to be corrected in a block)	Source: Model [1] Calibrate white balance: Checked [1]
Build orthomosaic (8 to 10 hrs)	Projection type: Geographic [1] Surface: Mesh [1] Blending mode: Mosaic (default) [1] Enable hole filling: Checked [1]

Figure 6. Processing workflow with corresponding parameters in Metashape for generating Orthomosaic from UAS imagery. [1]Parameters selected based on online tutorial; [2]Parameters selected using trial and error approach.

Images were aligned using the photo alignment process, involving tie point detection, selecting matching point pairs, and estimating improved camera coordinates. Metashape

generates a point cloud as a 3D representation of tie-points. The highest alignment accuracy was used in conjuction with the original NIR image spatial resolution and the medium setting with the RGB images for tie point pair selection (Agisoft, 2017b). Being the first step in the workflow, Alignment setting plays an important role in estimating tie point positions, to accurately tie the images together. The key point limit was set to 60,000 and tie point limit was set to 0 to retain all matched points. A key point is a feature point with unique texture or high contrast found on multiple overlapping images. Using a higher key point value improves the chances for a successful alignment. A larger key point limit ensures more points are sampled by Metashape, potentially with a higher accuracy (Agisoft, 2017b). A tie point is a key point found on two or more images and used to optimize model performance. When using a tie point limit of 0, no prefiltering occurred, processing times were longer, but image correction was improved. Using the highest quality setting requires longer processing times, as it upscales the imagery by factor of 4 and helps acquire more accurate camera positions, is recommended for research purposes (Agisoft, 2017b).

The complex canopy structure of dense vegetation along with relief displacement made it extremely difficult to identify distinct spatial features between adjacent images and affected the geometric alignment between the photos. Medium alignment setting smooths the data with a 2x resampling and does not require accurate feature point location compared to high alignment, which uses the original spatial resolution of the photos (Agisoft, 2017b). Hence it was used to minimize the parallax and differing reflectance values to achieve additional calibrated images.

Optimization, using the adaptive camera model fit, includes a least squares bundle adjustment [71], which estimates the internal and external camera orientation plus measurement parameters, estimating focal length (via exif data or user input), if unknown, and corrects camera lens distortion. It is important to perform optimization in order to reduce the lens distortion effects on the forest structures in the photos (Agisoft, 2017b). After optimization, the standard error of unit weight (SEUW) value was between 0.1 and 0.3, below the recommended SEUW tolerance of 1.0.

A dense point cloud was derived from the images generated from the optimized camera parameters. Medium quality and aggressive depth filtering mode [72] were used for both the NIR and RGB imagery as reconstruction parameters. Metashape creates depth maps for each image. In order to remove the outliers and noise from the aerial imagery depth filtering was recommended by Agisoft (2017b) to use. We aligned the images with highest settings whereas dense cloud was generated at medium quality which might impact the elevation but does not impact the orthophoto as the amount of points generated are usually more than sufficient to generate the final orthoimage. Another important factor to consider was the computer memory as when we tried generating the dense cloud with high settings it ran out of memory and gave an error. To overcome the processing error, we applied the medium setting. Processing time for two blocks together was 8-10 hours.

2.3.2 **Mesh Generation**

Polygonal mesh generation created a 3D surface model based on the point cloud (dense or sparse). The height field option (which represents planar surfaces) was selected for the mesh generation. The height field is a surface type that represents topographic surface

models. It requires lower amounts of memory to process large datasets (Agisoft, 2017b). The dense cloud was used as the source data in processing though it requires longer processing time, it generates high quality result. Medium quality which produces little less detailed feature formations but help remove more noise or artifacts (Saczuk, 2018), was used for both NIR and RGB data polygon count generation; and, high settings were avoided as it can cause model visualization problem due to very high number count. Default interpolation setting and all point classes were used. Using interpolation helps the software interpolate surface areas around each dense cloud point by creating a circle of certain radius around them and fills some hole automatically (Agisoft, 2017b). The processing time was around 1-2 hours for two blocks.

2.3.3 **Color Calibration**

Portions of the RGB imagery exhibited vignetting; thus, color correction was applied to before orthomosaic was generated. Vignetting is defined as the reduction in an image's brightness towards the edge when compared with its center [73]. Vignetting arises due to the changes in irradiance over the image plane due to sensor geometry [74], and color correction balances the brightness variation across the imagery block (Agisoft, 2017b). As the data was acquired at various times of the day, changing illuminance was anticipated. If color calibration is not utilized, Metashape only blends images in overlapping areas, and does not change the brightness values (digital numbers) of the original images. The software's white balance option was used to correct each band independently. White balance adjusted the brightness values so the image looks more "natural" by removing color casts. Calibrations times vary based on the number of images in a block.

2.3.4 Orthomosaic

In the final stage of the process, an orthomosaic was generated using the mesh model for an elevation reference and blending along the photo's seamlines. Pixel size was kept to default (i.e. image resolution, 1.3 cm for the NIR and 2.0 cm for the RGB). Hole filling option was kept on to remove any salt-and-pepper effects caused in part by shadows and to ensure there are no tiny gaps in the imagery. The software corrects image distortion followed by a multi-view stereo reconstruction procedure to place each pixel located in its correct XYZ position (Agisoft, 2017b).

The orthomosaic for each block was exported as a TIFF with no compression or tiling and reprojected to UTM NAD83 zone 16N (EPSG:26916) projected coordinate system. Dense points clouds were exported in ASPRS LAS format. The model was also exported as a KMZ file for use in Google Earth. Metadata documentation (PDF) for each block included all processing parameter specifications such as processing times for each segment, numbers of tie points, and number of dense cloud points, camera calibration information including point locations and errors, and orientation.

2.4 Results and Discussion

Metashape generated tie-points and orthomosaics with medium sized data gaps for the NIR data and large data gaps in the RGB data processing. With the NIR data, gaps occurred over water and dense forest areas. However, with RGB data, the low accuracy GNSS receiver quality on the UX5 potentially caused the data gaps due to poor quality initial estimation parameters. Collected image coordinates and orientation parameters were used for initial approximation in the photogrammetric processing. Higher accuracy

GNSS enables much higher fidelity in the initial approximations, and the remaining image orientation, relative orientation, and block adjustment were calculated using photogrammetric aero-triangulation, which occurs in the image alignment and optimization steps. For both Ogontz and Wedens Bay (Figure 8 a; Figure 10 a, b), the software was able to generate tie-points for coastal areas. Large open areas made it easy for Metashape to generate tie-points in Sturgeon River Delta (Figure 9 b) and it was the only study site with no gaps in the RGB imagery.

Initially, only one block was processed at a time due to computer memory concerns. Later, multiple adjacent blocks were processed simultaneously, and in some cases, this increased the number of tie-points. Figure 7 shows the photogrammetric processing of three adjacent blocks aligned in Metashape. Figures 8, 9, and 10 show complete mosaicked NIR and RGB blocks. The mosaicking was completed using MosaicPro in ERDAS IMAGINE software (Hexagon, 2016), and proved efficient in generating seamless mosaics. Each flight block had different lighting condition due to varying acquisition times during the day. This may impact additional digital image processing such as reduction of shadow effects by topographic normalization. This procedure may not be completed in a mosaic of all the blocks. Instead, topographic normalization would have to be performed in each block prior to creating the full mosaic. It should be noted that in many cases, image mosaics were better for classification when flown on days with cloud cover, due to fewer shadows, blurriness and glare.

All of the processed NIR blocks showed small data gaps, with the lowest number of gaps in the Sturgeon Delta and Wedens Bay (Figures 9a and 10a); whereas Ogontz Bay (Figure 8a) showed the highest amount of gap in the mosaicked imagery. The gaps visible in Wedens Bay NIR imagery were in areas not flown due to lack of a clear line of sight of the aircraft. The relief displacement of trees on large scale images, aircraft rotations caused by wind, the complex geometry of dense forested areas, and low oblique imagery, all contributed created problems for Metashape and other SfM software to find matching tie points, which led to huge gaps with the RGB imagery. In future studies we may increase the overlap to 90% by flying at higher elevations, if approved by the FAA. This would reduce the low oblique look angle and relief displacement. Final orthomosaics were generated at ground resolution of approximately 1.3 cm for the NIR and 2.0 cm spatial resolution for the RGB data.

It is important to experiment with the settings and options of photogrammetric software when processing such large amounts of data. For many of the NIR and RGB blocks, the process was run using each available setting, (Low, Lowest, Medium, High, Highest and Ultra High) to ascertain which resulted in acceptable imagery quality and minimal data gaps in the block mosaics. For several cases, using the high settings for alignment created huge image gaps, while the medium settings did not. Performing realignment after the initial alignment process was crucial. Many blocks showed improved alignment on successive attempts. Metashape did process water areas close to beaches and vegetated areas if there were identifiable features in adjacent images such as underwater rocks, sand bars and emergent vegetation. It has been observed when working with dense forest areas

and acquiring a large digital dataset with lower accuracy GNSS, medium settings may work best for the alignment. Running the low setting during alignment might align a several more images in the blocks, but should be avoided as images are downscaled by factor of 16, leaving out important details (Agisoft, 2017b). Significant downscaling was evaluated but never achieved full image alignment.

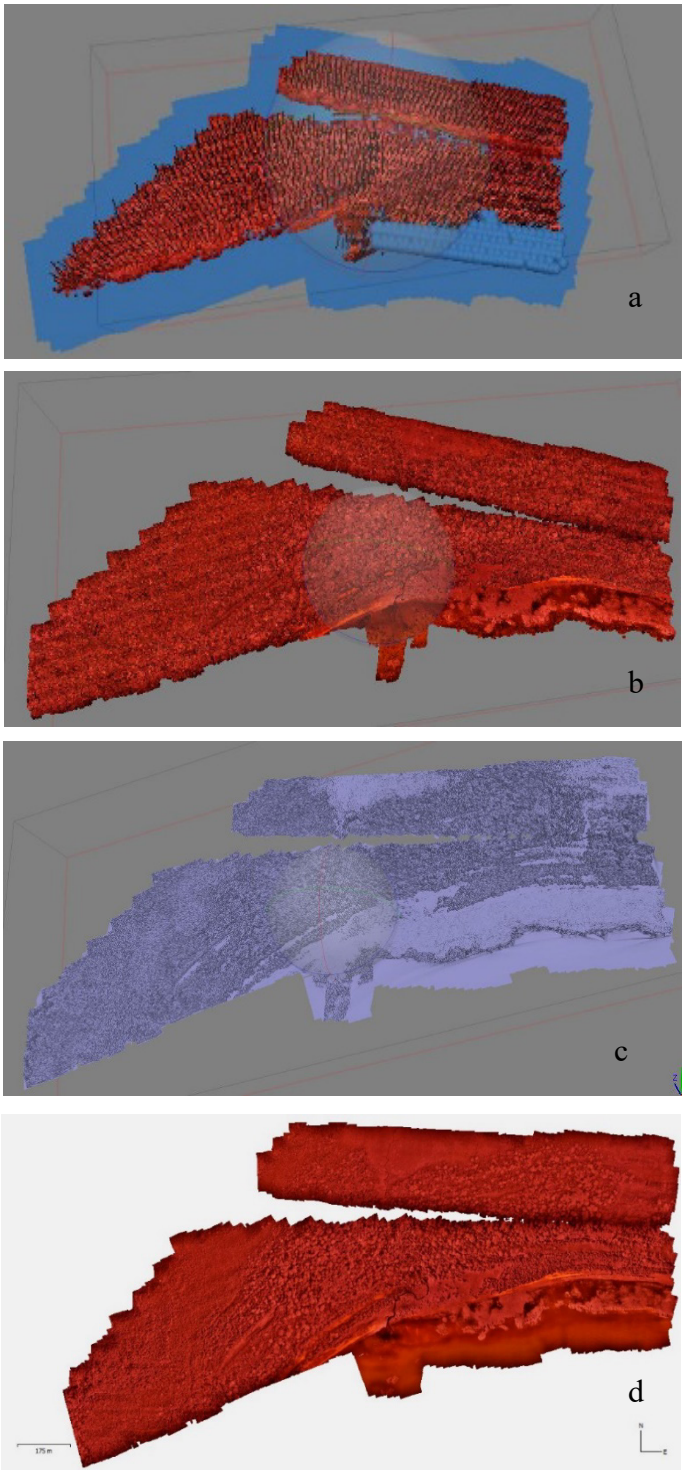

Figure 7. Tie points (a), dense cloud (b), 3D-Mesh (c), and orthomosaic (d) image generated from Metashape as part of photogrammetric workflow.

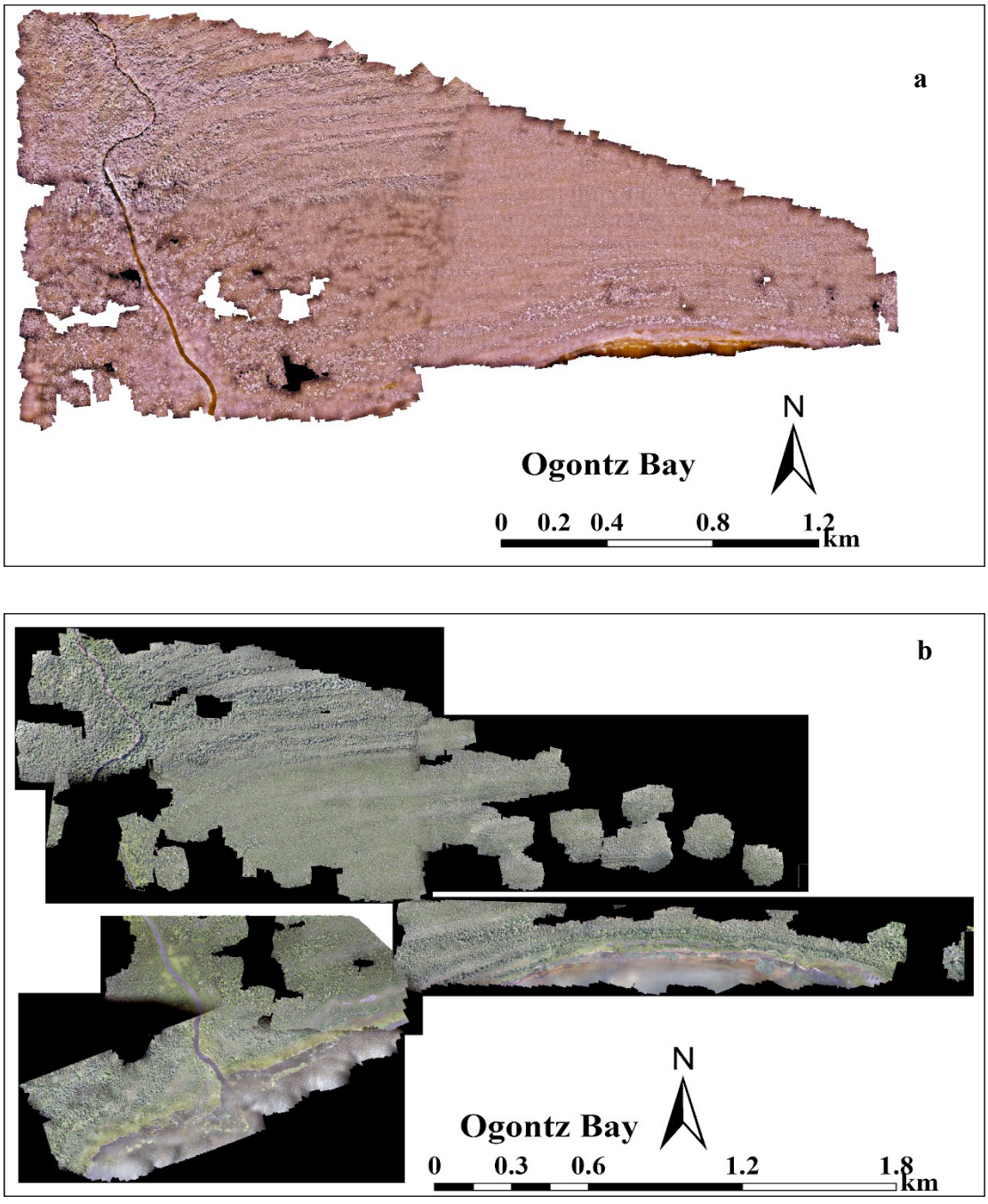

Figure 8. NIR (a) and RGB (b) mosaics of Ogontz Bay.

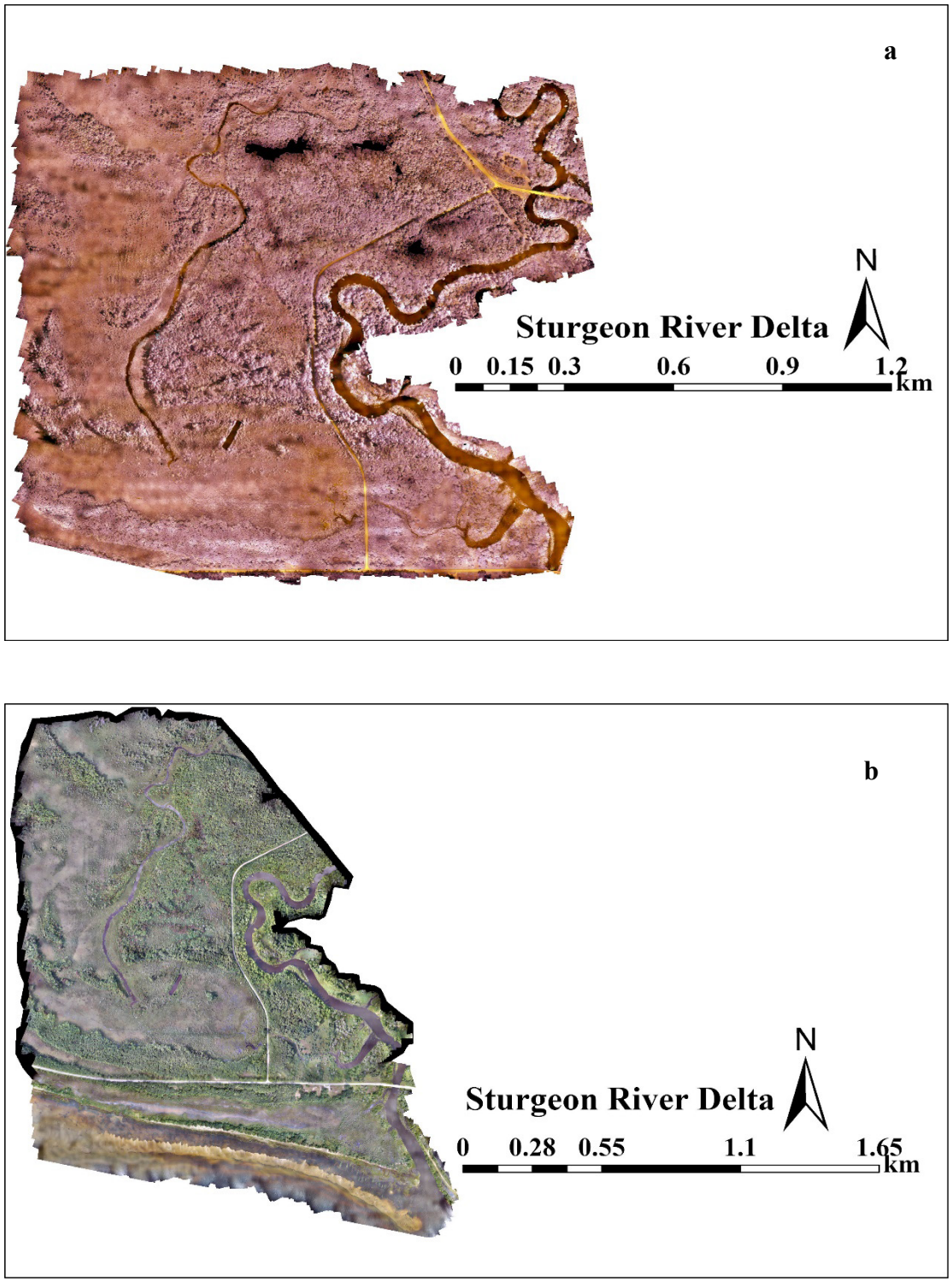

Figure 9. NIR (a) and RGB (b) mosaics of the Sturgeon River Delta.

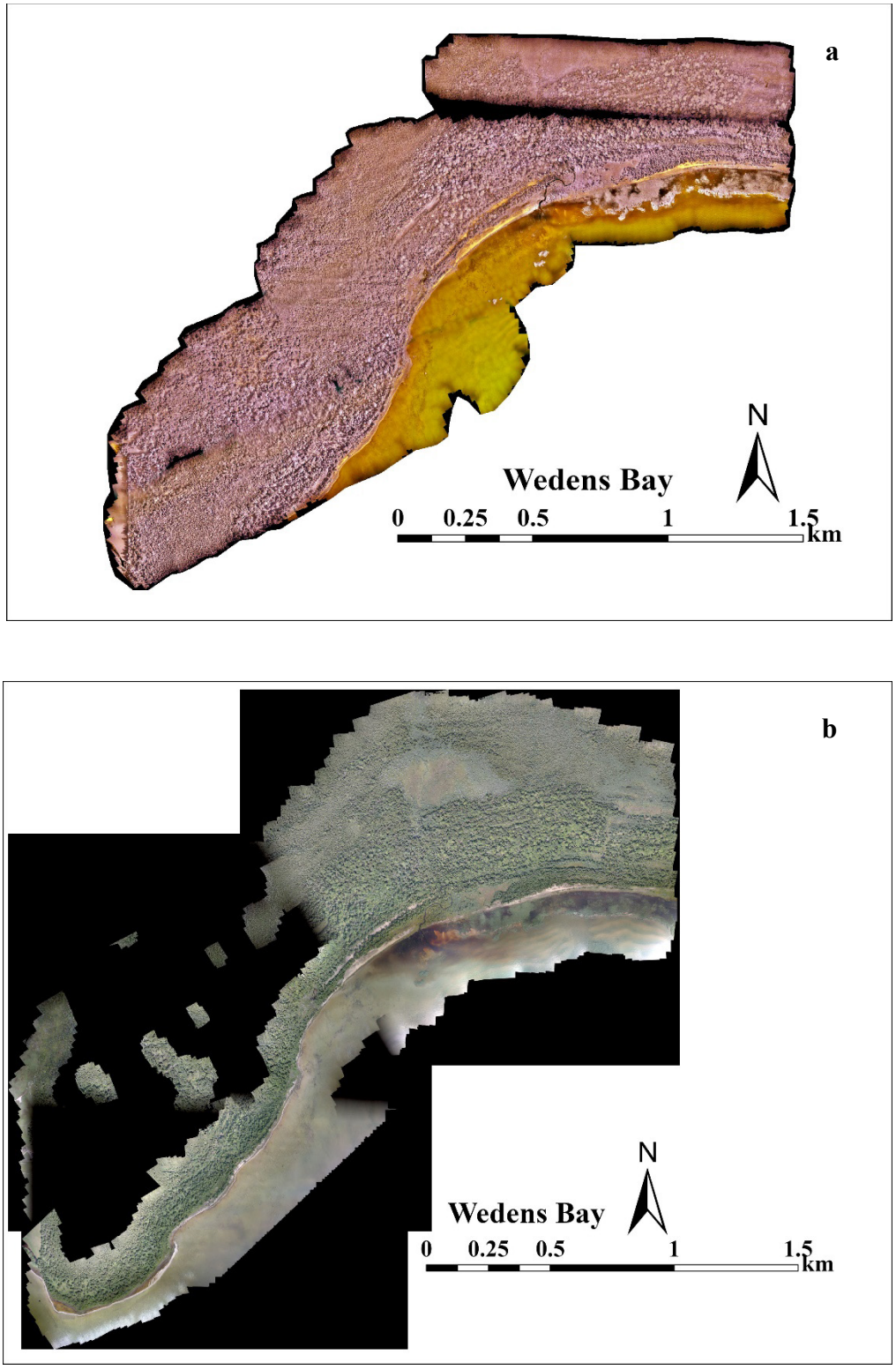

Figure 10. NIR (a) and RGB (b) mosaics of Wedens Bay.

With Metashape, higher accuracy requirements increased processing times which also depended on the complexity of the image texture. Due to the physical size of the raw data and the new data created with each processing, a large hard drive (5 to 8 terabytes) and adequate RAM were necessary. Thirty-five blocks, each having 800 to 1500 images, were processed for the three study sites. Each image was approximately 10 MB, consisting of 7,360 rows × 4,912 columns. The process was performed on a computer with 3.4 GHz CPU, Intel i5 processor using 64-bit Microsoft Windows 10 operating system with 16 GB of RAM (64 GB and GPU enabled PCs recommended for faster and larger data process). Increasing the computing capability enables processing the dataset for entire area at once, rather than individual blocks. It took 60 to 65 days to process the entire dataset. Cloud processing can be another option, but it's also time consuming and expensive.

2.5 **Conclusion**

The purpose of this applications paper was to discuss UAS image SfM photogrammetric workflow when working in a remote, dense forest environment, and acquiring large datasets with high spatial resolution image to create orthomosaics. This goal was achieved reasonably well. The methods described should help researchers and professionals to design and select an appropriate workflow.

The study demonstrated the flexibility of a UAS platform managed by a single person to collect data at different locations and times. Compared to human piloted aircraft

platforms, UAS allows higher spatial resolution, cloud free data due to low altitude flying heights, pilot safety, minimum requirements for takeoff and landing, and cost savings.

High image overlap (80%) and use of a higher grade GNSS on the UAS (UX5-HP) helped achieve good quality orthoimages with NIR data; whereas with the RGB data SfM did not achieve the same quality due to lower grade GNSS on the UX5 UAS. A study by Dandois et al. [75] showed that using high image overlap (>80%) in forested environment help achieve higher point cloud density. Higher flying heights covers more area as it provides a wider field of view, and may increase chances of matching identical features in homogenous forest and wetland cover imagery. In addition, the dense forest canopy negatively impacted image matching. Higher flying heights with increased image overlap as high as 90% is recommended. Higher flying heights help limit the amount of movement in the trees between image sets as the distance between the trees get smaller. Any movement in-between the image-sets adds error in the geometry, thus reducing number of tie-points. Increasing the overlap does increase the chance of finding a greater number of tie-points but it comes with a trade-off, as it increases the uncertainty in vertical measurements affecting the accuracy of the elevation model.

Flying at higher altitude, with appropriate FAA waivers should improve image alignment due to the reduction in oblique viewing angles, and perpendicular flight lines should reduce image gaps. Current FAA regulation required the aircraft within the visual line of sight and remain below 122 m (400 ft) above ground level (AGL). A recent study done by Seifert et al. [76] showed that higher overlap and flying altitudes impacts image reconstruction details and accuracy. All of the individually processed orthoimages were

mosaicked into one single seamless mosaic for each study site. There were some variation in shadow and sunlight as the images were taken at different times throughout the day, from early morning to late afternoon with different camera settings. Therefore, certain image enhancement techniques, such as topographic normalization and histogram adjustments should be completed by block by block before creating the mosaics. It is also recommended that data acquisition take place in the months of July and August as an optimal season for mapping forest areas due to longer days and higher amount of sunlight. Wind speed variation, increased aircraft rotations (yaw, pitch and roll), and tree crowns movement caused blurred images in several blocks, but the 80% overlap used in this study help overcome some of the issues during processing.

We concluded UAS imagery coupled with the SfM and traditional photogrammetry technique offers great potential for future research in vegetation and wetland classification, identification and mapping at the species level, to observe shoreline changes. It is efficient and affordable providing imagery at reduced cost over manned aircraft. UAS systems can also be used with multispectral, hyperspectral, thermal, and LiDAR sensors [77]. UAS imageries are an efficient and affordable data at reduced cost over manned aircraft systems or high-resolution private satellites.

Acknowledgments

The authors are grateful to the USDA Forest Service for the funding of this project. We are grateful to Jim Ozenberger, Hiawatha National Forest for his advice and recommendations. Particular thanks to Jeff L. Sloan and Mark Bauer at the National Unmanned Aircraft Systems Project Office, USGS and to Gordon Maclean for his wetlands mapping expertise.

Funding

This research was funded by the USDA Forest Service, Agreement Number 17-PA-11091000-023 and by the College of Forest Resources and Environmental Sciences Acknowledgments

Document references

Agisoft. L. 2017a. AgiSoft PhotoScan Professional (Version 1.3.0) (Software). URL: http://www.agisoft.com/downloads/installer/.

Agisoft. L. 2017b. Photoscan User Manual: Professional Edition, Version 1.3. URL: https://www.agisoft.com/downloads/user-manuals/.

CAA. 2015. An introduction to unmanned aircraft systems. URL: https://www.caa.co.uk/Consumers/Unmanned-aircraft/Our-role/An-introduction-to-unmanned-aircraft-systems/ (last date accessed: 21 November 2019).

DoD. U.S.D.o.D. 2019. UNMANNED AIRCRAFT SYSTEMS (UAS). URL: https://dod.defense.gov/UAS/ (last date accessed: 21 November 2019).

FAA. 2018. Small Unmanned Aircraft Regulations (Part 107). URL: https://www.faa.gov/news/fact_sheets/news_story.cfm?newsId=22615 (last date accessed: 21 November 2019).

Hexagon. G. 2016. ERDAS IMAGINE (Version 16.00) (64-bit). URL: https://download.hexagongeospatial.com/downloads/imagine/erdas-imagine-2016-64-bit (last date accessed: 21 November 2019).

ICAO. 2011. UAS Documents / Cir 328 AN/190 Unmanned Aircraft Systems (UAS). URL: https://www.icao.int/Meetings/UAS/Pages/UAS_Documents.aspx (last date accessed: 21 November 2019).

Markets. 2018. Unmanned Aerial Vehicle (UAV) Market by Application (ISR, Precision Agriculture, Product Delivery), Class (Tactical, MALE, HALE, UCAV), System (Avionics, Sensors, Payload), MTOW (<25Kg, 25-150Kg, >150kg), Range, Type, and Region - Global Forecast to 2025. URL: https://www.marketsandmarkets.com/Market-Reports/unmanned-aerial-vehicles-uav-market-662.html (last date accessed: 21 November 2019).

NASA. 2017. Mini-Sniffer. URL: https://www.nasa.gov/centers/dryden/multimedia/imagegallery/Mini-Sniffer/Mini-Sniffer_proj_desc.html (last date accessed: 21 November 2019).

NASA. 2008. The Promise of ERAST: Dryden Flight Research Center. URL: https://www.nasa.gov/centers/dryden/news/X-Press/stories/102904_people_erast.html (last date accessed: 21 November 2019).

Saczuk, E. (2018). –3-D Mesh Surface. *Processing UAS Photogrammetric Images in Agisoft Photoscan Professional.*

Trimble. 2019a. Trimble Inpho UASMaster. URL: https://geospatial.trimble.com/products-and-solutions/trimble-inpho-uasmaster (last date accessed: 5 November 2019).

Trimble, 2019b. Trimble UX5 Aerial Imaging Solution for Agriculture. URL: **https://www.trimble.com/agriculture/ux5** (last date accessed: 5 November 2019).

3 Fine-Scale Mapping of Natural Ecological Communities Using Machine Learning Approaches

Authors: Parth Bhatt[1], Ann Maclean[1], Yvette Dickinson[2], and Chandan Kumar[3]

Affiliations: [1]College of Forest Resources and Environmental Science, Michigan Technological University, [2]Scion (New Zealand Forest Research Institute), Rotorua 3020, New Zealand, [3]Geology and Geological Engineering, Colorado School of Mines, Golden, CO 80401, USA

(This work is published in the Journal of "Remote Sensing" under the special issue "Advanced Earth Observations of Forest and Wetland Environment": **Bhatt, P., Maclean, A., Dickinson, Y., & Kumar, C. (2022). Fine-Scale Mapping of Natural Ecological Communities Using Machine Learning Approaches. *Remote Sensing*, *14*(3), 563; https://doi.org/10.3390/rs14030563**)

Abstract

Remote sensing technology has been used widely in mapping forest and wetland communities, primarily with moderate spatial resolution imagery and traditional classification techniques. The success of these mapping efforts varies widely. The natural communities of the Laurentian Mixed Forest are an important component of Upper Great Lakes ecosystems. Mapping and monitoring these communities using high spatial resolution imagery benefits resource management, conservation and restoration efforts. This study developed a robust classification approach to delineate natural habitat communities utilizing multispectral high-resolution (60 cm) National Agriculture Imagery Program (NAIP) imagery data. For accurate training set delineation, NAIP imagery, soils data and spectral enhancement techniques such as principal component analysis (PCA) and independent component analysis (ICA) were integrated. The study evaluated the importance of biogeophysical parameters such as topography, soil characteristics and gray level co-occurrence matrix (GLCM) textures, together with the normalized difference vegetation index (NDVI) and NAIP water index (WINAIP) spectral indices, using the joint mutual information maximization (JMIM) feature

selection method and various machine learning algorithms (MLAs) to accurately map the natural habitat communities. Individual habitat community classification user's accuracies (UA) ranged from 60 to 100%. An overall accuracy (OA) of 79.45% (kappa coefficient (k): 0.75) with random forest (RF) and an OA of 75.85% (k: 0.70) with support vector machine (SVM) were achieved. The analysis showed that the use of the biogeophysical ancillary data layers was critical to improve interclass separation and classification accuracy. Utilizing widely available free high-resolution NAIP imagery coupled with an integrated classification approach using MLAs, fine-scale natural habitat communities were successfully delineated in a spatially and spectrally complex Laurentian Mixed Forest environment.

Keywords

remote sensing; northern mixed temperate forest; natural habitat communities; laurentian mixed forest; upper midwest; michigan; image classification; vegetation classification; machine learning; feature selection; RF; SVM; NAIP; DEM; GLCM texture; PCA; ICA

3.1 Introduction

Ecosystems are defined as "a community of organisms and their physical environment interacting as an ecological unit" [1]. Land cover grouped into types and systems by resource managers led Arthur Tansley [78] to coin the term "ecosystem". Ecosystems with spatially related features are considered higher order, larger scale ecosystems, referred to as "macroecosystems" [4]. When ecosystems are viewed as macroscale patterns they can be divided into ecoregions [79]. The term "ecoregion" was first

proposed by Orie Loucks [80], a Canadian forest researcher. Ecoregions play an important role in resource conservation and management by considering the natural process and patterns of communities in a particular region which provide ecosystem sustainability [81]. Many different factors (vegetation, soils, spatial and temporal scales, landform and bedrock geology) are utilized to classify these systems, and numerous ecological classification schemes exist. Spatial and temporal dimensions of ecosystem integrity can be addressed using scale (level of detail) and a hierarchical structure approach [2]. Various geographic ordering schemes were developed by Bailey [4, 81] to identify and delineate ecoregion boundaries. Additionally, having a hierarchical classification scheme allows ecosystems to be presented at different spatial scales [6, 7]. A holistic ecological framework was introduced by Rowe and Barnes [7, 8] using a landscape ecosystem, or geo-ecosystems, approach which incorporates factors such as climate, landforms, soil characteristics, hydrology and biota. An example of a widely used hierarchical classification scheme for wetlands and deep-water habitats for the United States was developed by Cowardin [9]. It divides ecological taxa into hierarchal systems or subsystems to provide mapping uniformity across the United States.

Selecting or developing an appropriate ecological classification scheme is critical for the classification to be useful to the end user. There are numerous existing classification schemes [6, 8, 9, 12] and selection of an inappropriate scheme can limit the end product's accuracy and utility. To classify a landscape, whether *in situ* or using remotely sensed data, it is important to have a classification scheme which reduces or eliminates confusion between various landscape features requiring separation [11]. Traditionally many resource management agencies (federal, state and private) use field sampled

regional vegetation classes focusing on the dominant vegetation species while ignoring associated plants, animals and other organisms which are repeatedly found under similar environmental conditions [82] and focuses on describing native ecosystem types minimally impacted by anthropogenic activities [12]. For this study, the hierarchical classification framework of Cohen et al. [12] was utilized. Their publication, "Natural Communities of Michigan: Classification and Description", published by the Michigan Natural Features Inventory (MNFI) provides detailed information on separating Michigan's complex landscape into understandable and describable components labeled as natural habitat communities. The foundation of this classification is based on the work completed by Chapman [13], and first published by Kost et al. [14]. It is important to understand the difference between a plant community, such as the ones used in the National Land Cover Classification [36], and a natural habitat community [12]. The latter differs from other hierarchical classifications schemes in that Cohen et al. [12] regards them "as an assemblage of interacting plants, animals, and other organisms that repeatedly occurs under similar environmental conditions across the landscape and are predominantly structured by natural processes rather than modern anthropogenic disturbances". To date, no study has been performed using a natural habitat community level classification scheme.

Along with the classification scheme, it is important to choose appropriate field collection methods and data sources. Commonly used field methods for data collection (e.g. collecting location points via Global Navigation Satellite System (GNSS) and vegetation sampling) are labor intensive, costly, and time consuming. Sampling is confined to small areas due to limited access and safety concerns [21]. With technical

advances in geospatial technology, an alternative and/or complimentary approach to traditional field data collection techniques is available. Remotely sensed imagery provides a practical, economical approach to monitor and measure biogeophysical factors. Hence it is efficient for large area monitoring [22, 83, 84]. Fine scale mapping is critical to locate and map endangered habitats particularly with escalating global climate change impacts. Hence high spatial resolution imagery, such as the National Agriculture Imagery Program (NAIP), is important. The NAIP program is managed by the Aerial Photography Field Office (APFO) of the United States Department of Agriculture (USDA). It has 8-bit radiometric and 60 cm spatial resolutions, with 4 spectral bands (near infrared (NIR), red, green and blue). NAIP data is nominally cloud free and widely available at no cost [85]. It has been used for wetland mapping, land cover classification, forest cover type mapping, forest health monitoring and other resource management projects [86-88].

Additionally, selection of the correct classification algorithm is dependent on image spatial resolution, chosen classification scheme and landscape complexity. In the last two decades the remote sensing community has steadily increased its use of Machine Learning (ML) classification techniques [26-31] as the limitations of traditional parametric classification techniques, such as maximum likelihood, are realized. Machine Learning Algorithms (MLAs) use a nonparametric approach to model and classify data, and do not require normally distributed data [89]. Numerous land use/cover classification studies have shown the advantages of using MLAs such as Random Forest (RF), and Support Vector Machine (SVM) [28, 32-35]. MLAs were utilized in the classification of

the 2001 National Land Cover Database (NLCD) [36]. They have also been used with NAIP imagery for accurate land cover classification [39, 85].

Factors such as training set quality, selection of the optimum number of ancillary datasets, and training parameters affects the performance of MLAs [89, 90]. Poor quality training data impacts the accuracy of MLAs. Use of image transformations, such as Principal Component Analysis (PCA) and Independent Components Analysis (ICA), reduces or eliminates redundant spectral information. Ancillary data such as landform, soil characteristics, hydrography and expert knowledge of the study area are important to create high quality training sets. Use of valid ancillary dataset also plays a crucial role in the classification of vegetation communities. It is important to understand which ancillary datasets are impacting classification accuracies. Feature selection methods identify the best ancillary data before executing MLAs, and reduce the complexity of the method (e.g. "Hughes Phenomenon" [43]) and overall computational time [89]. Researchers have shown the usefulness of feature selection methods and the use of multiple ancillary data to improve land cover classification [39, 85]. Examples include combining high spatial resolution data with ancillary layers using ML approaches to improve classification results of complex wetland environments [40, 85, 91].

The Upper Midwest is part of the Laurentian Mixed Forest and is an extremely complex landscape in terms of geomorphology and vegetation due to extensive regional glaciation [92, 93]. A Laurentian Mixed Forest province occurs in between the boreal forest and the broadleaf deciduous forest transition zones [94]. This has led to unique and complex landforms which dictate topography, soil characteristics, hydrography and vegetation

communities [92]. Although, there are a number of completed studies using grouped species classifications in this region [82, 95-97], to the best of our knowledge, no study has been performed using a natural habitat community level classification scheme [12] with MLAs.

Hence, the goal of this study was to develop a robust methodological classification approach to identify and accurately classify spectrally similar natural habitat communities of the complex Laurentian Mixed Forest region using the MNFI natural habitat communities classification scheme [12]. To achieve that, we proposed an integrated approach of spectral enhancement techniques coupled with elevation, soils, and field data to take accurate training data. Classification accuracies were compared between two commonly used MLAs, RF and SVM, using various ancillary data derived from feature selection methods along with the high spatial resolution NAIP dataset.

3.2 Study Area, Data and Methods

3.2.1 Study Area

The study site (Figure 11), is the Sturgeon River watershed (HU5 Id 20207) (45°50'27"N, 86°40'30"W) located in the western half of the Hiawatha National Forest, adjacent to the head of Big Bay de Noc. The study area encompasses approximately 3,151 ha (7,7861 ac) and contains a wide variety of natural habitat communities. Dominant vegetation is composed of upland and lowland deciduous, conifer and mixed forest types as well as palustrine wetlands [17]. The influence of the Great Lakes and various landforms creates distinct climatic zones across the area with summer

temperatures ranging from 22°C (71°F) near the Great Lakes shoreline to 27° to 29°C (81° to 85°F) warmer inland. Winter temperatures range from an average high of -2°C (28°F) and to an average low of -11°C (13°F). Winters are long and snowy, with average snowfall around 142 cm (56 inches) along the Lakes Michigan and Huron shorelines, to 554 cm (218 inches) near Lake Superior. The study area is part of a glacial lake plain and is a nearly level lake plain that was covered with water from Glacial Lake Algonquin. The soils on the landform are derived from predominantly sandy lacustrine deposits [92, 98]. Soil drainage classes range from poorly to excessively drained, and soil pH ranges from neutral to extremely acidic. The area contains numerous wetlands with a complex hydrography.

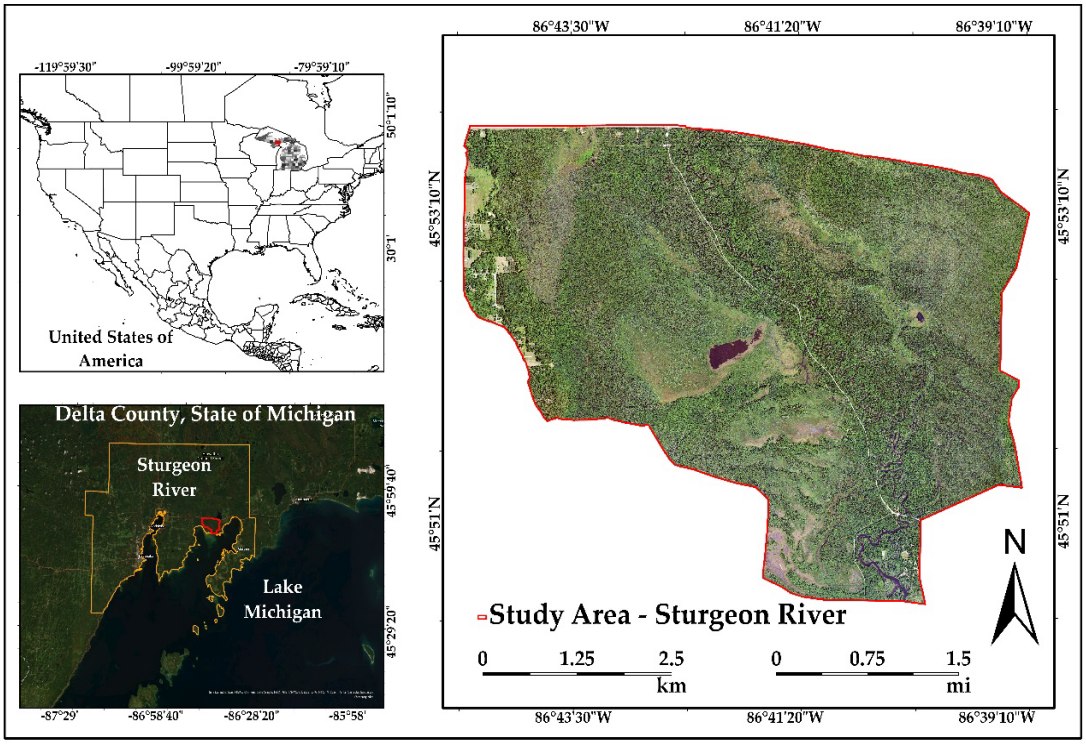

Figure 11. Geographical location of Sturgeon River watershed and the image of research area presented by RGB composition using bands 1, 2, and 3 from the NAIP imagery.

3.2.2 Imagery

National Agriculture Imagery Program (NAIP) is flown during the active growing season and is also known as “leaf-on” imagery, which is needed for habitat classification. The four band (red, green, blue, near- infrared) aerial imagery was acquired at approximately 16,000 feet above ground level (AGL) with a Leica ADS100 airborne digital sensor (Leica Geosystems). The image has a spatial resolution of 60 cm with 8-bit radiometric resolution. The spectral range of the 4-bands ranges between 435 and 882 nm (Figure 12). The data was preprocessed by the contractor to reduce radiometric and geometric distortions. NAIP imagery tiles dated 25 July 2018 and 11 August 2018 were downloaded from the United States Geological Service (USGS) Earth Explorer (https://earthexplorer.usgs.gov/, accessed on: 14 July, 2021). A LiDAR derived 1 m Digital Elevation Model (DEM) was obtained from The Natural Resources Conservation Service (NRCS). All datasets were registered to the Universal Transverse Mercator (UTM), Zone 16 North, North American Datum of 1983 (NAD83). The spatial resolution for all the datasets is 60 cm. Where resampling was required, the data was reprojected using a two-dimensional affine coordinate transformation with nearest neighbor sampling with a fundamental vertical accuracy of ±24.5 cm and meets all FGDC (Federal Geographic Data Committee) standards.

ERDAS IMAGINE® 2020 (https://www.hexagongeospatial.com/products/power-portfolio/erdas-imagine, accessed on: 14 July, 2021) and ArcPro 2.7 (https://www.esri.com/en-us/store/arcgis-pro, accessed on: 14 July, 2021) were used for image transformation. IMAGINE’s Spatial Model Editor Toolbox was used to generate

Normalized Vegetation Index (NDVI) and a Modified Water Index (WINAIP), Gray Level Co-occurrence Matrix (GLCM) Textures, Aspect and Slope (%). ArcPro tools were used to generate random points (Create Random Points) and to extract multi raster values (Extract Multi Values to Points). The "caret" package [45] of the R programming language [99] was used for MLA implementation.

Spectral Band Names	Wavelength (nm)	Spatial Resolution (cm)
Blue (B)	435 – 495 nm	60
Green (G)	525 – 585 nm	
Red (R)	619 – 651 nm	
Near-Infrared (NIR)	808 – 882 nm	

Figure 12. Spectral characteristics of the NAIP Data (Leica Geosystems, 2020).

3.3 Methods

3.3.1 Utility of Image Transformations

Multiple workflows have been developed by the remote sensing community for delineating and mapping vegetation. They are dependent on environmental factors (e.g. soil characteristics (drainage, slope, pH), hydrography, landform, climatic conditions) [100], as well as data collected in the field, expert image interpretation (manual and computer assisted), and an appropriate classification scheme [9, 12, 40, 91, 101-103]. The delineation and classification workflow used in this study is presented in Figure 13. Inter-class spectral variability is important to differentiate natural communities. However, locally high variance occurs not only due to changes in vegetation, but also site

conditions and the high spatial resolution of the imagery [104]. When selecting training sets, it is important to understand how these factors influence training set statistics and to generate adequate training data to encompass the variation. Having polygon training sets with well delineated feature boundaries is critical to generate valid training set point matrices for the Machine Learning Algorithms (MLAs) [89].

To fully utilize spectral reflectance information, and at the same time, reduce redundant information between bands, an integrated approach of spectral transformation techniques (Principal Components Analysis (PCA) and Independent Components Analysis (ICA) were utilized. PCA is a widely employed transformation using a linear transformation and generates uncorrelated components [105, 106]. PCA derived components have been used to map wetlands vegetation, assess change detection, evaluate vegetation anomalies, and geological features [107-111]. PCA uses second-order statistics and assumes the data are normally distributed and correlated. PCA has been utilized since the launch of the Landsat 2 Multi Spectral Scanner which consisted of 4 bands [112]. ICA considers higher-order statistics, and each transformed component is considered non-Gaussian [113]. ICA has been shown to identify details in an image even when the feature occupies a small area [114]. However, it has not been extensively used in vegetation and land use/cover classification [111, 115-117]. Both PCA and ICA were used to draw accurate training classes for MLA. The components of the PCA transformation were not used in the classification process as components 3 and 4 contained information critical to delineating the emergent marsh natural habitat communities.

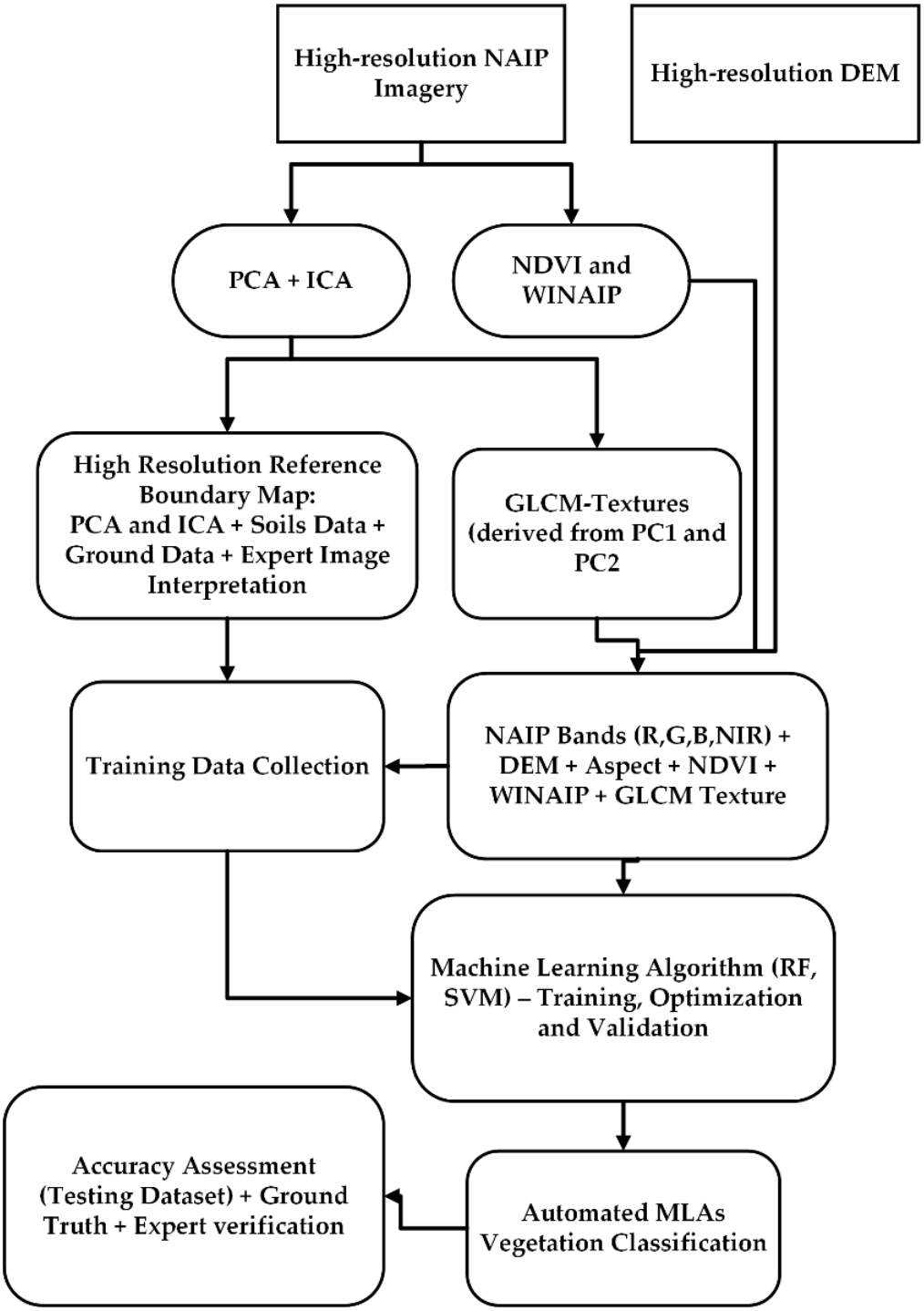

Figure 13. Workflow diagram explaining the methods adapted for vegetation classification using spectral enhancement techniques, indices and machine learning algorithms.

3.3.2 **Vegetation and Moisture Indices**

Spectral Indices have been used extensively to evaluate, monitor and map vegetation both qualitatively and quantitatively [118]. Two spectral indices such as Normalized Vegetation Index (NDVI) and a Modified Water Index (WINAIP) were derived from the NAIP bands. NDVI indicates the biomass abundance and vigor as well as differentiating vegetation from non-vegetated areas [119, 120]. NDVI was generated using NAIP bands 4 (NIR) and 1 (red). WorldView Water Index (WV-WI) was proposed by Wolf [121] and uses WorldView satellite band combinations of Coastal Blue (425nm) and the second Near Infrared channel (NIR2) (950nm). Previous water indices for satellite imagery were based on NDWI [122] which used NIR and Short Wave Infrared (SWIR) channels. Based on Wolf's index a custom water index was developed for this study by replacing the Coastal Blue (425nm) band with NAIP Blue (435nm) and NIR2 (950nm) band with NAIP NIR (882nm). The modified index is referred to as the WINAIP.

3.3.3 **Texture**

Plant communities often share similar spectral reflectance characteristics which leads to confusion and misclassification. In such scenarios, texture differences may be useful, even critical, to correct classification. A grey-level co-occurrence matrix (GLCM) originally referred to as a "gray-tone spatial-dependence matrix" by Haralick et al. [123], uses second-order metrics to analyze relationships between pairs of pixels and computes both angular relationships and directionality to measure the spectral and physical distance between two neighboring pixels [124]. GLCM texture analysis has been used in

numerous studies to classify various features including urban areas, forests, agriculture and wetlands [102, 123-125].

The GLCM texture was derived from the NAIP first and second PCA components. These components explained 94% (component 1) to 99% (components 1 and 2) of the variability in the image. Three different GLCM measures of texture (contrast, entropy, and standard deviation) were calculated with PCAs 1 and 2. GLCM was performed in ERDAS IMAGINE (Hexagon Geospatial, 2020), with a grayscale level of 32 and 3×3, 5×5 and 7×7 processing windows. Two different Euclidean geometry XY offsets (2, 2 and 2, -2) were used. The derived means from the texture measures were used in the classification.

3.3.4 **Topographical Characteristics**

At fine scales, natural habitat communities are controlled by soils, local topography, lake effect climate zones and in some instances past disturbances such as fire and wind throw. Extensive glaciation in the Upper Midwest has created a wide variety of surficial geologic features. These features are made up of interacting landform patterns which have been described [98, 126] as combinations of "relief-topography (surface shape) and geological parent material." Rowe [8, 98, 127] stated that "repetitive patterns in vegetation can be traced directly to repetitive patterns of topography associated with specific types of surficial material of landforms." Drawing on this body of research, 1-meter DEM generated from Lidar imagery collected in 2015 helped identify important topographic features with high positional accuracy. The DEM was downloaded from the National Resource Conservation Service at the recommendation of the US Forest Service.

Hillshade (Multi-Directional Oblique Weighted - MDOW), aspect and slope (%) were generated from the DEM. Aspect and slope were evaluated as input ancillary data into the MLAs and Hillshade aiding in manual training set delineation.

3.3.5 **Selection of Input Ancillary Data Layers**

When imagery alone can't adequately classify the data, the incorporation of ancillary data is important. Once ancillary data layers are selected, understanding their contribution towards classification is important [128] with the goal of optimizing and creating an accurate classification. Variable selection has been used in many applications including data mining and machine learning, network anomaly detection, natural language processing, bioinformatics and image processing [128]. There are many different feature selection methods available [129].

In this study, the Joint Mutual Information Maximization (JMIM) [44], a filter-based variable selection method was implemented in R using the "praznik" package [130]. This method uses 'mutual information' and 'maximum of the minimum' criteria to calculate the contribution of each input variable. This method evaluates each variable's importance. The JMIM method was performed prior to running the MLA classification. Those with higher JMIM values were used as ancillary data inputs. Along with the JMIM method, the "varImp" function was used [44] from the "caret" package [45, 131]. It evaluates the implemented MLA and identifies the best ancillary data layers for improving the classification [129, 131]. The varImp method is implemented after the RF classification is performed. The scores produced for each variable helped select different variable combinations for the MLAs classifications.

Based on Joint Mutual Information Maximization (JMIM) and "varImp" scores the following variables were used as inputs in the Machine Learning Algorithms (MLAs):

- 4 bands of NAIP imagery
- Elevation from DEM
- Contrast Texture (C1*7) calculated from PC1 (7×7) moving window, C2*7 calculated from PC2 (7×7) moving window
- Normalized Vegetation Index (NDVI), and Modified Water Index (WINAIP) derived from NAIP imagery.

Feature selection methods have been primarily used in geology applications to reduce the complexity of the dataset where there are large number of bands (i.e. Hyperspectral data) [111]. In this study, both feature selection methods were implemented. However, as this is an uncommon approach for natural resource applications [132-134], along with feature section methods various combinations of the ancillary data were manually selected and evaluated as well. These are listed in the results section.

3.3.6 **Collection of Training Samples**

An adequate number of training samples is crucial to achieve optimum classification results. As a 'rule of thumb' in ML, the number of training samples should be 10 times (preferably 100 times) the total number of variables [89, 135]. How the training samples are selected also plays a crucial role and requires expert knowledge of the spectral and spatial variation within and between the natural communities [11]. Additionally, the choice of classification algorithm, the number of input variables and the spatial extent of each natural habitat community influences the number of training samples required. [89,

136]. Researchers have noted that large and accurate training datasets are preferable regardless of the MLA used [25, 89, 137]. Training samples were generated within manually delineated training set polygons (Figure 14) using stratified random sampling in ArcMap 10.7.1 with a minimum of 5 m distance between points. Different spectral enhancement techniques (PCA, ICA), soils, elevation data, and ground truth were utilized to delineate the training polygons. Figure 15 presents the natural communities within the study area and the number of training and test points collected for each. The points were assigned natural habitat community class names and ids. Using the X and Y locations of the training sample points, pixel values for all of the input ancillary data layers were extracted for use in the MLAs.

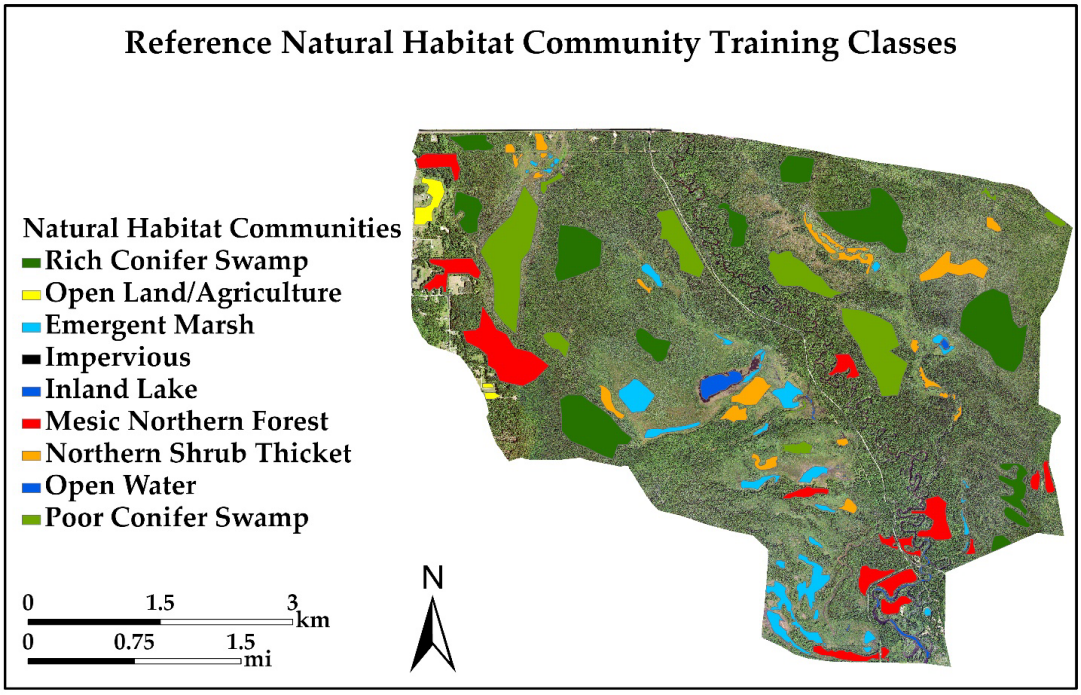

Figure 14. Reference natural habitat community training data map showing polygons to be used for generating random points.

Vegetation Community Type (Code)	Area (hectares)	Training Data	Testing Data
Open Land (OL)	10.6	466	155
Emergent Marsh (EM)	64.7	3,205	1,068
Rich Conifer Swamp (RCS)	202.5	4,057	1,352
Poor Conifer Swamp (PCS)	142.9	2,272	757
Northern Shrub Thicket (NST)	54.9	2,620	873
Mesic Northern Forest (MNF)	108.3	3,814	1,271
Inland Lake (IL)	8.3	386	128
Open Water (OW)	5.3	292	97
Impervious Surfaces (IS)	5.5	301	100
Total	603	17,413	5,801

Figure 15. Vegetation communities, area and the number of randomly generated training and testing points for input into the MLAs.

3.3.7 **Utilization of MLAs for Natural Communities Classification**

The training samples derived from the input ancillary data layers were used to train both Random Forest (RF) and Support Vector Machine (SVM). Parameter optimization, validation, and accuracy assessment were performed for both algorithms. "Caret" package [45] available in "R" programming language was used to implement the MLAs. RF and SVM classifiers are discussed briefly below.

3.3.7.1 Random Forest

RF is an ensemble classifier method developed by Brieman [138], which uses a set of non-parametric, Classification and Regression Tree (CART) rules to make predictions [139]. Decision Trees (DT) are generated using the values of a random vector sampled independently from the input vector and distributed equally among all the trees in the forest [27, 31, 140, 141]. It then uses the majority of votes from the tree's assemblages

and assigns that value to each of the unknown vectors [40, 89]. Random Forest works on a ‘bagging’ (or bootstrap aggregating) approach, which generates training datasets by randomly drawing replacements of the original training set for each selected feature/feature combination [31, 138, 142]. RF uses two thirds of the data to train the trees and the remaining one third data to provide an independent estimate of overall accuracy (OA) [26, 89]. The classifier is computationally efficient but can be prone to overfitting [143, 144]. The forest can grow to a user-defined largest number of trees (Ntree) by optimizing the number of RF created trees exhibiting high variance and low bias [26, 138]. The m_{try} parameter controls the number of variables randomly selected at each split in the tree building process and has a sensitive influence on RF performance. It can be adjusted if needed as part of the tuning process [145, 146]. RF advantages include its ability to work with spatially large, complex datasets with correlated variables, rank variable importance, and improved classification accuracies [89, 138]. We used the default parameters provided with the “rf” method in the caret package and used “center” and “scale” to standardize the ancillary data [45, 147]. RF tends to work robust without optimization parameters [89].

3.3.7.2 Support Vector Machine

SVM is a supervised machine learning algorithm developed by Vapnik [148] based on statistical learning theory. The classifier is inherently binary and tries to identify a boundary or a hyperplane which separates two classes closest in feature space. The hyperplanes associated with the class are parallel to the optimal separating hyperplane and the samples located on these hyperplanes are called support vectors [148, 149].

However, in the real-world, data distributions are often non-linear, noisy and may not be easily separated, which promotes over fitting. Projecting the input data to a higher dimension feature space helps overcome this issue, assuming that a linear boundary exists in the higher dimensional feature space [89, 150]. If a linear higher dimensional feature space doesn't exist, a kernel function can be used, and for this study a radial basis function (RBF) kernel was used [151]. We used the default "svmRadial" method from the caret package [45]. SVM contains two important model parameters, "cost" (C) and "sigma" (σ). Higher C values can lead to a more complex decision boundary and less generalization [89]. Whereas a higher σ affects the overall shape of the separating hyperplane and may influence overall accuracy. The "caret" package estimates approximate value for the cost and σ parameter directly [45, 147, 152]. RBF parameters are determined by a grid search algorithm using m-fold cross-validation (m-FCV) approach. The grid search method tests different pairs of parameters, and the one with higher cross validation accuracy is selected [153]. Centering and scaling was done to standardize the ancillary data [45, 147].

Cross-validation procedure prevents overfitting issues with the data [149, 154]. To select and evaluate optimum parameters, a 10-fold cross validation was used for both RF and SVM. It is the recommended number of folds for comparing machine learning algorithms performances [155].

3.3.8 **Accuracy Assessment and Classification Differences**

Thematic accuracy assessment is an important component in evaluating the "correctness" of a classification. Products with low accuracy have limited, if no utility to the end-user as they are composed of misinformation. Stratified random sampling was selected for the accuracy assessment points. This sampling approach insures unbiased sample selection and adequate sampling for each habitat since a minimum number of samples is specified for each class [156, 157]. Using the methodologies developed by Congalton and Green [11] error matrixes, overall accuracies, kappa and Z-scores with a 95% confidence limits where calculated.

Differences in the output classifications occur as the MLA algorithms do not process the data the same way. Processing differences do create different end products. Differences from the two MLA outputs were assessed in ArcPro 2.7.

3.3.9 **Classification Post-Processing**

Classified data, including the natural habitat community classifications resulting from the MLAs manifest a 'salt and pepper' appearance due to the spectral variability encountered by the classifier [10, 158]. A single pixel is an arbitrary usually square, delineation which may have little or no relation to the actual mapping of a natural habitat community [11, 159, 160]. It is common practice to remove noise using a majority filter and a specified window size [10] to create homogenous polygons suitable for accuracy assessment. To make the natural habitat community classes easily identifiable and aesthetically pleasing on the map we applied a 7×7 moving window majority filter.

3.4 Results

Natural habitat community classification was evaluated using RF and SVM with various input ancillary datasets including NAIP spectral bands, topographical layers, textural measures, and spectral indices to classify the natural communities (Figure 19). The training and testing datasets were split 75% and 25%. The appropriateness of the input datasets was evaluated based on the overall accuracy (OA) and kappa (k) of test samples (5,801 pixels). OA indicates the ratio between total number of pixels and total accurately classified pixels and the k (kappa) shows measurement of agreement between the accurately classified data and the reference data [11]. Along with OA and k, UA and PA for each community class was evaluated as well. User's Accuracy (UA) and Producer's Accuracy (PA) shows accuracy of each community class, as described by Congalton [11], UA and PA shows commission and omission errors of individual class respectively. Z-scores with 95% CI were evaluated as well. Along with that, a difference map was generated as well to evaluate the classifier differences.

3.4.1 Ancillary Data and Feature Selection Methods

Total of 19 ancillary datasets were evaluated in this study as shown in Figure 17. Contrast texture image provided the most detailed information compared to Ent and SD. Hence, 2 more images were generated using 3X3 and 5X5 moving windows to evaluate impact of window size on the natural habitat community MLA classification. JMIM and varImp scores were calculated for all of these input ancillary datasets and shown in Figure 17 from higher to lower scores. Classifications using RF and SVM were generated

using all possible combinations of the above-mentioned ancillary data layers (Figure 19) to verify the robustness of feature selection methods. Ancillary data layers which had lower scores in the feature selection method (Figure 17), showed similarly poor performance in the MLA classifications (Figure 19 and 20).

3.4.2 Classification Results

The classifications for both MLAs can be grouped into 3 broad categories. Those with OAs between 50 and 59%, those between 60 and 69%, and those greater than 70%. Those with the lowest accuracies used the fewest number of input ancillary data, ranging from 4 (National Agriculture Imagery Program (NAIP) bands only) to 5 (all NAIP bands and the addition of derived ancillary data such as slope, aspect, Normalized Difference Vegetation Index (NDVI) and WaterIndex-NAIP (WINAIP). Improved OAs were seen with the addition of various combinations of texture. Classifications with the highest accuracies included using all of the input ancillary data (Input 3) to those using a combination of derived indices and textures. Figure 19 shows the overall accuracy (OA), kappa (k) and confidence intervals (CI) for the natural habitat community classifications derived from various input variable combinations. RF has OAs and associated k's ranging from 56.02 % (k = 0.46) for Input 1 to 79.96% (k = 0.75) for Input 3. SVM values were between an OA of 59.01% (k = 0.49) for Input 1 to 75.85% (k = 0.70) for Input 4. Using Cohen's categorization of kappa value ranges, classifications from Inputs 2 and 3-4 (Figure 20) have substantial agreement. The remainder have moderate agreement.

Using the four multispectral (NAIP) bands (Input 1) achieved a low OA (56.02%, k = 0.46) with RF and with SVM (OA = 59.01%, k = 0.49) (Figure 19). Incorporating the DEM with the NAIP bands provided a significant improvement in OA (12 to 17% increase) regardless of the MLAs. Using slope and aspect with the NAIP bands did not significantly improve the OA. Similarly, vegetation and water indices did not differ significantly compared to just using four NAIP bands. When all variables (Figure 19), including the four NAIP bands, three topographic layers, ten texture layers and two indices were used, the OA improved to almost 80% for RF and 74% for SVM (Figure 19). Figure 18 shows the graphical representation of OA and k for NAIP bands, all ancillary dataset and the final classification approach. Input 4 ancillary data layers were used for the final classification (Figure 21 and 22), having 79.45% OA for RF and 75.85% for SVM. Between Input 3, which used nineteen ancillary data layers and Input 4, which used only nine ancillary data layers, no significant statistical differences were observed (Figure 19 and 20).

Z-scores with a 95% confidence limit are calculated for all k values and are shown in Figure 20. The scores for each classification, regardless of input variable combination, show the classification to be meaningful and significantly better than a random classification. Pairwise Z-scores are also presented in Figure 20. The scores indicate all of the classification results for RF and SVM with the same input variables are not statistically different as all have an absolute value < 1.96.

Figures 21 and 22 present the final classification results from input data 4 (Figure 19) for RF and SVM. There are 5 natural habitat community classes (Figures 21 and 22) with 4

non-habitat community classes (Open Land, Impervious, Inland Lake, and Open Water) which are not considered natural habitats under the current classification scheme, but reflect human influences on the landscape, such as agricultural/open land, roads, and must be included. Input data 3 has a slightly higher OA, but is not statistically significant (Z-score) compared to input data 4 which has fewer variables. Fewer variables shorten the computing time, which is an important consideration for classification of large areas. However, the kappa and Z-score are only 2 measures of classification quality as they only consider the overall classification and not the accuracy of the individual natural habitat community classes.

Figure 25 presents the error matrix for the final RF and SVM natural habitat communities classification. User's (UA) and producer's accuracies (PA) are also presented. A total of 5,801 randomly generated ground truth testing points were used for accuracy assessment (Figure 25). Each natural habitat community class had at least the minimum number points to create a 95% confidence interval, and was based on the percent area each class made up of the total area.

The PA and UA calculations show the accuracies of the natural habitat communities are split into 2 groups. Those with accuracies above 85% and those with accuracies between 60 and 75% (Figure 25). Open Land (OL), Emergent Marsh (EM), Mesic Northern Forest (MNF), Inland Lake (IL), Open Water (OW) and Impervious Surface (IS) have PA between 84 and 100%. Rich Conifer Swamp (RCS), Poor Conifer Swamp (PCS) and Northern Shrub Thicket (NST) have PA between 41 and 81%. These lower PA accuracies can be explained by the prevalence of tag elder (*Alnus incana*), red osier dogwood

(*Cornus sericea*), white pine (*Pinus strobus*), red maple (*Acer rubrum*) across all three communities [12]. Sphagnum mosses (*Sphagnum* spp.), bunchberry (*Cornus canadensis*), balsam fir (Abies balsamea), paper birch (*Betula papyrifera*), black spruce (*Picea mariana*), huckleberry (*Gaylussacia baccata*), sensitive fern (*Onoclea sensibilis*) are found in both Rich and Poor Conifer Swamp communities [12]. The presence of these species in both communities contributes to the lower UA and PA (Figure 25). Also contributing to the Northern Shrub Thicket's lower UA and PA was the misclassification between it and Emergent Marsh. This is due to the large areas of spatial intermixing of the two communities. Similar observations were made with the classifier difference map (Figure 23), where majority of confusion with the SVM classification was observed in RCS, PCS, and NST natural habitat communities. Areas in red show where differences in the natural habitat communities occur between the MLA. Otherwise the classification results were in agreement.

3.4.3 **Figures and Schemes**

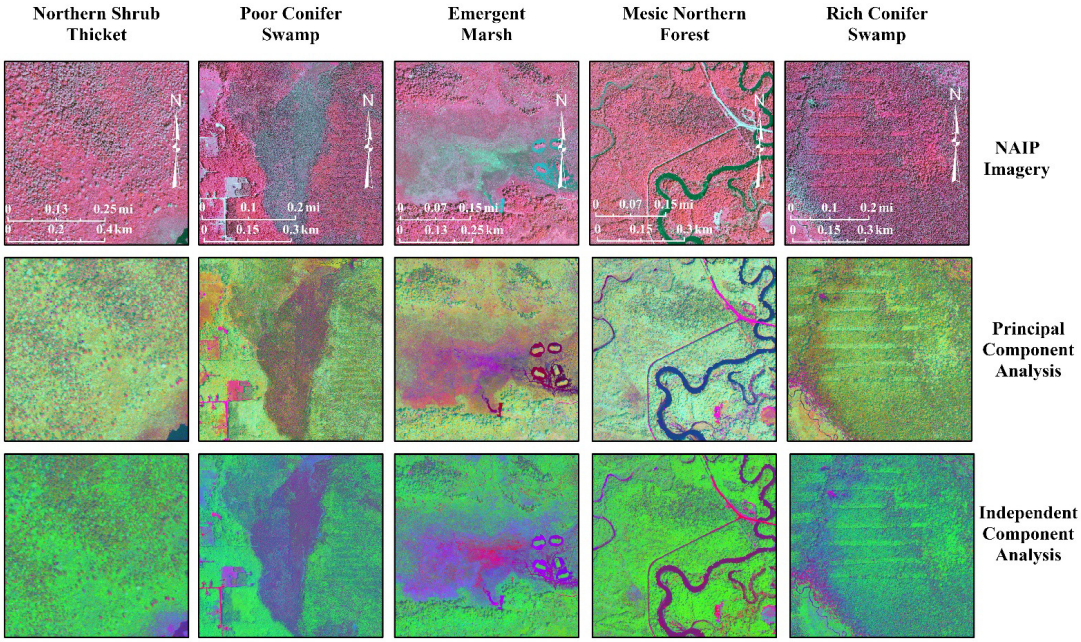

Figure 16. Enhanced natural habitat communities shown using PCA and ICA component combinations (R:3, G:2, B:1) compared to the original NAIP spectral band combinations.

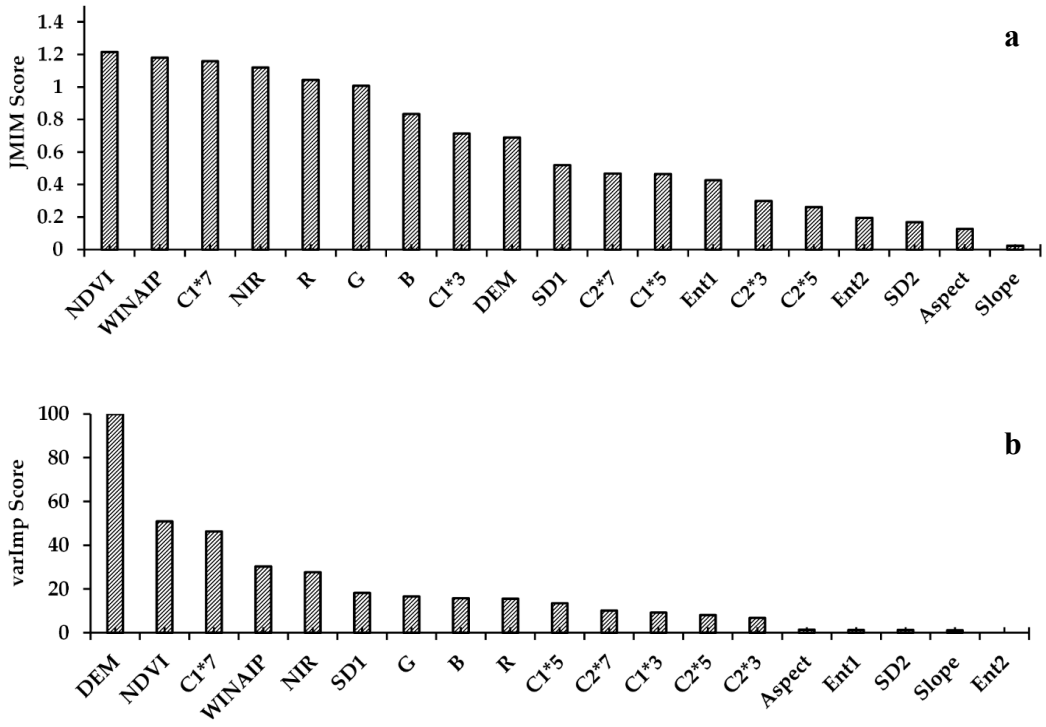

Figure 17. Ancillary data importance scores using (a) JMIM and (b) RF based varImp calculations. R — Red, G — Green, B — Blue, NIR — Near-Infrared, DEM — Digital Elevation Model, Slope, Aspect, C1 — Contrast Texture (PC1, 7×7 moving window), C2 — Contrast Texture (PC2, 7×7 moving window), Ent1*7 — Entropy Texture (PC1, 7×7 moving window), Ent2*7 — Entropy Texture (PC2, 7×7 moving window), SD1*7 — Standard Deviation Texture (PC1, 7×7 moving window), SD2*7 — Standard Deviation Texture (PC2, 7×7 moving window), NDVI — Normalized Difference Vegetation Index, WINAIP — Modified Water Index-NAIP, C1*3 — Contrast Texture (PC1, 3×3 moving window), C2*3 — Contrast Texture (PC2, 3×3 moving window), C1*5 — Contrast Texture (PC1, 5×5 moving window), C2*5 — Contrast Texture (PC2, 5×5 moving window). Note: varImp score for Ent 2 = 0 (no bar).

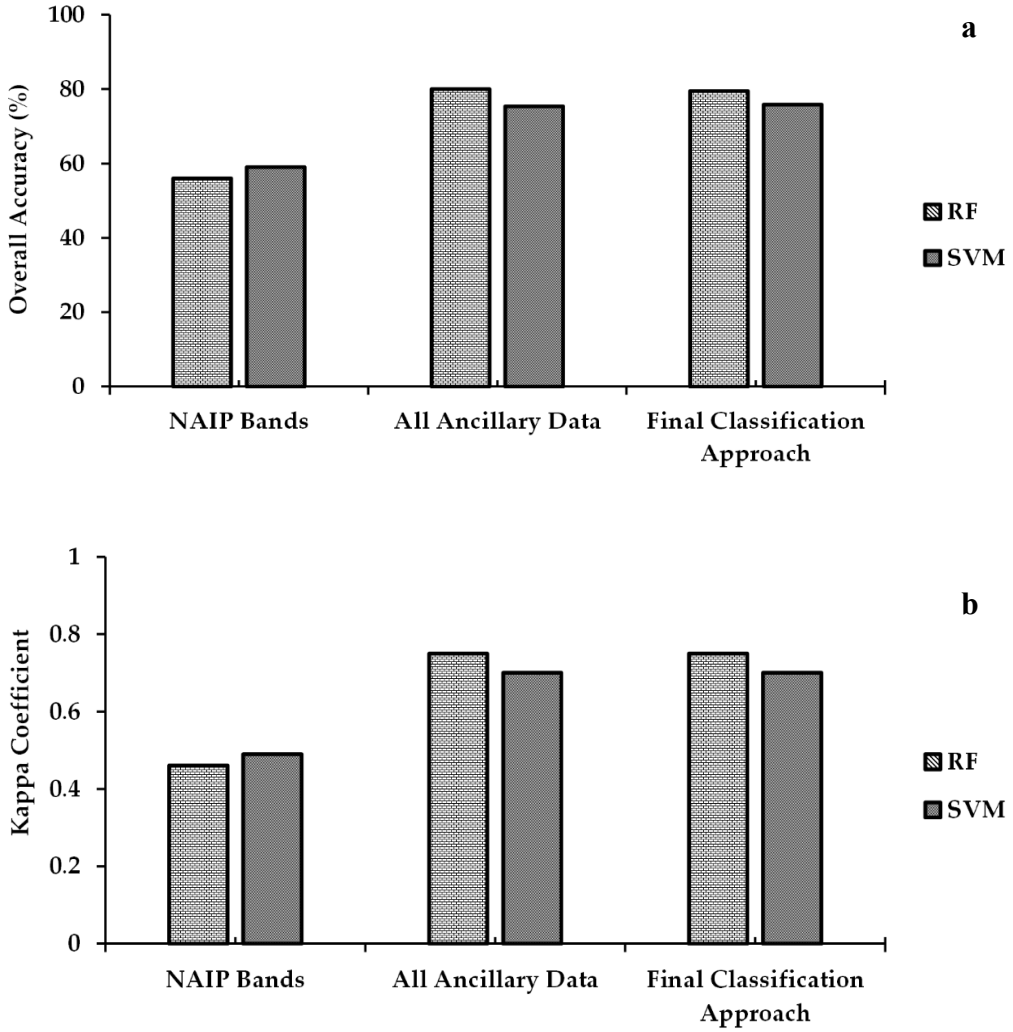

Figure 18. Accuracy Statistics (a) overall accuracy and (b) kappa coefficient of MLAs of different variable combinations (Table 3 - NAIP Bands - Input 1, All Ancillary Data - Input 13, Final Classification Approach - Input 14)

Input Data	Variable Combinations	OA (%) (RF)	k (RF)	OA (%) (SVM)	k (SVM)
1	NAIP bands	56.02	0.46	59.01	0.49
2	NAIP bands + DEM	73.09	0.67	71.21	0.65
3	NAIP + DEM + Asp+ Slp + Tex + NDVI + WINAIP + Tex2 + Tex3	79.96	0.75	75.35	0.70
4	**NAIP + DEM + Tex1 + NDVI + WINAIP (JMIM based optimal input variables)**	**79.45**	**0.75**	**75.85**	**0.70**

Figure 19. Overall accuracy (OA) and kappa coefficient (k) for the input variable combinations. Input 4 (bolded) has the highest OA and k and was used for the final natural communities classification. Abbreviations: Asp — Aspect, Slp — Slope, Tex — GLCM Texture (Contrast, Entropy, Standard Deviation 7×7), Tex1 — Contrast (7×7) Tex2 — Contrast (3×3), Tex3 — Contrast (5×5).

Input Number	Variable Combinations	k (RF)	Z-score (RF)	k (SVM)	Z-score (SVM)	Z-score (Pairwise)	95% CI (RF)	95% CI (SVM)
1	NAIP bands	0.46	2.37	0.49	2.72	-0.34	±1.28	±1.27
2	NAIP bands + DEM	0.67	5.02	0.65	5.09	0.196	±1.15	±1.17
3	NAIP + DEM + Asp + Slp + Tex + NDVI + WINAIP + Tex2+ Tex3	0.75	6.29	0.70	6.13	0.467	±1.02	±1.11
4	**NAIP + DEM + Tex1 + NDVI + WINAIP**	**0.75**	**6.29**	**0.70**	**6.13**	**0.467**	**±1.04**	**±1.10**

Figure 20. Kappa, associated Z-scores and 95% confidence intervals for the input variable combinations. The pairwise Z-Score indi-cates if the classifications from RF and SVM with the same input variables are statistically different. Abbreviations: Asp — Aspect, Slp — Slope, Tex — GLCM Texture (Contrast, Entropy, Standard Deviation 7×7), Tex1 — Contrast (7×7), Tex2 — Contrast (3×3), Tex3 — Contrast (5×5).

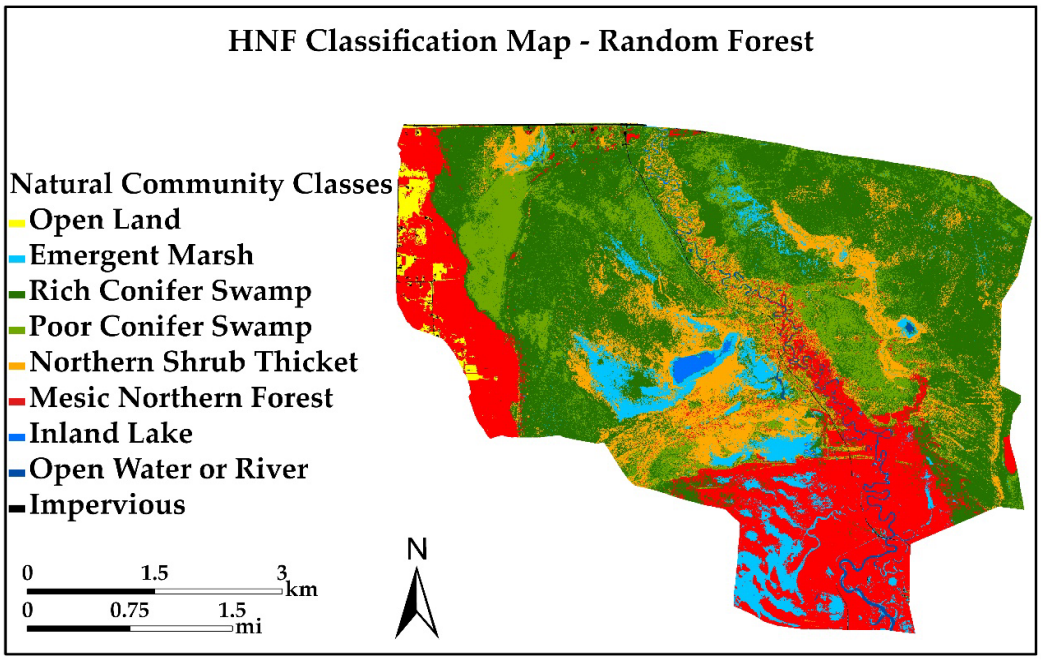

Figure 22. RF classified study area based on the MNFI classification system.

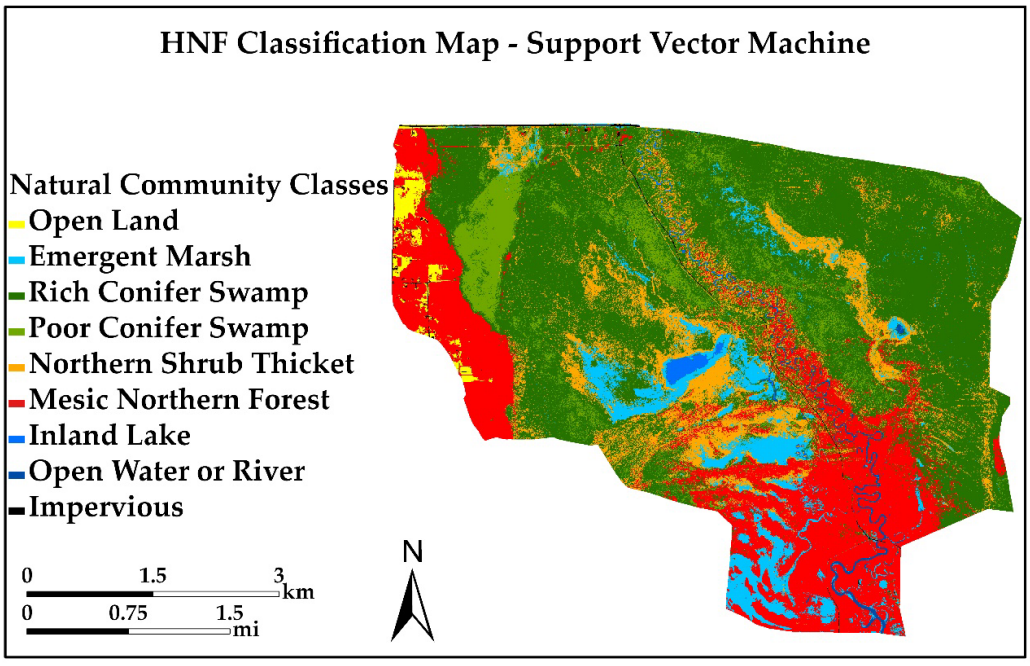

Figure 21. SVM classified study area map based on the MNFI classification system.

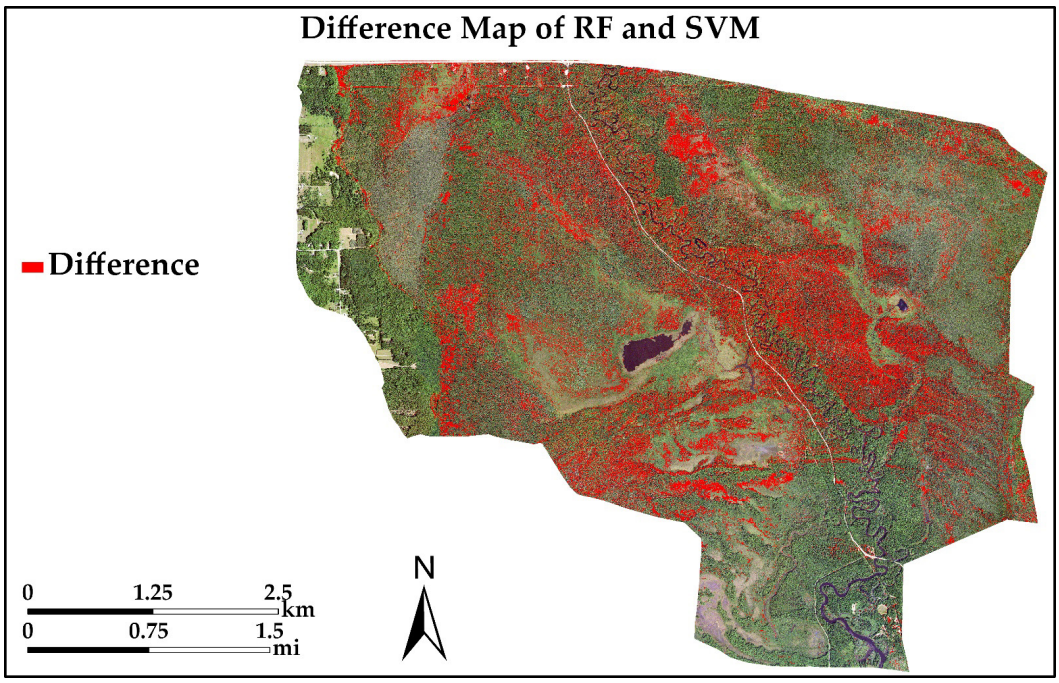

Figure 23. Map showing natural habitat community classification differences between Random Forest and Support Vector Ma-chine. Differences are shown in red whereas no differences are in no color.

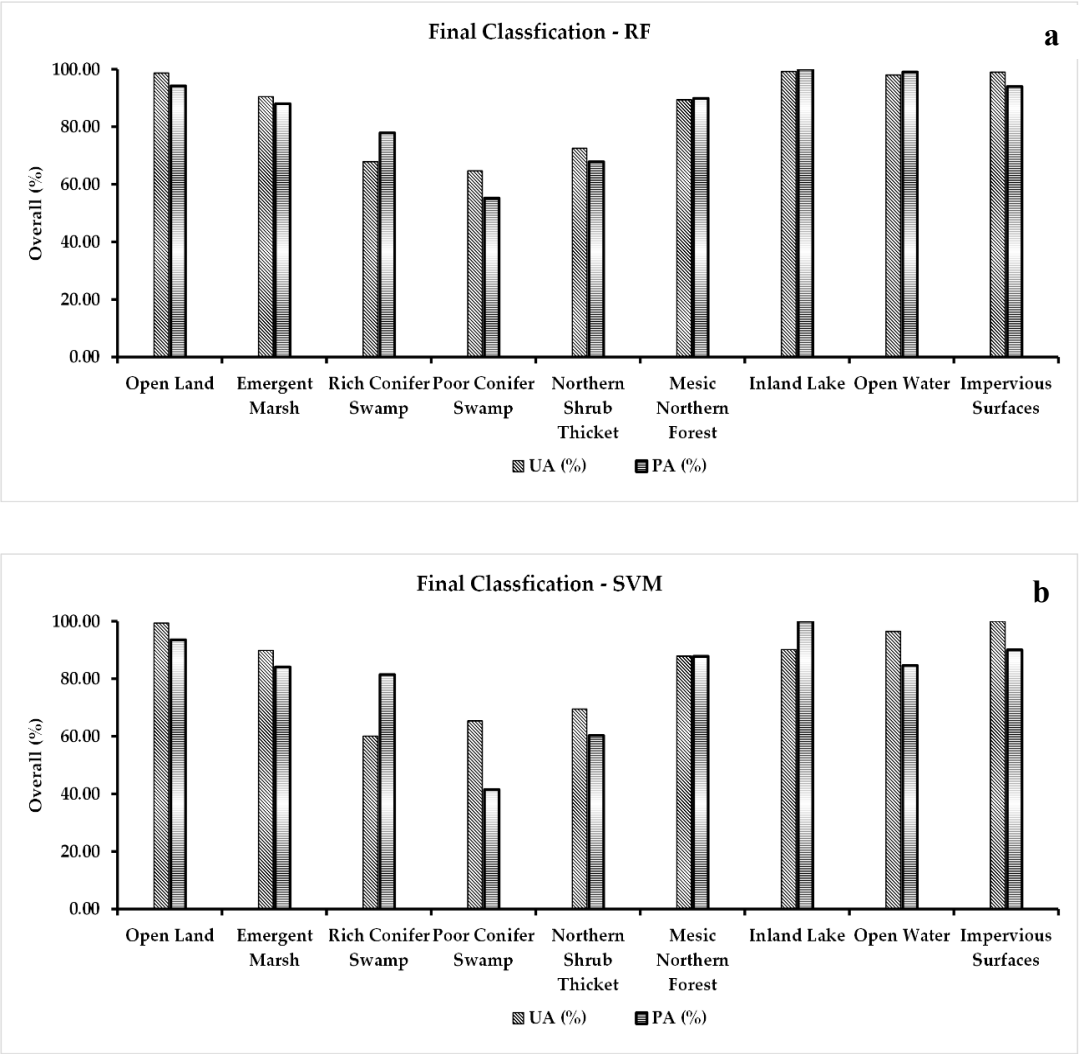

Figure 24. User's and Producer's Accuracy obtained through (a) RF and (b) SVM using final classification approach, NAIP bands, DEM, Texture (Contrast — PC1, PC2) and spectral indices (NDVI, WINAIP).

RF	OL	EM	RCS	PCS	NST	MNF	IL	OW	IS	**Total**	**UA (%)**	**PA (%)**
OL	**146**	0	0	0	0	1	0	0	1	**148**	98.64	94.19
EM	0	**940**	20	8	61	10	0	0	0	**1039**	90.47	88.01
RCS	0	42	**1053**	275	128	53	0	0	1	**1552**	67.85	77.88
PCS	0	10	176	**418**	23	17	0	1	1	**646**	64.70	55.22
NST	0	59	81	37	**592**	47	0	0	0	**816**	72.55	67.81
MNF	9	14	22	19	69	**1142**	0	0	3	**1278**	89.36	89.85
IL	0	1	0	0	0	0	**128**	0	0	**129**	99.22	100.00
OW	0	2	0	0	0	0	0	**96**	0	**98**	97.96	98.97
IS	0	0	0	0	0	1	0	0	**94**	**95**	98.95	94.00
Total	**155**	**1068**	**1352**	**757**	**873**	**1271**	**128**	**97**	**100**	**5801**	**OA = 79.45%, k = 0.75**	

SVM	OL	EM	RCS	PCS	NST	MNF	IL	OW	IS	**Total**	**UA (%)**	**PA (%)**
OL	**145**	0	0	0	0	1	0	0	0	146	99.31	93.55
EM	0	**898**	21	6	66	7	0	0	1	999	89.88	84.08
RCS	0	71	**1101**	371	196	93	0	0	0	1832	60.09	81.43
PCS	0	3	139	**314**	11	11	0	1	1	480	65.41	41.48
NST	0	81	72	35	**526**	43	0	0	0	757	69.48	60.25
MNF	10	12	19	31	74	**1116**	0	0	8	1270	87.87	87.80
IL	0	0	0	0	0	0	**128**	14	0	142	90.14	100.00
OW	0	3	0	0	0	0	0	**82**	0	85	96.47	84.53
IS	0	0	0	0	0	0	0	0	**90**	90	100.00	90.00
Total	**155**	**1068**	**1352**	**757**	**873**	**1271**	**128**	**97**	**100**	**5801**	**OA = 75.85%, k = 0.70**	

Figure 25. Error matrixes and accuracy statistics derived from the final (Input 4) Random Forest and Support Machine vector classifications. RF — Random Forest, SVM — Support Vector Machine; OL — Open Land, EM — Emergent Marsh, RCS — Rich Conifer Swamp, PCS — Poor Conifer Swamp, NST — Northern Shrub Thicket, MNF — Mesic Northern Forest, IL — Inland Lake, OW — Open Water, IS — Impervious Surface; UA — User's Accuracy, PA — Producer's Accuracy, OA — Overall Accuracy, k — Kappa.

3.5 Discussion

3.5.1 Feature Selection and Importance of Ancillary Datasets

Ancillary datasets such as NAIP (National Agriculture Imagery Program) multispectral bands, DEM, aspect, slope, spectral indices, PC1 and PC2 based texture layer were used and selected by implementing feature selection method. The utility of these input datasets was determined and compared for the automated MLAs. The selection of ancillary data was done not only based on the variable importance but on OA and k values as well. Both of the feature selection methods (i.e. JMIM, varImp) proved to be important for seeing differences in ancillary data contribution towards MLAs accuracies (Figure 17 a, b).

The JMIM (Figure 17a) scores are independent of the classification algorithm and are generated prior to running the MLAs. The ranking serves as a guide to the potential contribution of the variables and assists in initial variable selection. This is importance when there are numerous inputs to choose from. By contrast, the varImp (Figure 17b) ranks the importance of input variables for only Random Forest and is generated after the classification is performed. This ranking allows confirmation of input variable importance and validates the original selection of the input variables. The order of variable listing is not expected to be the same given where each is calculated in the workflow. However, the first nine listed variables are closely similar for both feature selection approaches. The approach also confirms the lower contribution of useful information of certain variables such as slope and aspect.

With spectral indices, both NDVI and WINAIP were helpful in improving the accuracies. NDVI was critical for calculating green biomass present in the area and assisted in discriminating Mesic Northern Forest from Northern Shrub Thicket. With WINAIP, even though the NAIP bandwidths are not similar match as the WV-WI bandwidths, initial results showed the modified index contributed to differentiating standing water bodies, emergent marsh, and shadows efficiently. Of the three calculated GLCM texture measures, contrast provided the most useful information for classification. Emergent Marsh, Northern Shrub Thicket and Water had smooth textures hence low mean contrast values; whereas Mesic Northern Forest, Rich and Poor Conifer Swamps had high mean contrast values due to a rough texture. Average mean contrast values in the study area ranged from 0 to 285. To determine the best texture window size and evaluate finer scale changes in texture, 3 different moving window sizes were evaluated (3×3, 5×5 and 7×7) using Contrast. The largest window size (7×7) performed well for entropy and standard deviation (Figure 17 a, b) providing unique information. However, contrast texture outperformed both entropy and standard deviation in differentiating natural habitat communities. Only the first two PCA components were used to generate GLCM-Texture. PCs 1 and 2 explained 96.74% of the variability in the original NAIP data. Feature selection methods (JMIM and varImp) may not necessarily improve accuracy, but they helped reduce the model complexity by allowing selection of variables which contributed the greatest amount of information to the classification.

3.5.2 **MLAs Classifier Performance**

Overall, Random Forest (RF) outperformed Support Vector Machine (SVM), including the classification with the highest Overall Accuracy (OA) and Kappa (k). In comparison to SVM model, RF model was more robust at handling a higher number of ancillary data (Figure 19). Our observation showed that DEM can be considered as important ancillary data in classifying and increasing the model accuracy of the community types. Smallest changes in elevation reflects variation in soil types and drainage patterns which can influence the natural habitat community of the area [40]. The model which was used for the final classification (Input 4), showed a 6.36% increase in OA for RF and 4.64% in SVM, compared to Input 2 where we only used 2 ancillary data layers. Therefore, users who wish to increase the model OA in a similar environmental condition should consider using elevation as ancillary data along with texture and spectral indices. Evaluating the three GLCM textures, contrast proved to be the most useful followed by entropy and standard deviation (Figure 17).

Both RF and SVM showed major confusion between RCS, PCS, and NST classes. RCS and PCS have variety of tree species of similar type which can cause confusion in the classification. NST is another community class which shares similar vegetation types as RCS and PCS, and showed lower UA and PA as well (Figure 24 a, b). Due to the close spectral similarities between these classes, they have a lower UA and PA overall compared to other classes (Figure 24 a, b). Classes with higher spectral dissimilarity showed maximum accuracy (i.e. OL, EM, MNF, IL) and vise-versa. When we look at the overall UA and PA for the community classes, in general RF (Figure 24 a) performed better over SVM (Figure 24b). For example, all five natural habitat community classes

(EM, RCS, PCS, NST, MNF) showed better or close UA and PA as compared to SVM (Figure 24 a, b).

The final classified maps from RF (Figure 21) and SVM (Figure 22) algorithms shows that RF delineated the natural community boundaries better over SVM. Figure 23 shows the classification difference map between RF and SVM. Areas of disagreement are shown in red. Most of the confusion occurs between rich conifer swamp, poor conifer swamp and northern shrub thicket and are responsible for errors of commission and omission in the accuracy assessment matrix (Figure 25). These areas occur along the glacial lake shoreline (west side of study area), in the riparian area of the Sturgeon River (center of study area), on moraines (southeast corner of study area). Areas such as open land, open water, impervious surface and marsh shows agreement across the landscape for both MLAs. Higher confusion was observed in the SVM accuracy assessment matrix resulting in lower PA and UA when compared to RF. It is important to also visually assess the final classifications, not just matrices, to fully understand the MLA performance.

3.5.3 Overall Performance of MLAs with Natural Habitat Communities Classification

The classification results are similar to outcomes of previous studies where RF outperformed SVM model. SVM model tends to work better with smaller number of classes whereas RF can work with larger number of classes [89]. In the past, Rodriguz-Galiano et al. [28, 161] successfully used RF to map and classify 14 classes using Landsat TM and ancillary datasets with high OA. Berhane et al. [40] discriminated 22

wetland classes and achieved the highest OA with using RF with WorldView-2 multispectral data along with various ancillary data. Higher accuracies with RF classifications compared to SVM classifications were also observed by Adam et al. [162] for land-use/cover classification. Hayes et al. [39] used RF classifier to successfully classify 9 landcover classes using NAIP bands and additional ancillary data like spectral indices, elevation data, texture etc. Land cover classification is common in remote sensing community, but this is the first time natural communities of Michigan classification system [12] has been used to classify a complex Laurentian Mixed Forest system at the natural habitat community level.

3.5.4 Importance of Reference Vegetation Map

The color infrared (CIR) combination (R: 4, G: 3, B: 2) of high-resolution multispectral data, and high spectral contrast from the feature extraction techniques (PCA, ICA), helped differentiate natural habitat community types. Ancillary data such as the soils map (soil moisture, pH, drainage as well as prior fieldwork and knowledge of the study site contributed important information. Figure 14 shows the reference natural habitat community map, where nine different classes were delineated, including five community types (Figure 15). The component combination (R:4, G:3, B:2) from PCA and ICA (Figure 16) transformation showed outline boundaries between forest, marsh, swamps, thickets, open land and water groups. Figure 16 shows how the differences in texture from the five natural habitat communities were enhanced and visualized using the PCA and ICA components compared to the original NAIP imagery. This distinction between different natural habitat communities permits more accurate boundary delineation for

better training data as compared with present traditional maps, which are drawn at larger scale having lower spatial resolution (i.e. NWI, NLCD maps). Both RF and SVM models require good training data in order to perform well [89].

3.5.5 Impact of Number of Training Samples and Quality of Sample Data on MLAs

The reference vegetation map was used to generate random training points for the 9 classes within delineated polygons. Data from field validation, expert knowledge and limited very-high spatial resolution UAS dataset [17] for the area provides a reliable and accurate reference map. The total number of training points (i.e. 23,214) were divided into 75% and 25% respectively for the training and testing purpose (Figure 15). Potentially, an increase in the number of training and testing points could achieve higher classification accuracies. For example, this study used a minimum distance of 5 m between the randomly generated points for each community class. If the distance decreased to 3 m, it would allow a greater number of points for training and testing. Researchers have shown in the past that training sample size can play a crucial role in the classification accuracies for supervised machine learning algorithms [89, 136]. Required number of training data also depends on the classification algorithm, number of ancillary data and size and complexity of the study area [136].

3.5.6 Validation of Classified Community Vegetation Map Using Field Data and Expert's Observation

The study area is in a rural remote location where land use and cover changes are minimal. Parts of the study area are protected from exploitation and development. There is limited access which constrains field verification due to lack of roads, a complex network of land ownership, where most private lands cannot be traversed, and many of the natural communities also prohibit ground truthing for safety reasons. Where possible, ground surveys were conducted during the summers of 2018, 2019 and 2020. However, field work in 2020 and 2021 was severely curtailed due to the COVID-19 pandemic. Additional reference data was collected by observations made by an expert interpreter from the NAIP imagery outside of the reference area polygons as well as using United States Forest Service (USFS) stand compartment maps [52]. This was the first time the Laurentian Mixed Forest of the Hiawatha National Forest (HNF) was classified using the natural communities classification system [12], as a result it was not possible to directly compare it to any previously available maps.

3.5.7 **Future Works**

Future research will involve assessing the robustness of this classification approach to other study sites with different natural communities, varying landforms and soil conditions. Consideration will be given to mapping spatially larger areas, such as an entire watershed, as well as looking at smaller areas with limited natural communities such as fens. In Michigan, there are 5 different fen communities [12], and they can exist adjacent to each other. Being able to accurately map natural communities at different scales is important to understand, describe, document and restore natural habitat community diversity.

Consideration must also be given to what classes should be incorporated into the classification for areas influenced by modern anthropogenic distributions such as agriculture, mining and development. Non-natural habitat community classes were added as needed in this study. This is not a robust approach. These classes need to be well defined, mutually exclusive and hierarchical in structure.

3.6 **Conclusions**

Community classification for Laurentian Mixed Forest is challenging due to the complexity of the landscape. In this paper, for the first time, a natural habitat community level classification using an integrated approach of spectral transformation and enhancement techniques, field data, ancillary datasets and MLAs was implemented. Use of feature selection methods such as JMIM and varImp evaluated the utility of a wide variety of ancillary data including elevation, various measures of texture, and vegetation and soil moisture indices and guided the selection of best performing ancillary data. High-spatial resolution data and machine learning algorithms contributed to a successful and accurate classification.

Five complex natural habitat communities and 4 non-natural habitat communities were successfully classified. Due to the spectral limitation of the four NAIP bands, the classification showed confusion between similar natural habitat communities (e.g. Rich Conifer Swamp vs Poor Conifer Swamp vs Northern Shrub Thicket) with accuracies ranging from 72.55% down to 64.70% (Figure 25). Discrimination between Mesic

Northern Forest, Emergent Marsh, Impervious, Open Land, and Water (Open Water and Inland Lake) have higher accuracies (100% to 89.36%) (Figure 25).

RF and SVM both showed promising performance for classifying a complex Laurentian Mixed Forest community. RF outperformed SVM in the final classification results, SVM performed well when the number of ancillary datasets were less. The choice of MLAs may vary for the users depending on the site, type of communities being mapped, number of ancillary datasets and quality of the training data. In R parameter optimization is allowed and can help provide better performance, use of optimization parameters may increase the processing times of the classifiers. In this study we used the default parameters of the classifiers as they were accurate enough and achieved the desired results. We also think using more spectral bands might improve the classification and can help overcome the complexity of the vegetation classes.

Acknowledgments

We would like to thank the College of Forest Resources and Environmental Science for their support. Thanks Ian Anderson (Chief Product Owner) of Hexagon Geospatial for his crucial help at the start of this project, Jim Ozenberger of the Hiawatha National Forest for assistance with field work, and Emily Clegg with the Nature Conservancy providing technical support.

Funding

This research was funded by US Forest Service, Hiawatha National Forest (Grant Number 17-PA-11091000-023), The Nature Conservancy (Grant Number R45984), and the College of Forestry and Environmental Science.

Conflicts of Interest

The authors declare no conflict of interest.

4 Comparison of High-Resolution NAIP and Unmanned Aerial Vehicle (UAV) Imagery for Natural Vegetation Communities Classification Using Machine Learning Approaches

Authors: Parth Bhatt[1,*], Ann L Maclean[1]

[1]College of Forest Resources and Environmental Science, Michigan Technological University, Houghton, MI 49931, USA

(This work is currently under review in the journal of "GIScience & Remote Sensing" under special issue "Remote sensing for sustainable forest and wetland management under climate change", Submission ID: 226232668)

Abstract

To map and manage forest vegetation including wetland communities, remote sensing technology has been shown to be a valid and widely employed technology. In this paper, two ecologically different study areas were evaluated using free and widely available high-resolution multispectral (NAIP) and ultra-high-resolution multispectral unmanned aerial vehicle (UAV) imagery located in the Upper Great Lakes Laurentian Mixed Forest. Three different machine learning algorithms, random forest (RF), support vector machine (SVM) and averaged neural network (avNNet), were evaluated to classify complex natural habitat communities as defined by the Michigan Natural Features Inventory. Accurate training sets were developed using both spectral enhancement and transformation techniques, field collected data, soils data, texture, spectral indices and expert knowledge. The utility of the various ancillary datasets improved classification results significantly. Using the RF classifier, overall accuracies (OA) between 83.8 and 87.7% with kappa (k) values between 0.79 to 0.85 for the NAIP imagery and between 87.3 and 93.7% OA with k

values between 0.83 to 0.92 for the UAV dataset were achieved. Based on the results, we concluded RF to be a robust choice for classifying complex forest vegetation including surrounding wetland communities. The study provides an approach to working with two different imagery datasets using machine learning algorithms to classify spatially and spectrally complex natural community habitats. A discussion of advantages and disadvantages of each dataset is presented.

Keywords

natural community habitats, NAIP, UAV, drone imagery, image classification, land cover classification, machine learning, feature selection, random forest, support vector machine, neural networks, GLCM Texture, PCA, ICA, NDVI, water index

4.1 Introduction

A key goal of forest management is to maintain and preserve the forest's natural biodiversity and protect the pristine landscape [163] by using efficient, affordable science based practices. In order to maintain a balance between biological diversity and societal needs, it is important to have a management plan which can achieve these goals [164]. Within the natural resource community there are many widely available mapping and monitoring techniques used for management, monitoring and conservation planning. Field surveys and aerial photography are traditional techniques for obtaining information about forest conditions, and identifying tree species or habitats, but are expensive, time-consuming and have limitations [165]. Aerial photography and satellite imagery

interpretations provide areal coverage, but are constrained by temporal, spectral and spatial resolutions. Free or low-cost multispectral imagery commonly have spatial resolutions between 10 and 30 m. This information is employed for vegetation monitoring, predicting species abundance in association with environmental changes, and mapping habitats for species distribution modeling [166-169].

Within the remote sensing community, research on forest land use/cover classification using various satellite imagery datasets, piloted aircraft, as well as unmanned aerial vehicle (UAV) data is well documented [36, 39, 85, 170, 171]. Land use/cover classifications have used well defined, non-overlapping categories [4, 79, 172, 173] to classify forests, wetlands, grasslands etc. Natural community habitats have a more broader definition based not only on the canopy, but understory vegetation, soil attributes, and landform [12, 169]. Natural habitats often have the same plant species in more than one community [12], and this increases classification complexity and challenges due to the spectral similarities between them [10, 158]. Overcoming this complexity requires high spatial resolution imagery to provide more detail for improved feature delineation via the use of spectral transformations such as texture.

Along with the high spatial resolution imagery, the accuracy of the classification depends on the classification algorithm and ancillary datasets. Use of Machine Learning (ML) classification approaches has exponentially increased in the last decade [174] and has been used in a variety of environmental and natural resource applications [27, 28, 30, 39, 89, 170]. Ancillary datasets play an equally important role. In the past, researchers have used various environmental and geomorphological variables to improve classification

results [39, 40, 91, 111, 172, 175]. These datasets help overcome the imagery's spectral resolution limitations. It is important to understand the contribution each ancillary dataset provides to improving the classification. Widely available feature selection methods help evaluate the importance of the ancillary datasets [129] as they reduce data complexity [43] and improve computational times [89]. The robustness of the approach used in this study was compared with a previous study done by the authors [38].

The key focus of this research is to explore the usefulness of ultra-high spatial resolution UAV imagery for classifying complex natural community habitats and compare the results to classifications derived from high spatial resolution National Agricultural Imagery Program (NAIP) imagery. Researchers have used NAIP and UAV datasets for delineating and mapping land cover, identifying tree species, delineating wetlands, habitat mapping, and invasive species mapping, [17, 38, 46, 104, 176-178]. However, a direct comparison between the two datasets for natural habitat community classification has not been completed.

4.2 Materials

4.2.1 Study Areas

Upper Midwest forests are classified as Laurentian Mixed Forest (LMF) which is made up of complex geomorphology and vegetation due to the extensive glaciation which occurred over thousands of years. The area is dominated by sandstone and limestone bedrock [17, 92]. The forest falls under IUCN category IV and contains diverse upland

and lowland ecosystems, including extensive pristine coastal forests and wetlands. The area has number of natural community habitats which are rare and vulnerable [12]. Two study sites, Point aux Chenes (PAC) Bay (Figure 26) (HUC12-040301120108) and Carp River Mouth (CRM) (Figure 27) (HUC12-40700020307) [179] were selected because of the combination of rare and vulnerable natural community habitats within relatively small geographic areas. Several of the communities (Interdunal Wetlands, Open Dunes and Wooded Dune and Swale Complex) are considered imperiled within Michigan due to rarity and/or vulnerability due to restricted ranges [12]. The PAC site encompass 420 ha (1,038 ac) and 790 ha (1,952 ac) for CRM. The study areas are located within glacial lake and outwash plain landforms respectively [92]. Current threats to these areas include unauthorized off-road vehicle use, poorly designed or degraded road and stream crossing structures which create physical barriers to hydrologic function, roads that parallel coastlines with inadequate drainage structures, and the presence and/or expansion of non-native invasive species.

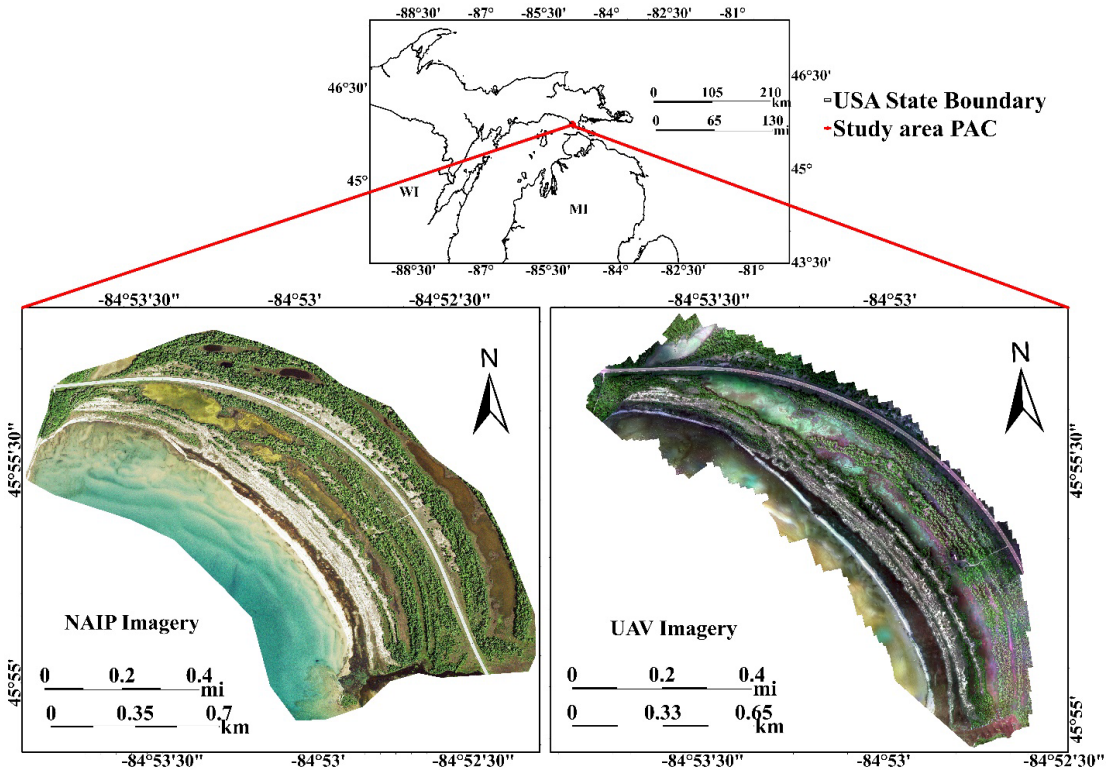

Figure 26. Pointe aux Chenes Bay study area. The shoreline is adjacent to Lake Michigan.

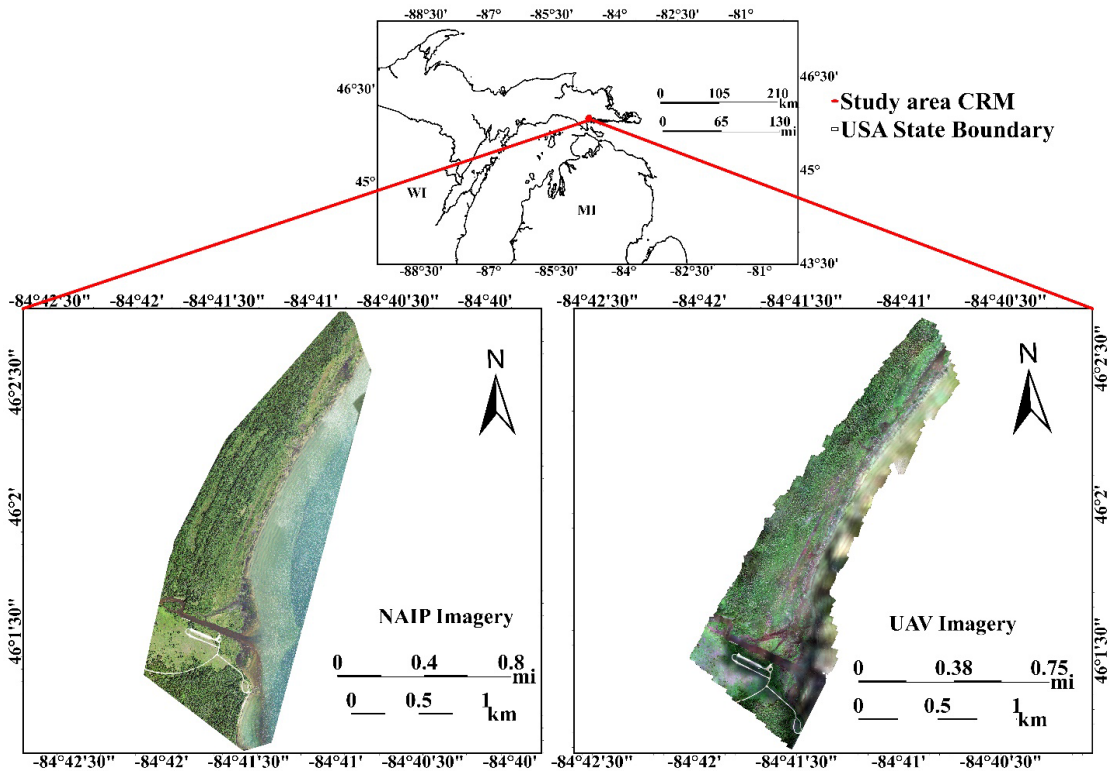

Figure 27. Mouth of the Carp River study area. The shoreline is adjacent to Lake Huron.

4.2.2 **Datasets and Software**

High-resolution multispectral NAIP and ultra-high-resolution UAV imagery were used for the study. NAIP imagery has four bands (Blue (420 - 492 nm), Green (533 - 587 nm), Red (604 - 664 nm) and Near-Infrared (683 - 920 nm)) [180] and was acquired 4,877 m (16,000 feet) above ground level (AGL) with a Leica ADS100 airborne digital sensor. The imagery has 8-bit radiometric resolution with 0.6 m spatial resolution. Imagery tiles dated 11 August 2018 and 6 September 2018 were downloaded from USGS Earth Explorer for Point aux Chenes Bay (PAC) and Carp River Mouth (CRM) respectively.

UAV data were collected in August 2019 using a fixed-wing Trimble UX5-AG aircraft. The UX5-AG has a 1 m wingspan with 2.5 kg weight and is capable of flying up to 45 minutes with a cruise speed of 80 km/h. Imagery with 80% overlap was acquired using a five-band (Blue (475 ± 20 nm), Green (560 ± 20nm), Red (668 ± 20 nm), Red Edge (717 ± 20 nm), and Near-Infrared (840 ± 20 nm)) Micasense camera mounted onboard. Flying height was between 104 and 134 m (341 ft - 440 ft) with a 7 cm spatial resolution for the PAC and 9 cm for the CRM. The spatial resolution varied due to the flying height and differences in terrain geometry. Using the onboard high-accuracy GNSS positioning data, the UAV images were processed and mosaicked with Agisoft Metashape 1.5.3 software using the standard workflow procedure provided by the USFS UAV office [70].

ERDAS IMAGINE (Hexagon Geospatial, 2021) was used to generate Principal Component Analysis (PCA), spectral indices, and Gray- Level Co-Occurrence (GLCM) texture layers for both sets of imagery. Random training points were generated using

ArcPro software. Machine learning algorithms were implemented using the “caret” [45] package within R [99] programming language.

4.3 Methods

Spectral variability and similarity within and between the vegetative components of the natural community habitats created classification challenges and was documented by Bhatt et al. [38]. However, the high spatial resolution NAIP and UAV imagery combined with ML permitted utilization of the variability [104]. All NAIP and UAV spectral bands were utilized for training set generation. An integrated classification approach incorporating ancillary data (image transformation and enhancement techniques), field data, and expert knowledge was developed [11, 12, 40, 91, 101, 102, 181]. Accurately delineated training area polygons were critical for optimal performance of Machine Learning Algorithms (MLAs) [89].

4.3.1 Image Transformation Techniques

Principal Component Analysis (PCA) is commonly used for various classification applications, and is one of the most widely used transformation techniques and generates uncorrelated components [10, 105]. It has been used by natural resource managers to map vegetation, evaluate change detection, and observe vegetation distribution [107-110]. By contrast, ICA uses higher-order statistics and considers each component to be non-Gaussian [113]. The transformation highlights minute details in the imagery even when the feature occupies a small area [114]. However, it has been used minimally to map vegetation communities and for land use/cover classification [115-117]. Components

from both transformations were visually assessed for edge detection within and between the natural habitat communities to generate valid training sets.

4.3.2 **Texture**

Similar spectral signatures occur between the natural habitat communities and increase the difficulty of accurate separation during training set development and classification. However, the communities do display various types of texture traditionally used in manual interpretation. Different texture statistics can detect unique information and spatial patterns for features which are hard to separate using only spectral information [102, 123-125]. In the past, texture-based variables have been incorporated by researchers into species detection, for fine-scale wetlands classification, and in land use land cover classification [19, 40, 161, 182, 183]. GLCM texture measures were calculated from the first and second PCA components and created two uncorrelated texture datasets. For both the NAIP and the UAV imagery, first (55.38 to 67.72%) and second (27.02 to 38.32%) principal components contributed the highest to explaining the data variability [105]. Four GLCM texture measures (contrast, entropy, standard deviation, dissimilarity) were calculated. Contrast measures the local variations present in the image, entropy measures the randomness within the data, standard deviation looks at its frequency of occurrence with reference and neighboring pixel values, and dissimilarity measures the differences in elements of the GLCM from each other [123, 124]. Data were generated with a 32-bit grayscale level and two Euclidean geometry offsets (2, 2 and 2, -2). Window sizes of 3×3, 5×5, 7×7 and 9×9 were evaluated.

4.3.3 Spectral Indices

Spectral indices have been used extensively to map and monitor vegetation [38, 40, 118]. The normalized vegetation index (NDVI) [119] was employed. While two modified water indices based on the WorldView water index (WV-WI) proposed by Wolf [121] were developed. The water index for the NAIP imagery (WINAIP) using its blue and near-IR bands, and a water index for the UAV imagery (WIUAV) using its blue and near-IR bands of the Micasense camera created customized indices.

4.3.4 Evaluation of Ancillary Datasets

When classifying natural community habitats, inputting multispectral imagery alone was not adequate to accurately classify the data. With manual interpretations ancillary data such as soils maps are traditionally used for improved boundary delineation and vegetation classification. It made sense to provide the ML classifiers with this type of information as well. DEMs, Grey Level Co-Occurrence Matrix (GLCM) textures (contrast, entropy, standard deviation, dissimilarity) and spectral indices (NDVI, WINAIP, WIUAV) were calculated. The next step was to understand each ancillary dataset's contribution to classification improvement as using all of them does not guarantee the best result. Ancillary input dataset selection approaches have been used in many remote sensing applications (i.e., data mining, natural language processing, bioinformatics, image processing, and mineral mapping) [111, 128, 129], but have not been extensively used in natural resource classification [38]. Input data selection (also known as variable or feature selection) approaches are fast, cost-effective, and provide

insight into the contribution of each ancillary dataset [129]. For this study, joint mutual information maximization (JMIM) [44], a filter-based method, was used.

4.3.5 **Training Set Development**

Training polygons, from which the ML training points are selected, were manually drawn with careful consideration given to vegetation community species, soil drainage classes and pH, elevation and landform, information highlighted in the PCA and ICA components, ground truth data, and expert knowledge of the areas. Eight natural community habitat classes and three non-community habitat classes were identified (Figure 28).

Multiple training sets created with randomly selected training points were developed across the study sites to capture spectral and spatial variability. More training polygons (812 for UAV vs 136 for NAIP) were needed to classify the UAV imagery because the higher spatial resolution provided greater detail. Manual delineation of training polygons for the NAIP and UAV imagery was selected based on its successful use in previous research [38].

4.3.6 **Image Classification**

In a recent study completed by Bhatt et al. [38] with NAIP imagery, RF was shown to be a better classifier for natural community habitats compared to SVM. Along with RF and SVM, another ML algorithm, averaged neural network (avNNet) from the caret [45] package was tested. These classifiers have been extensively used for land-use/land-cover

classifications [39, 40, 136, 169, 184-187]. Within the training polygons 75% of the randomly selected training points were used to develop the training sets. The remaining 25% were reserved for accuracy assessment and a 10-fold cross validation to avoid overfitting issues [155]. Default training parameters were accepted for each classifier, and "center" and "scale" were implemented to standardize the ancillary datasets [45, 147]. Classifications were executed using the "caret" package [45] in the "R" programming language [99]. Results for the three classifiers were compared using Overall Accuracy (OA) and kappa coefficient (k) [11]. Individual communities were evaluated employing User's Accuracy (UA) and Producer's Accuracy (PA) [11]. Between 10 and 15 ground truth observations were made for each natural habitat community class during field visits to each study site.

	Natural community	Common trees, plants, shrubs
1	Emergent Marsh (EM)	Sedges, musk grasses, common reed, common waterweed, coontail, waterlily (Cohen et al. 2014)
2	Submergent Marsh (SM)	Musk grasses, common waterweed, coontail, waterlily, pond-lilies (Cohen et al. 2014)
3	Great Lakes Marsh (GLM)	Broad-leaved cat-tail, waterlily, pond-lilies, coontail, duckweed, sedges, reed grass, tag alder, green ash, paper birch (Cohen et al. 2014)
4	Northern Shrub Thicket (NST)	Sedges, grasses, ferns, tag alder, bog birch, dogwoods, winterberry, willows, black ash, tamarack, black spruce, white pine, northern white-cedar (Cohen et al. 2014)
5	Interdunal Wetlands (IW)	Sedges, rush, willow, tamarack, jack pine, northern white-cedar (Cohen et al. 2014)
6	Rich Conifer Swamp (RCS)	Northern white-cedar, white pine, tamarack, spruce, red maple, black ash, tag alder, balsam fir, birch (Cohen et al. 2014)
7	Wooded Dune & Swale Complex (WDSC)	Pines, oaks, red maple, balsam fir, sedges, rush, ferns, tag alder, willows, black spruce, black ash, tamarack, northern white-cedar, aspen (Cohen et al. 2014)
8	Sand & Gravel Beach (SGB)	Marram grass, Baltic rush, willow, pitcher's thistle, sea rocket (Cohen et al. 2014)
9	Open Water (OW)	Lake Michigan, Lake Huron, inland lakes, rivers and ponds
10	Open Land (OL)	Open land areas including agriculture and quarries
11	Impervious Surfaces (IS)	Roads, houses, cars, other manmade structures

Figure 28. Natural community habitats and associated vegetation components. Communities 9-11 were developed for land uses not natural community habitats.

4.3.7 **Accuracy Assessment and Post-classification Refinement**

Accuracy assessment was completed using the reserved test points plus independently collected field points. These are referred to as validation points. Evaluations were completed by comparing classification values against the validation points [11]. Using the resulting accuracy assessment matrices, UA and PA values were calculated for each habitat class.

"Salt and pepper" effects [158] were smoothed to create a more easily interpreted final classification map. A majority filter using a 7×7 moving window was run based in previous research [107].

4.4 Results and Discussion

Pixel based image classifications were run using RF, SVM, and avNNet with RF producing the best classifications for all combinations of imagery and ancillary data inputs. Figures 3 and 4 show the classification results for both types of imagery at each study site. The figures show zoomed-in snippets highlighting various mapped details. Visual assessment of the classifications showed the UAV classifications delineated finer detailed boundaries for each community. This is due in part to the finer spatial resolution when compared to the boundaries derived from the NAIP imagery. The NAIP imagery also presented a more generalized natural community habitat map with less "salt-and-pepper" artifacts [158] from the per pixel classification.

However, other factors besides spatial resolution contributed to boundary detail and location including radiometric and geometric preprocessing. The UAV imagery was preprocessed and mosaicked using Metashape. The resulting mosaic has areas of uneven lighting and specular reflectance, blurriness, and shadowing due to UAV pitch, roll and yaw caused by varying wind direction and speed as well as flying height variability. The NAIP imagery was preprocessed by the contractor and was acquired by a heavier aircraft, hence a more stable platform with a consistent flying height. Figures 5 and 6 highlight

some of the image variability of the UAV imagery caused by the UAV platform and environment factors, noted above, when compared to the NAIP imagery.

Texture was also a contributing factor to the detailed boundary variation. The natural habitat communities at both study sites exhibited significant amounts of local variation [123].The finer spatial resolution of the UAV imagery emphasizes the high degree of texture created within and between the natural communities. Each community exhibits distinctive patterns and shapes such as the well-defined ridge and valley complex associated with the Wooded Dune and Swale Complex. Contrast, using a 7×7 window size, was the most informative texture component when evaluated against entropy, standard deviation and dissimilarity using JMIM feature selection (Figure 7). Low contrast values were observed with smooth texture classes such as Open Water, Open Land and Impervious Surface. Highly textured community classes (i.e., Wooded Dune and Swale Complex, Rich Conifer Swamp, Northern Shrub Thicket) have a rougher texture represented by higher contrast values as illustrated in Figure 5. The red arrow points to a gray textured area in the UAV imagery which is Princess Pine (*Dendrolycopodium obscurum*) an endangered club moss and indicates a very small, but important, area of Wooded Dune Swale Complex. It is not visible on the NAIP imagery; rather the entire area is classified as Interdunal Wetland and does not provide the detail required to manage and protect this at-risk species.

Along with texture, other ancillary data sets were evaluated using JMIM feature selection. These included DEMs, NDVIs, and a modified water indexes specific to the NAIP and UAV imagery. The water index for each set of imagery differed due to the

NAIP having 4 spectral bands (B, G, R, near-IR) while the UAV has 5 bands (B, G, R, red edge and near-IR). JMIM scores were calculated for all of the spectral bands as well (Figure 7). At both study sites, the most important input features with the NAIP imagery were all of the NAIP spectral bands, NDVI, WINAIP, DEM and contrast textures (Figure 7). For the UAV data, the five Micasense spectral bands, followed by NDVI, WIUAV, DEM, and contrast textures (Figure 7) showed high importance.

Both NDVI and WINAIP, two of the highest JMIM scores, helped accurately delineate the community habitat classes. Classes such as WDSC, RCS, and NST showed higher values with NDVI compared to the rest of the habitat community classes. Incorporation of the DEM, NDVI, WINAIP, Contrast 1 and 2 increased the OA of the natural community classifications an average of 13.59% for NAIP and 18.22% for the UAV, when compared to only using the four spectral bands of NAIP and the five spectral bands of UAV (Figures 35 and 36). Overall, the UAV based classification outperformed the NAIP classification, due to the high-spatial resolution of the UAV, greater texture, and the additional red-edge band. It is important to remember JMIM based selection values do not guarantee more accurate classification, but the numbers provide quantitative guidance to input variable selection.

As noted, the PAC NAIP classification (Figure 3) was more generalized and contributed to Wooded Dune & Swale Complex and Emergent Marsh overprediction when compared to field observations. The UAV classification delineated the natural communities well except for Emergent Marsh, Interdunal Wetlands and Great Lakes Marsh. This confusion is due to the same vegetation components and water being found in all of them (Table 1);

hence spectral similarities between them. These communities are smaller in size and intermixed with more commonly occurring, larger area, communities and therefore have fewer validation points. Fewer points mean misclassifications have a greater impact on UA and PA and were lower compared to the other classes (natural communities) (Appendix A).

The PAC NAIP based classification achieved OAs between 86.28% and 88.33% using all input variables with RF. When the highest contributing variables based on the JMIM scores were used, the OAs ranged between 85.28% and 87.74%. Reducing the input variables from 15 to 9 did not significantly affect the OAs and kappa (k) (Table 2). However, using only the 4 NAIP bands accuracies decreased significantly and ranged from 72.49% to 77.15% (Table 2). This illustrates the important contribution made by the ancillary data (variables). The final classification had an OA of 87.74% and a k of 0.85. Similar results occurred with the PAC UAV imagery. Using all 16 available inputs with the UAV imagery, the OA was slightly lower (Table 3) compared to inputting the 10 JMIM selected inputs. Once again, using just the five UAV reflectance bands decreased OA between 5 and 8% with all three classifiers (Table 3). The final UAV imagery classification using RF achieved an OA of 93.74% and 0.92 k. Overall, the UAV classifications provided better end products than the NAIP classifications by a 6% increase in OA (0.7 k) using RF (Table 3).

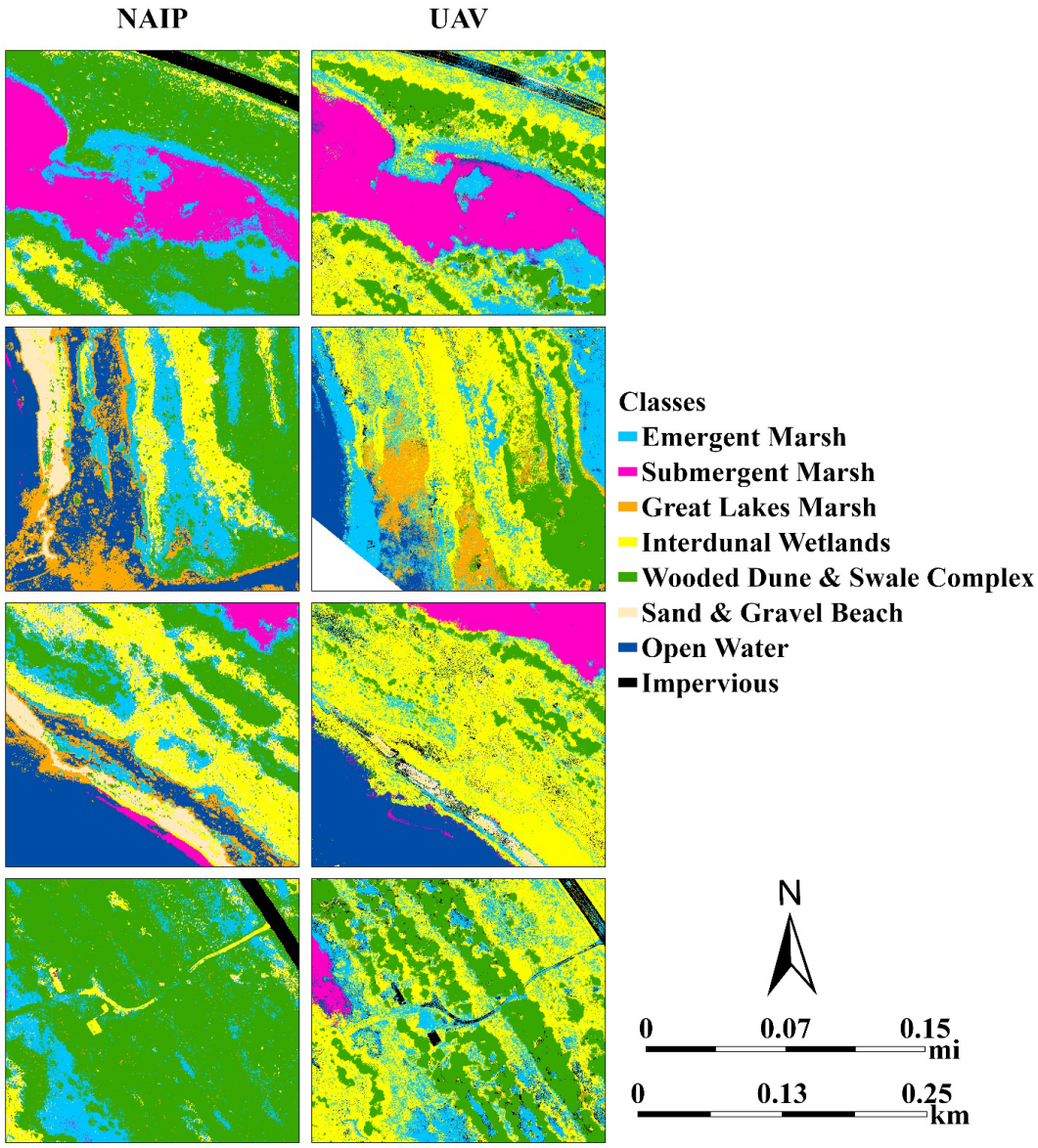

Figure 29. Selected areas of the PAC classification delineated by the RF classifier.

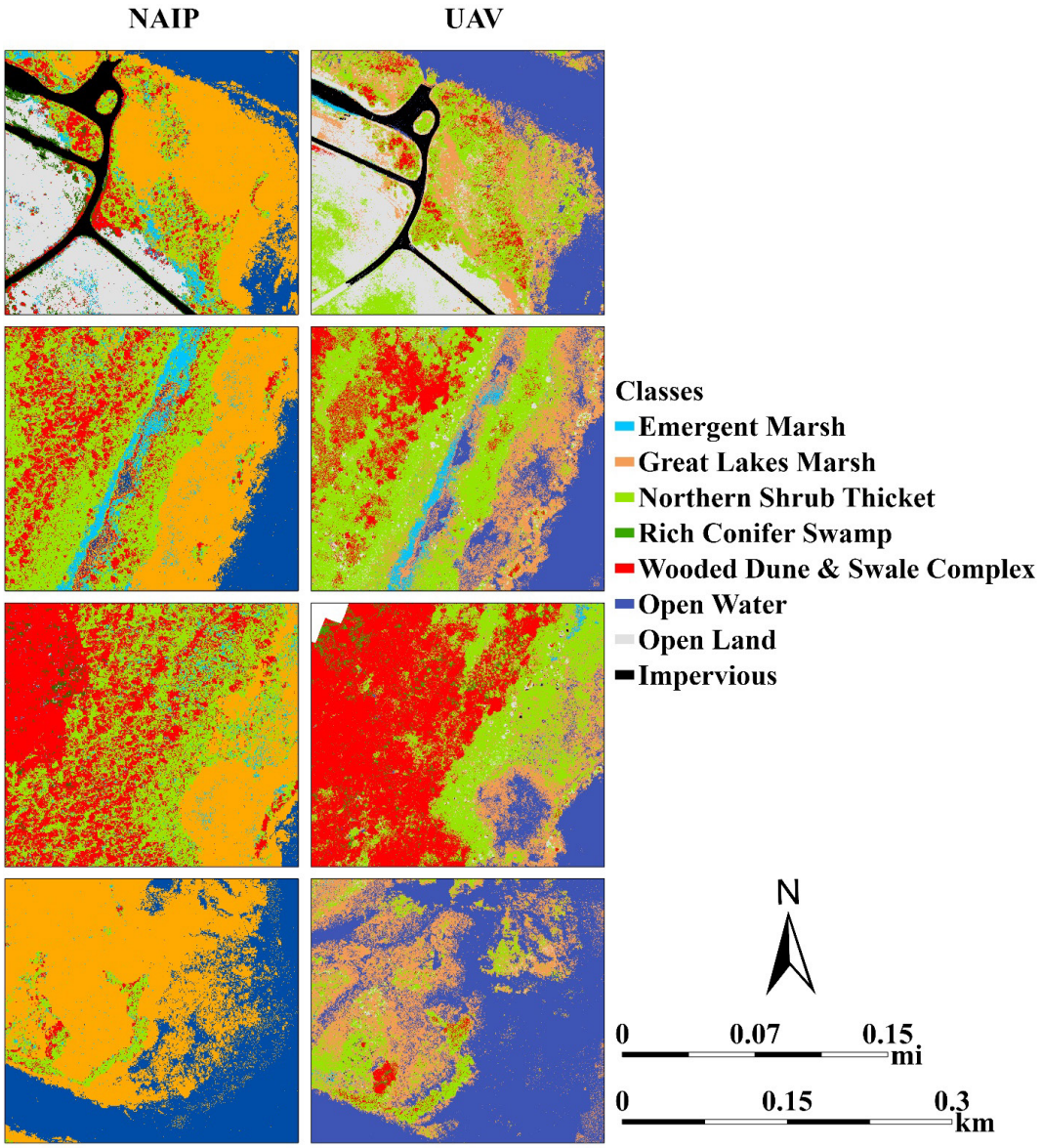

Figure 30. Selected areas of the CRM study site delineated by the RF classifier.

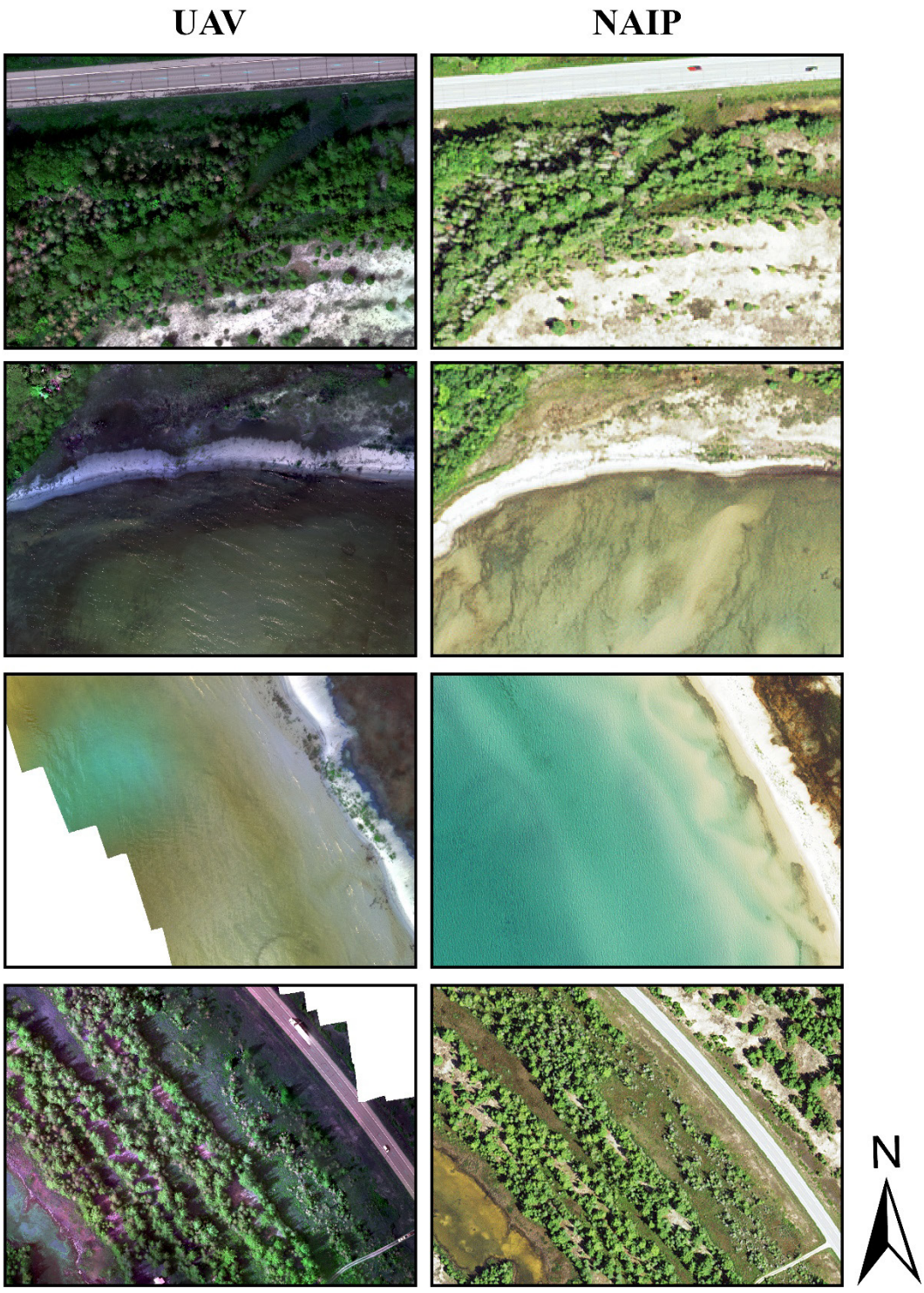

Figure 31. Spectral reflectance differences between UAV and NAIP imagery for PAC for the blue, green and red bands.

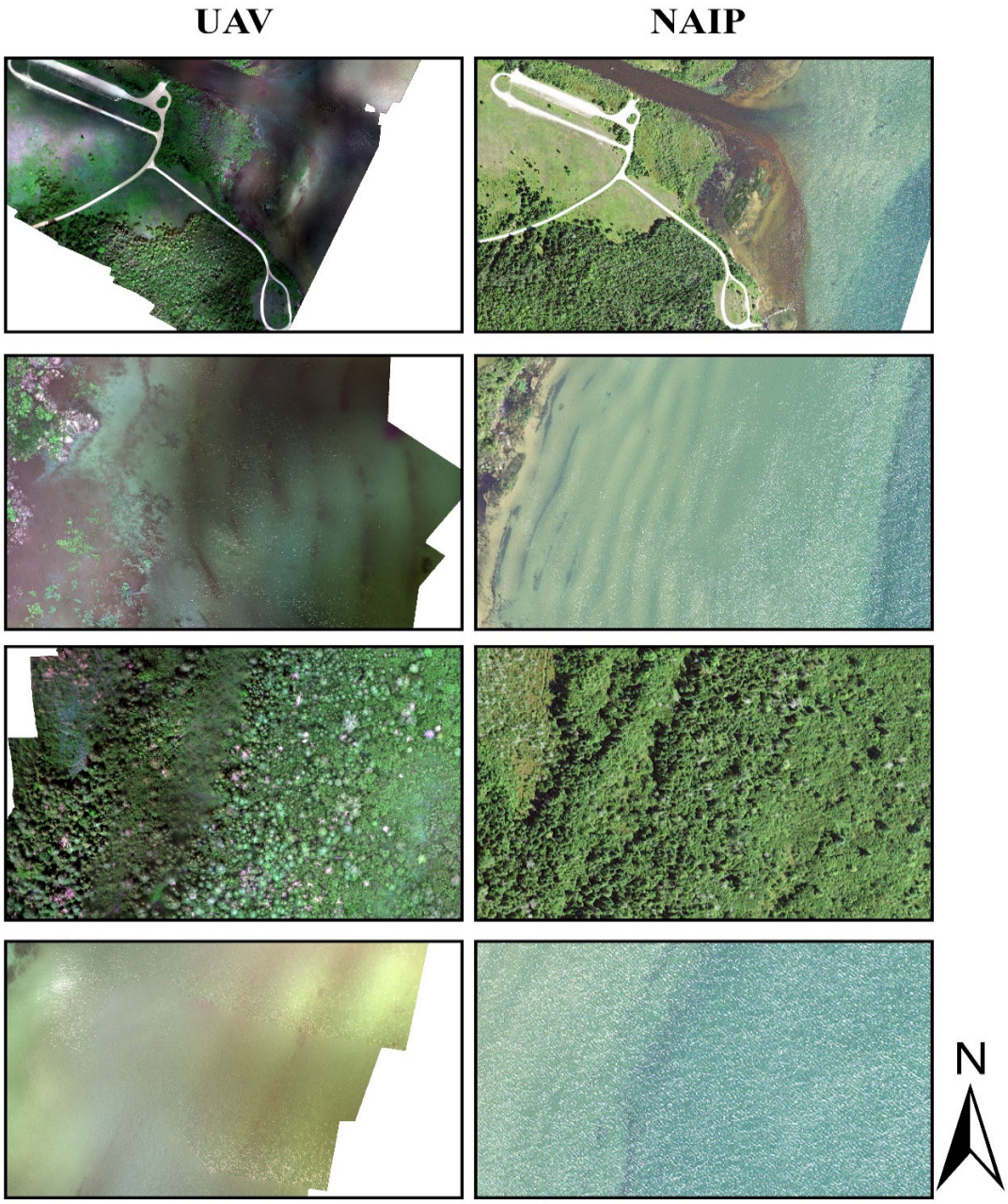

Figure 32. Spectral reflectance differences between UAV and NAIP imagery for CRM for the blue, green and red bands.

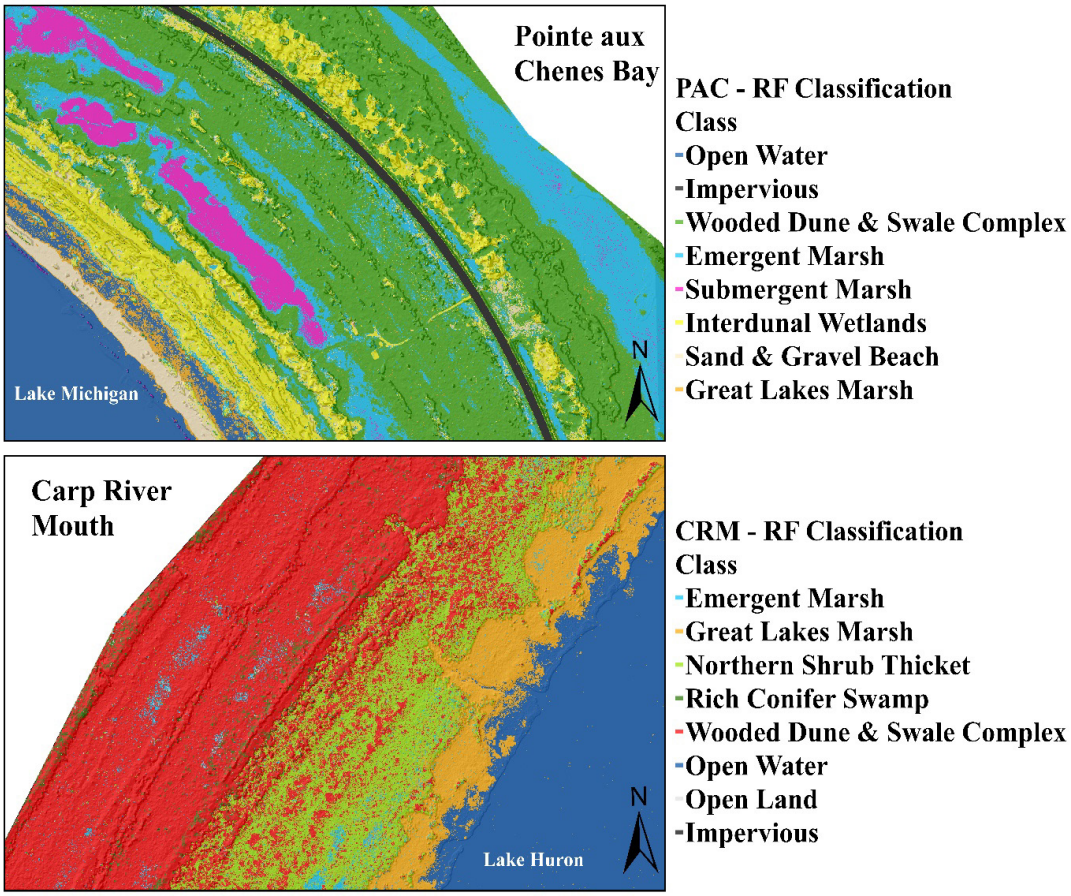

Figure 33. Landforms influence on vegetation for the PAC and CRM study sites draped over a Multi-Directional Oblique Weighted (MDOW) hillshade.

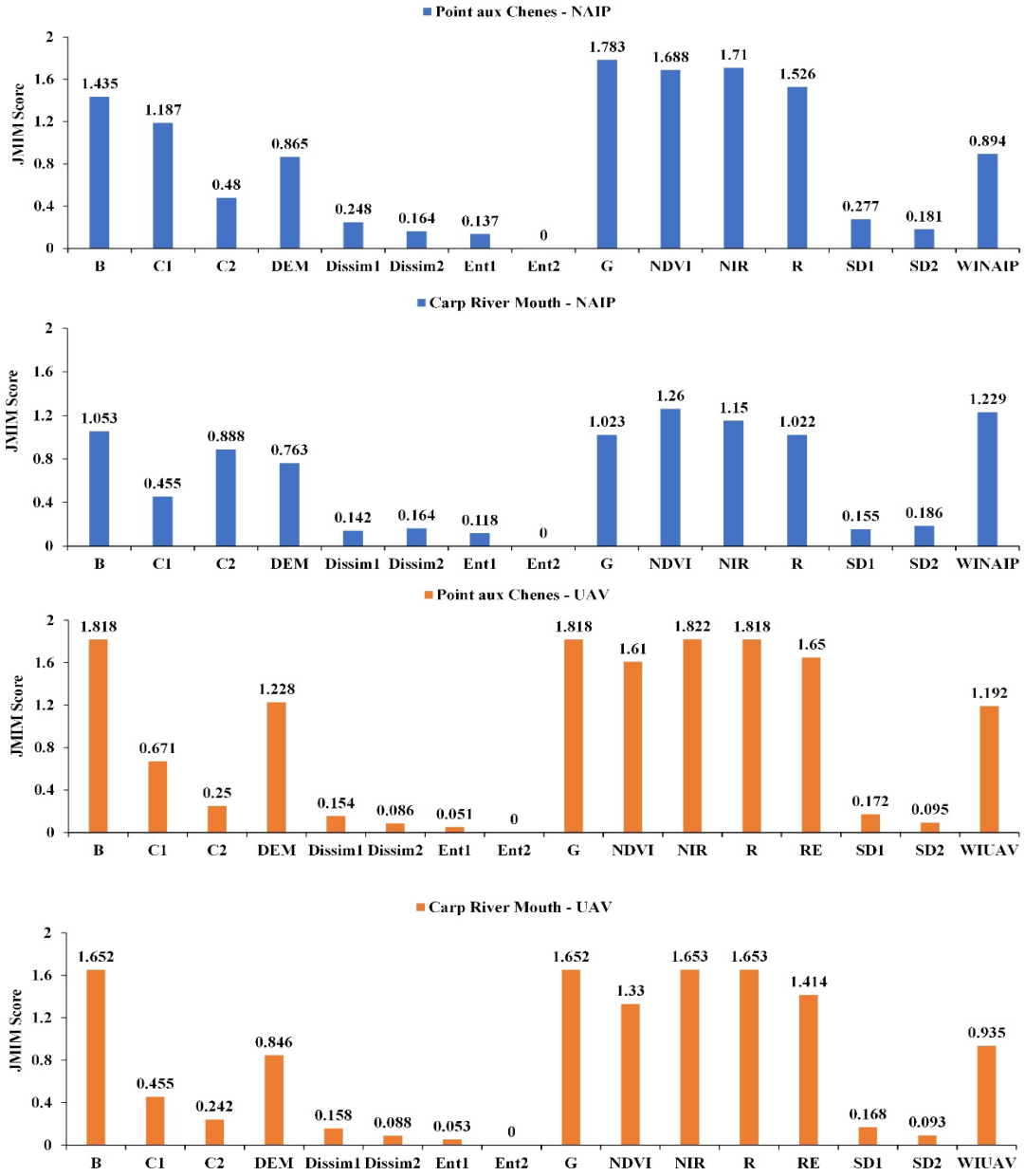

Figure 34. Ancillary dataset (variable) importance scores using JMIM feature selection method. R-red, G-green, B-blue, NIR-near-infrared, RE-red edge, DEM-digital elevation model, C1-contrast texture (PC1, 7×7 moving window), C2-contrast texture (PC2, 7×7), Ent1- entropy texture (PC1, 7×7), Ent2-entropy texture (PC2, 7×7), SD1-standard deviation texture (PC1, 7×7), SD2-standard deviation texture (PC2, 7×7), Dissim1-Dissimilarity texture (PC1, 7×7), Dissim2-Dissimilarity texture (PC2, 7×7), NDVI-normalized difference vegetation index, WINAIP- NAIP modified water index, WIUAV-UAV modified water index.

Ancillary Data/Variables (NAIP)	Classifier	PAC OA (%)	k	CRM-OA (%)	k
R, G, B, NIR	RF	77.15	0.72	67.26	0.57
	SVM	75.33	0.69	65.50	0.55
	avNNet	72.49	0.65	65.11	0.53
NAIP + DEM + GLCM-Texture (7×7) - PC 1, 2 (Contrast, Entropy, Standard Deviation, Dissimilarity) + NDVI + WINAIP	RF	88.33	0.86	84.80	0.80
	SVM	87.04	0.84	83.57	0.79
	avNNet	86.28	0.83	80.95	0.75
Final Classification - NAIP + DEM + GLCM-Texture (7×7) - PC 1, 2 (Contrast) + NDVI + WINAIP	**RF**	**87.74**	**0.85**	**83.85**	**0.79**
	SVM	86.13	0.83	83.06	0.78
	avNNet	85.28	0.81	79.60	0.74

Figure 35. Accuracy assessments for the NAIP classifications at PAC and CRM.

Ancillary data/Variables (UAV)	Classifier	PAC - OA (%)	k	CRM - OA (%)	k
R, G, B, Red Edge, NIR	RF	87.06	0.83	75.51	0.67
	SVM	86	0.82	75.34	0.66
	avNNet	78.80	0.73	70.04	0.58
UAV (R, G, B, RE, NIR) + DEM + GLCM-Texture (7×7) - PC 1, 2 (Contrast, Entropy, Standard Deviation, Dissimilarity) + NDVI + WIUAV	RF	93.02	0.91	86.77	0.82
	SVM	89.13	0.87	84.46	0.80
	avNNet	85.14	0.81	80.52	0.73
Final Classification - UAV (R, G, B, RE, NIR) + DEM + GLCM-Texture (7×7) - PC 1, 2 (Contrast) + NDVI + WIUAV	**RF**	**93.74**	**0.92**	**87.31**	**0.83**
	SVM	91.07	0.89	86.16	0.81
	avNNet	85.09	0.81	81.13	0.74
UAV (R, G, B, NIR) + DEM + GLCM-Texture (7×7) - PC 1, 2 (Contrast) + NDVI + WIUAV (without red edge)	RF	93.39	0.92	86.70	0.82
	SVM	90.56	0.88	86.14	0.81
	avNNet	84.22	0.80	80.78	0.74

Figure 36. Accuracy assessments for the UAV classifications at PAC and CRM.

The NAIP and UAV classifications for the CRM study site achieved higher accuracies with RF compared to SVM and avNNet. Final NAIP classification OA was 83.85% with 0.79 k (Figure 35). The UAV OA and k were 87.31% and 0.83 respectively (Table 3). Both classifications performed best using JMIM scores to select input variables compared to using all available data (Figures 35 and 36). Using only the NAIP spectral bands decreased the OA by 16% (Figure 35), and with the UAV the accuracy decreased 11.8% (Figure 36). These results are similar to those seen with the PAC study site and the work completed by Bhatt et al. [38]. They indicate the robustness of the classification approach across different landforms. Considering landform, the CRM is more complex compared to PAC (Figure 8). CRM is an eroded Dune and Swale complex, while the PAC is made up of narrowly separated dunes and swales [179].

The confusion matrix for NAIP CRM classification (Appendix A) shows both lower UAs and PAs for EM, NST and RCS. The matrix shows confusion for EM and NST occurring across all habitats, which is an indication that improved training sets with less variability (smaller standard deviations) are needed. The misclassification of the RCS is primarily with Wooded Dune & Swale Complex. This confusion is the result of a high percentage of same species in both natural communities including northern white cedar, tamarack, white pine and tag alder (Table 1). Landform is also a strong indicator for Wooded Dune & Swale Complex (Figure 8). However, if the swales are widely spaced between the dunes, the texture changes and contributes to the error particularly with the coarser NAIP spatial resolution (Figure 8). The UAV classification shows lower UAs and PAs for Great Lakes Marsh, Northern Shrub Thicket and Rich Conifer Swamp. Again, the poor classification of Great Lakes Marsh and Northern Shrub Thicket are due to high

variability in the training sets. The same error seen in NAIP classification between RCS and Wooded Dune & Swale Complex continues here.

JMIM scores range between 0 and 2 regardless of the measurement units of the input variables. This allows direct comparison between the variables in ascertaining the unique contribution each input makes to the classification. Plots of the JMIM scores (Figure 7) show the input variables (ancillary data) maintain the same pattern of importance for the two sets of imagery across both study sites. The same results were seen with work completed by Bhatt et al. [38]. The spectral bands and the NDVI, which is derived from the spectral bands, have the highest scores; followed by texture, water index and the DEM.

4.5 Conclusions

Based on the results from this study and from Bhatt et al. [38], RF is recommended as a classifier of choice when working with ecologically complex natural community habitats. SVM and avNNet always produced classifications with lower accuracies. It can be argued that tuning the RF parameters could improve the classifications. However, parameter tuning is time consuming and not cost effective given the acceptable accuracies for natural community habitat delineation and identification. Categorizing the k values into 3 groups, good ($k < 0.80$) [188, 189], strong (k 0.80 - 0.90) and almost perfect ($k > 0.90$) [190] for the classifications shows strong to almost perfect relationships between “truth” and the classifications (Figures 35 and 36). This further supports the use of RF. This pixel-based machine learning classification approach

coupled with high and ultra-high spatial resolution imagery, spectral transformation and enhancement techniques, field data, soils data, and various ancillary datasets proved to be efficient and robust for classifying complex vegetation and wetland communities in a Laurentian Mixed Forest (LMF) in the Upper Midwest.

Most studies classifying land use/cover are for specific resource management purposes and categorize the imagery into narrowly defined, non-overlapping classes. However, classifying imagery into well defined, robust natural community habitats provides a holistic approach to resource management and is more representative of the variability of actual field conditions. Until recently there were no natural community habitat classification studies of the complex Laurentian Mixed Forest in the Upper Great Lakes. Inventorying, monitoring and preserving these pristine habitats, particularly along coastlines is increasingly important given the impacts of climate change. Field-based monitoring alone is not able to complete these tasks in a timely, cost-effective manner.

Which imagery is best for natural community habitat classification is unclear. For areal coverage, NAIP is more comprehensive as it is acquired by aircraft flying at a constant speed and altitude. It undergoes rigorous radiometric and geometric corrections, and mosaics are easy to create. Plus, the data is free. However, the temporal resolution is not ideal, especially for catastrophic events such as fires and flooding as well as phenological timed events. UAV imagery offers advantages for these types of studies as the platform can be airborne in a short time frame and is ideal for data collection over small geographic areas which are accessible [46]. However, accessibility becomes a problem due to Federal Aviation Administration (FAA) regulations requiring the drone be keep in

line of sight at all times and in locating take-off and landing sites, especially for fixed wing UAVs. Though this limitation can potentially be overcome by using a rotary-wing UAV instead of a fixed wing [49].

Performing radiometric and geometric corrections on the UAV imagery was time consuming. Current processing software has its limitations both in photogrammetric robustness and ease of use. The physical size of the UAV imagery is also an important consideration, and adequate computing resources and storage space are prerequisites. Processing times also need to considered. It took 88 hours to preprocess the imagery and generate the final orthomosaics for the study areas.

In the future studies, it is recommended to test the efficacy of the red edge band and derived indices, and compare them to traditional indices like NDVI. Red edge indices have been used in the past with Sentinel-2A, Rapid-Eye, WorldView-2, and UAV imagery to observe vegetation phenology, spatial variability of crop growth, leaf area index, and burn severity assessments [191-195]. It was beyond the scope of this study to complete that. If future technology permits UAV data to be collected in the mid-IR, its utility should also be investigated.

A Appendix A

RF (NAIP - PAC)	EM	SM	GLM	IW	WDSC	SGB	OW	IS	**UA (%)**	**PA (%)**
EM	**518**	11	0	13	21	20	1	0	88.7	89.0
SM	11	**329**	0	0	0	0	0	0	96.7	96.7
GLM	0	0	**101**	0	4	2	11	0	85.6	60.1
IW	2	0	0	**285**	29	87	0	1	70.5	85.0
WDSC	46	0	44	17	**941**	20	0	0	88.1	94.1
SGB	5	0	1	20	5	**223**	0	0	87.8	63.3
OW	0	0	22	0	0	0	**292**	0	93.0	96.0
IS	0	0	0	0	0	0	0	**124**	100.0	99.2
OA = 87.74%, k = 0.85										

RF (UAV - PAC)	EM	SM	GLM	IW	WDSC	SGB	OW	IS	**UA (%)**	**PA (%)**
EM	**467**	1	11	25	2	1	4	24	87.2	86.1
SM	1	**223**	0	3	0	0	3	0	96.9	96.9
GLM	0	**0**	**28**	1	4	0	1	1	80	53.8
IW	52	1	2	**465**	7	2	3	9	85.9	89.7
WDSC	1	0	4	4	**673**	0	0	1	98.5	97.5
SGB	3	0	0	4	0	**117**	0	2	92.8	95.9
OW	5	5	3	5	1	0	**1137**	0	98.3	98.7
IS	13	0	4	11	3	2	3	**366**	91.0	90.8
OA = 93.74%, k = 0.92										

Figure 37. NAIP and UAV classification accuracy assessment matrices for PAC. EM - Emergent Marsh, SM - Submergent Marsh, GLM - Great Lakes Marsh, IW - Interdunal Wetlands, WDSC - Wooded Dune & Swale Complex, SGB - Sand & Gravel Beach, OW - Open Water, IS - Impervious Surface.

RF (NAIP - CRM)	EM	GLM	NST	RCS	WDSC	OW	OL	IS	**UA(%)**	**PA(%)**
EM	**175**	23	48	3	23	0	6	0	62.9	53.3
GLM	29	**1192**	39	0	2	3	1	0	94.1	89.5
NST	31	83	**404**	9	157	0	0	1	58.9	61.4
RCS	3	0	4	**95**	42	0	0	0	65.9	42.6
WDSC	87	26	162	108	**1494**	0	2	0	79.5	86.7
OW	0	7	0	0	0	**897**	0	0	99.2	99.6
OL	3	0	1	8	4	0	**283**	0	94.6	96.9
IS	0	0	0	0	0	0	0	**119**	100.0	99.1
OA = 83.58%, k = 0.79										

RF (UAV - CRM)	EM	GLM	NST	RCS	WDSC	OW	OL	IS	**UA(%)**	**PA(%)**
EM	**206**	13	9	0	0	2	3	1	88.0	85.5
GLM	21	**544**	122	1	9	42	19	0	71.8	65.8
NST	8	164	**875**	10	121	0	36	1	72.0	74.5
RCS	0	0	1	**44**	22	0	0	0	65.6	35.5
WDSC	0	3	121	69	**871**	0	1	0	81.8	85.1
OW	4	78	5	0	0	**3255**	0	2	97.3	98.6
OL	1	23	41	0	0	1	**615**	1	90.1	91.2
IS	1	2	1	0	0	1	0	**119**	95.9	95.9
OA = 87.31%, k = 0.83										

Figure 38. NAIP and UAV classification accuracy assessment matrices for the CRM. EM - Emergent Marsh, GLM - Great Lakes Marsh, NST – Northern Shrub Thicket, RCS – Rich Conifer Swamp, WDSC - Wooded Dune & Swale Complex, OW - Open Water, OL Open Land, IS - Impervious Surface.

Acknowledgements

We would like to thank the College of Forest Resources and Environmental Science, Michigan Technological University for their support. We also thank Ian Anderson (Chief Product Owner) of Hexagon Geospatial for his crucial help at the beginning of this project, Jim Ozenberger of the Hiawatha National Forest for assistance with field work and Emily Clegg of The Nature Conservancy for providing technical support. We would like to acknowledge Dr. Curtis Edson and Ben Miller who helped in UAV flight planning and data collection.

Funding

This research was funded by the US Forest Service, Hiawatha National Forest (Grant Number 17-PA-11091000-023), The Nature Conservancy (Grant Number R45984) and the College of Forest Resources and Environmental Science.

Reference List

1. Lincoln, R., G. Boxshall, and P. Clark, *A dictionary of ecology, evolution and systematics. â Cambridge University Press, Cambridge*. 1982, England.
2. King, A.W., *Considerations of scale and hierarchy.* Ecological integrity and the management of ecosystems, 1993: p. 19-45.
3. Jensen, M.E., C.H. McNicoll, and M. Prather, *Application of ecological classification to environmental effects analysis.* Journal of Environmental Quality, 1991. **20**(1): p. 24-30.
4. Bailey, R.G., *Ecosystem geography: from ecoregions to sites*. 2009: Springer Science & Business Media.
5. Bailey, R., et al., *Design and use of ecological mapping units.* Ecosystem management: Principles and applications, 1994. **2**: p. 95-106.
6. Bailey, R., *Ecoregions of the United States (map).* Ogden, UT: US Department of Agriculture, US Forest Service, Intermountain Region, 1976.
7. Barnes, B.V., *The landscape ecosystem approach and conservation of endangered spaces.* Endangered Species Update, 1993. **10**(3&4): p. 13-19.
8. Rowe, J.S. and B.V. Barnes, *Geo-ecosystems and bio-ecosystems.* Bulletin of the Ecological Society of America, 1994. **75**(1): p. 40-41.
9. Cowardin, L.M., et al., *Classification of wetlands and deepwater habitats of the United States*. 1979, US Department of the Interior, US Fish and Wildlife Service.
10. Jensen, J.R., *Introductory digital image processing: a remote sensing perspective*. 2015: Prentice Hall Press.
11. Congalton, R.G. and K. Green, *Assessing the Accuracy of Remotely Sensed Data : Principles and Practices, Third Edition*. 2019, Milton: Chapman and Hall/CRC.
12. Cohen, J.G., et al., *A field guide to the natural communities of Michigan*. 2014: Michigan State University Press.
13. Chapman, K.A., *Michigan natural community types.* Michigan Natural Features Inventory, Ohio Dept of Natural Resources, 1986.
14. Kost, M.A., et al., *Natural communities of Michigan: classification and description.* Michigan Natural Features Inventory, 2007. **21**(1).
15. By Earth Resources Observation and Science (EROS) Center, U. *USGS EROS Archive - Aerial Photography - National Agriculture Imagery Program (NAIP)* 2018 [cited 2022 May 21]; Available from: https://www.usgs.gov/centers/eros/science/usgs-eros-archive-aerial-photography-national-agriculture-imagery-program-naip?qt-science_center_objects=0#qt-science_center_objects.
16. Samiappan, S., et al., *Using unmanned aerial vehicles for high-resolution remote sensing to map invasive Phragmites australis in coastal wetlands.* International Journal of Remote Sensing, 2016. **38**(8-10): p. 2199-2217.
17. Bhatt, P., *Mapping Coastal Wetland and Phragmites on the Hiawatha National Forest Using Unmanned Aerial System (UAS) Imagery: Proof of Concepts*. 2018, Michigan Technological University.

18. Husson, E., O. Hagner, and F. Ecke, *Unmanned aircraft systems help to map aquatic vegetation.* Applied Vegetation Science, 2014. **17**(3): p. 567-577.
19. Feng, Q., J. Liu, and J. Gong, *UAV Remote Sensing for Urban Vegetation Mapping Using Random Forest and Texture Analysis.* Remote Sensing, 2015. **7**(1): p. 1074-1094.
20. National Land Imaging Program, U. *UAS Supports Science*. 2020 [cited 2022 May, 21]; Available from: https://www.usgs.gov/programs/national-land-imaging-program/science/uas-supports-science.
21. Lee, K. and R. Lunetta, *Wetland and environmental application of GIS.* 1996, Lewis Publishers, New York.
22. Silva, T.S., et al., *Remote sensing of aquatic vegetation: theory and applications.* Environ Monit Assess, 2008. **140**(1-3): p. 131-45.
23. Hubert-Moy, L., et al., *A comparison of parametric classification procedures of remotely sensed data applied on different landscape units.* Remote Sensing of Environment, 2001. **75**(2): p. 174-187.
24. Al-Doski, J., S.B. Mansorl, and H.Z.M. Shafri, *Image classification in remote sensing.* Department of Civil Engineering, Faculty of Engineering, University Putra, Malaysia, 2013. **3**(10).
25. Lu, D. and Q. Weng, *A survey of image classification methods and techniques for improving classification performance.* International journal of Remote sensing, 2007. **28**(5): p. 823-870.
26. Belgiu, M. and L. Drăguţ, *Random forest in remote sensing: A review of applications and future directions.* ISPRS Journal of Photogrammetry and Remote Sensing, 2016. **114**: p. 24-31.
27. Pal, M. and P.M. Mather, *An assessment of the effectiveness of decision tree methods for land cover classification.* Remote Sensing of Environment, 2003. **86**(4): p. 554-565.
28. Rodriguez-Galiano, V.F., et al., *An assessment of the effectiveness of a random forest classifier for land-cover classification.* ISPRS Journal of Photogrammetry and Remote Sensing, 2012. **67**: p. 93-104.
29. Kulkarni, A.D. and B. Lowe, *Random forest algorithm for land cover classification.* 2016.
30. Mountrakis, G., J. Im, and C. Ogole, *Support vector machines in remote sensing: A review.* ISPRS Journal of Photogrammetry and Remote Sensing, 2011. **66**(3): p. 247-259.
31. Pal, M., *Random forest classifier for remote sensing classification.* International Journal of Remote Sensing, 2005. **26**(1): p. 217-222.
32. Ghimire, B., et al., *An evaluation of bagging, boosting, and random forests for land-cover classification in Cape Cod, Massachusetts, USA.* GIScience & Remote Sensing, 2012. **49**(5): p. 623-643.
33. Hansen, M., R. Dubayah, and R. DeFries, *Classification trees: an alternative to traditional land cover classifiers.* International journal of remote sensing, 1996. **17**(5): p. 1075-1081.
34. Friedl, M.A. and C.E. Brodley, *Decision tree classification of land cover from remotely sensed data.* Remote sensing of environment, 1997. **61**(3): p. 399-409.

35. Rogan, J., et al., *Land-cover change monitoring with classification trees using Landsat TM and ancillary data.* Photogrammetric Engineering & Remote Sensing, 2003. **69**(7): p. 793-804.
36. Homer, C., et al., *Development of a 2001 national land-cover database for the United States.* Photogrammetric Engineering & Remote Sensing, 2004. **70**(7): p. 829-840.
37. Xie, Y., A. Zhang, and W. Welsh, *Mapping Wetlands and <I>Phragmites</I> Using Publically Available Remotely Sensed Images.* Photogrammetric Engineering & Remote Sensing, 2015. **81**(1): p. 69-78.
38. Bhatt, P., et al., *Fine-Scale Mapping of Natural Ecological Communities Using Machine Learning Approaches.* Remote Sensing, 2022. **14**(3): p. 563.
39. Hayes, M.M., S.N. Miller, and M.A. Murphy, *High-resolution landcover classification using Random Forest.* Remote sensing letters, 2014. **5**(2): p. 112-121.
40. Berhane, T.M., et al., *Decision-Tree, Rule-Based, and Random Forest Classification of High-Resolution Multispectral Imagery for Wetland Mapping and Inventory.* Remote Sens (Basel), 2018. **10**(4): p. 580.
41. Szantoi, Z., et al., *Analyzing fine-scale wetland composition using high resolution imagery and texture features.* International Journal of Applied Earth Observation and Geoinformation, 2013. **23**: p. 204-212.
42. Álvarez-Martínez, J.M., et al., *Modelling the area of occupancy of habitat types with remote sensing.* Methods in Ecology and Evolution, 2018. **9**(3): p. 580-593.
43. Hughes, G., *On the mean accuracy of statistical pattern recognizers.* IEEE transactions on information theory, 1968. **14**(1): p. 55-63.
44. Bennasar, M., Y. Hicks, and R. Setchi, *Feature selection using Joint Mutual Information Maximisation.* Expert Systems with Applications, 2015. **42**(22): p. 8520-8532.
45. Kuhn, M., et al., *Package 'caret'.* The R Journal, 2020.
46. Bhatt, P., C. Edson, and A. Maclean, *Image Processing in Dense Forest Areas using Unmanned Aerial System (UAS).* 2022.
47. Rango, A., et al., *Unmanned aerial vehicle-based remote sensing for rangeland assessment, monitoring, and management*. Vol. 3. 2009: SPIE. 1-15, 15.
48. Watts, A.C., V.G. Ambrosia, and E.A. Hinkley, *Unmanned Aircraft Systems in Remote Sensing and Scientific Research: Classification and Considerations of Use.* Remote Sensing, 2012. **4**(6): p. 1671-1692.
49. Colomina, I. and P. Molina, *Unmanned aerial systems for photogrammetry and remote sensing: A review.* ISPRS Journal of Photogrammetry and Remote Sensing, 2014. **92**: p. 79-97.
50. Gini, R., et al., *Use of Unmanned Aerial Systems for multispectral survey and tree classification: a test in a park area of northern Italy.* European Journal of Remote Sensing, 2017. **47**(1): p. 251-269.
51. Bendig, J., et al., *Estimating Biomass of Barley Using Crop Surface Models (CSMs) Derived from UAV-Based RGB Imaging.* Remote Sensing, 2014. **6**(11): p. 10395-10412.

52. Thamm, F.P., et al., *SONGBIRD – AN INNOVATIVE UAS COMBINING THE ADVANTAGES OF FIXED WING AND MULTI ROTOR UAS.* ISPRS - International Archives of the Photogrammetry, Remote Sensing and Spatial Information Sciences, 2015. **XL-1/W4**: p. 345-349.
53. Cai, G., J. Dias, and L. Seneviratne, *A survey of small-scale unmanned aerial vehicles: Recent advances and future development trends.* Unmanned Systems, 2014. **2**(02): p. 175-199.
54. Boon, M.A., A.P. Drijfhout, and S. Tesfamichael, *Comparison of a Fixed-Wing and Multi-Rotor Uav for Environmental Mapping Applications: A Case Study.* ISPRS - International Archives of the Photogrammetry, Remote Sensing and Spatial Information Sciences, 2017. **XLII-2/W6**: p. 47-54.
55. Husson, E., et al., *Unmanned aircraft systems help to map aquatic vegetation.* Applied Vegetation Science, 2014. **17**(3): p. 567-577.
56. Goodbody, T.R.H., et al., *Unmanned aerial systems for precision forest inventory purposes: A review and case study.* The Forestry Chronicle, 2017. **93**(01): p. 71-81.
57. Torresan, C., et al., *Forestry applications of UAVs in Europe: a review.* International Journal of Remote Sensing, 2016. **38**(8-10): p. 2427-2447.
58. Dunford, R., et al., *Potential and constraints of Unmanned Aerial Vehicle technology for the characterization of Mediterranean riparian forest.* International Journal of Remote Sensing, 2009. **30**(19): p. 4915-4935.
59. Dandois, J.P. and E.C. Ellis, *High spatial resolution three-dimensional mapping of vegetation spectral dynamics using computer vision.* Remote Sensing of Environment, 2013. **136**: p. 259-276.
60. Getzin, S., K. Wiegand, and I. Schöning, *Assessing biodiversity in forests using very high-resolution images and unmanned aerial vehicles.* Methods in Ecology and Evolution, 2012. **3**(2): p. 397-404.
61. Koh, L.P. and S.A. Wich, *Dawn of Drone Ecology: Low-Cost Autonomous Aerial Vehicles for Conservation.* Tropical Conservation Science, 2012. **5**(2): p. 121-132.
62. Carbonneau, P.E. and J.T. Dietrich, *Cost-effective non-metric photogrammetry from consumer-grade sUAS: implications for direct georeferencing of structure from motion photogrammetry.* Earth Surface Processes and Landforms, 2017. **42**(3): p. 473-486.
63. Chiang, K.W., M.L. Tsai, and C.H. Chu, *The development of an UAV borne direct georeferenced photogrammetric platform for Ground Control Point free applications.* Sensors (Basel), 2012. **12**(7): p. 9161-80.
64. Turner, D., A. Lucieer, and L. Wallace, *Direct Georeferencing of Ultrahigh-Resolution UAV Imagery.* IEEE Transactions on Geoscience and Remote Sensing, 2014. **52**(5): p. 2738-2745.
65. Eling, C., et al., *Development and Evaluation of a Uav Based Mapping System for Remote Sensing and Surveying Applications.* ISPRS - International Archives of the Photogrammetry, Remote Sensing and Spatial Information Sciences, 2015. **XL-1/W4**: p. 233-239.

66. Mian, O., et al., *Direct Georeferencing on Small Unmanned Aerial Platforms for Improved Reliability and Accuracy of Mapping without the Need for Ground Control Points.* ISPRS - International Archives of the Photogrammetry, Remote Sensing and Spatial Information Sciences, 2015. **XL-1/W4**: p. 397-402.
67. Gabrlik, P., *The use of direct georeferencing in aerial photogrammetry with micro UAV.* IFAC-PapersOnLine, 2015. **48**(4): p. 380-385.
68. Samiappan, S., et al., *Mapping of invasive phragmites (common reed) in Gulf of Mexico coastal wetlands using multispectral imagery and small unmanned aerial systems.* International Journal of Remote Sensing, 2016. **38**(8-10): p. 2861-2882.
69. US Forest Service, U.F.S. *Land Areas Report (LAR): Table 4 – Areas by State*. 2015 [cited 2019 16 February, 2019]; Available from: https://www.fs.fed.us/land/staff/lar/LAR2015/lar2015index.html.
70. Sloan, J.L., *National Unmanned Aircraft Systems Project Office: U.S. Geological Survey, Agisoft PhotoScan Workflow*. 2017, USGS.
71. Wolf, P.R., B.A. Dewitt, and B.E. Wilkinson, *Elements of Photogrammetry with Applications in GIS*. 2014: McGraw-Hill Education.
72. Agisoft, L. *Metashape User Manual: Professional Edition, Version 1.8.* 2022 [cited 2022 May, 2022]; Available from: https://www.agisoft.com/downloads/user-manuals/.
73. Kim, S.J. and M. Pollefeys, *Robust radiometric calibration and vignetting correction.* IEEE Trans Pattern Anal Mach Intell, 2008. **30**(4): p. 562-76.
74. Kelcey, J. and A. Lucieer, *Sensor Correction of a 6-Band Multispectral Imaging Sensor for UAV Remote Sensing.* Remote Sensing, 2012. **4**(5): p. 1462-1493.
75. Dandois, J., M. Olano, and E. Ellis, *Optimal Altitude, Overlap, and Weather Conditions for Computer Vision UAV Estimates of Forest Structure.* Remote Sensing, 2015. **7**(10): p. 13895-13920.
76. Seifert, E., et al., *Influence of Drone Altitude, Image Overlap, and Optical Sensor Resolution on Multi-View Reconstruction of Forest Images.* Remote Sensing, 2019. **11**(10).
77. Sankey, T., et al., *UAV lidar and hyperspectral fusion for forest monitoring in the southwestern USA.* Remote Sensing of Environment, 2017. **195**: p. 30-43.
78. Tansley, A.G., *The use and abuse of vegetational concepts and terms.* Ecology, 1935. **16**(3): p. 284-307.
79. Bailey, R.G., *Identifying ecoregion boundaries.* Environmental management, 2004. **34**(1): p. S14-S26.
80. Loucks, O.L., *A forest classification for the Maritime Provinces.* Proceedings of the Nova Scotian Institute of Science, 1962. **25**: p. 1958-1962.
81. Bailey, R.G., *Delineation of ecosystem regions.* Environmental management, 1983. **7**(4): p. 365-373.
82. Bergen, K.M. and I. Dronova, *Observing succession on aspen-dominated landscapes using a remote sensing-ecosystem approach.* Landscape Ecology, 2007. **22**(9): p. 1395-1410.
83. Ozesmi, S.L. and M.E. Bauer, *Satellite remote sensing of wetlands.* Wetlands ecology and management, 2002. **10**(5): p. 381-402.

84. Rundquist, D.C., S. Narumalani, and R.M. Narayanan, *A review of wetlands remote sensing and defining new considerations.* 2001.
85. Maxwell, A.E., et al., *Large-Area, High Spatial Resolution Land Cover Mapping Using Random Forests, GEOBIA, and NAIP Orthophotography: Findings and Recommendations.* Remote Sensing, 2019. **11**(12).
86. Maxwell, A.E., et al., *Modeling critical forest habitat in the southern coal fields of West Virginia.* International Journal of Ecology, 2012. **2012**.
87. Maxwell, A.E., T.A. Warner, and M.P. Strager, *Predicting palustrine wetland probability using random forest machine learning and digital elevation data-derived terrain variables.* Photogrammetric Engineering & Remote Sensing, 2016. **82**(6): p. 437-447.
88. Xie, Y., A. Zhang, and W. Welsh, *Mapping wetlands and phragmites using publically available remotely sensed images.* Photogrammetric Engineering & Remote Sensing, 2015. **81**(1): p. 69-78.
89. Maxwell, A.E., T.A. Warner, and F. Fang, *Implementation of machine-learning classification in remote sensing: An applied review.* International Journal of Remote Sensing, 2018. **39**(9): p. 2784-2817.
90. Michie, D., D.J. Spiegelhalter, and C.C. Taylor, *Machine learning, neural and statistical classification.* 1994.
91. Corcoran, J., J. Knight, and A. Gallant, *Influence of Multi-Source and Multi-Temporal Remotely Sensed and Ancillary Data on the Accuracy of Random Forest Classification of Wetlands in Northern Minnesota.* Remote Sensing, 2013. **5**(7): p. 3212-3238.
92. Jerome, D.S., *Landforms of the Upper Peninsula, Michigan*. 2006, Natural Resources Conservation Service. p. 56.
93. Wayne, W.J. and J.H. Zumberge, *The Quaternary of the U.S*, in *PLEISTOCENE GEOLOGY OF INDIANA AND MICHIGAN*. 2015, Princeton University Press. p. 63-84.
94. Lessard, V.C., R.E. McRoberts, and M.R. Holdaway. *Diameter growth models using FIA data from the Northeastern, Southern, and North Central Research Stations*. in *McRoberts, Ronald E.; Reams, Gregory A.; Van Deusen, Paul C., eds. Proceedings of the First Annual Forest Inventory and Analysis Symposium; Gen. Tech. Rep. NC-213. St. Paul, MN: US Department of Agriculture, Forest Service, North Central Research Station: 37-42*. 2000.
95. Archambault, L., B.V. Barnes, and J.A. Witter, *Ecological species groups of oak ecosystems of southeastern Michigan.* Forest Science, 1989. **35**(4): p. 1058-1074.
96. Host, G.E. and K.S. Pregitzer, *Ecological species groups for upland forest ecosystems of northwestern Lower Michigan.* Forest Ecology and Management, 1991. **43**(1-2): p. 87-102.
97. Zogg, G.P. and B.V. Barnes, *Ecological classification and analysis of wetland ecosystems, northern Lower Michigan, U.S.A.* Canadian Journal of Forest Research, 1995. **25**(11): p. 1865-1875.
98. Smith, M.-L., *Proceedings, land type associations conference: development and use in natural resources management, planning and research.* 2002.
99. Team, R.C., *R: A language and environment for statistical computing.* 2013.

100. Adam, E., O. Mutanga, and D. Rugege, *Multispectral and hyperspectral remote sensing for identification and mapping of wetland vegetation: a review.* Wetlands Ecology and Management, 2010. **18**(3): p. 281-296.
101. Whittaker, R.H., *Classification of natural communities.* The Botanical Review, 1962. **28**(1): p. 1-239.
102. Lane, C., et al., *Improved Wetland Classification Using Eight-Band High Resolution Satellite Imagery and a Hybrid Approach.* Remote Sensing, 2014. **6**(12): p. 12187-12216.
103. Akar, Ö. and O. Güngör, *Classification of multispectral images using Random Forest algorithm.* Journal of Geodesy and Geoinformation, 2012. **1**(2): p. 105-112.
104. Maxwell, A.E., et al., *Land cover classification and feature extraction from national agriculture imagery program (NAIP) Orthoimagery: A Review.* Photogrammetric Engineering & Remote Sensing, 2017. **83**(11): p. 737-747.
105. Dunteman, G.H., *Basic concepts of principal components analysis*. 1989, SAGE Publications Ltd: London. p. 15-22.
106. Jensen, J.R., *Introductory Digital Image Processing: A Remote Sensing Perspective*. 2015: Prentice Hall Press. 544.
107. Munyati, C., *Use of principal component analysis (PCA) of remote sensing images in wetland change detection on the Kafue Flats, Zambia.* Geocarto International, 2004. **19**(3): p. 11-22.
108. Dronova, I., et al., *Mapping dynamic cover types in a large seasonally flooded wetland using extended principal component analysis and object-based classification.* Remote Sensing of Environment, 2015. **158**: p. 193-206.
109. Almeida, T.I.R.d. and D.S. Filho, *Principal component analysis applied to feature-oriented band ratios of hyperspectral data: a tool for vegetation studies.* International Journal of Remote Sensing, 2004. **25**(22): p. 5005-5023.
110. Lasaponara, R., *On the use of principal component analysis (PCA) for evaluating interannual vegetation anomalies from SPOT/VEGETATION NDVI temporal series.* Ecological Modelling, 2006. **194**(4): p. 429-434.
111. Kumar, C., et al., *Automated lithological mapping by integrating spectral enhancement techniques and machine learning algorithms using AVIRIS-NG hyperspectral data in Gold-bearing granite-greenstone rocks in Hutti, India.* International Journal of Applied Earth Observation and Geoinformation, 2020. **86**.
112. Dwivedi, R. and T. Ravi Sankar, *Principal component analysis of Landsat MSS data for delineation of terrain features.* International Journal of Remote Sensing, 1992. **13**(12): p. 2309-2318.
113. Shah, C.A., et al. *ICA mixture model based unsupervised classification of hyperspectral imagery*. in *Applied Imagery Pattern Recognition Workshop, 2002. Proceedings.* 2002. IEEE.
114. Hyvärinen, A. and E. Oja, *Independent component analysis: algorithms and applications.* Neural networks, 2000. **13**(4-5): p. 411-430.
115. Shah, C., P.K. Varshney, and M. Arora, *ICA mixture model algorithm for unsupervised classification of remote sensing imagery.* International Journal of Remote Sensing, 2007. **28**(8): p. 1711-1731.

116. Shah, C.A., et al. *TOWARDS THE DEVELOPMENT OF NEXT GENERATION REMOTE SENSING TECHNOLOGY–ERDAS IMAGINE INCORPORATES A HIGHER ORDER FEATURE EXTRACTION TECHNOQUE BASED ON ICA*. in *Proceedings of the ASPRS 2007 Annual Conference*. 2007.
117. Li, F. and B. Xiao. *Aquatic vegetation mapping based on remote sensing imagery: An application to Honghu Lake*. in *2011 International Conference on Remote Sensing, Environment and Transportation Engineering*. 2011. IEEE.
118. Bannari, A., et al., *A review of vegetation indices.* Remote sensing reviews, 1995. **13**(1-2): p. 95-120.
119. Tucker, C.J., *Red and photographic infrared linear combinations for monitoring vegetation.* Remote sensing of Environment, 1979. **8**(2): p. 127-150.
120. Rouse, J., et al., *Monitoring vegetation systems in the Great Plains with ERTS.* NASA special publication, 1974. **351**: p. 309.
121. Wolf, A.F. *Using WorldView-2 Vis-NIR multispectral imagery to support land mapping and feature extraction using normalized difference index ratios*. in *Algorithms and Technologies for Multispectral, Hyperspectral, and Ultraspectral Imagery XVIII*. 2012. International Society for Optics and Photonics.
122. Gao, B.-C., *NDWI—A normalized difference water index for remote sensing of vegetation liquid water from space.* Remote sensing of environment, 1996. **58**(3): p. 257-266.
123. Haralick, R.M., K. Shanmugam, and I.H. Dinstein, *Textural features for image classification.* IEEE Transactions on systems, man, and cybernetics, 1973(6): p. 610-621.
124. Hall-Beyer, M., *Practical guidelines for choosing GLCM textures to use in landscape classification tasks over a range of moderate spatial scales.* International Journal of Remote Sensing, 2017. **38**(5): p. 1312-1338.
125. Maillard, P., *Comparing texture analysis methods through classification.* Photogrammetric Engineering & Remote Sensing, 2003. **69**(4): p. 357-367.
126. Cleland, D.T., et al., *Principles of land stratification for delineating ecosystems.* Taking an ecological approach to management. US Forest Service Watershed and Air Management, 1992: p. 40-50.
127. Cleland, D., et al. *Use of Ecological Units in Mapping Natural Disturbance Regimes in the Lake States*. in *Land Type Associations Conference: Development and Use in Natural Resources Management, Planning and Research*. 2001.
128. Hoque, N., D.K. Bhattacharyya, and J.K. Kalita, *MIFS-ND: A mutual information-based feature selection method.* Expert Systems with Applications, 2014. **41**(14): p. 6371-6385.
129. Guyon, I. and A. Elisseeff, *An introduction to variable and feature selection.* Journal of machine learning research, 2003. **3**(Mar): p. 1157-1182.
130. Kursa, M.B., *Praznik: High performance information-based feature selection.* SoftwareX, 2021. **16**: p. 100819.
131. Kuhn, M. and K. Johnson, *Applied predictive modeling*. Vol. 26. 2013: Springer.
132. Löw, F., et al., *Impact of feature selection on the accuracy and spatial uncertainty of per-field crop classification using support vector machines.* ISPRS journal of photogrammetry and remote sensing, 2013. **85**: p. 102-119.

133. Laliberte, A.S., D. Browning, and A. Rango, *A comparison of three feature selection methods for object-based classification of sub-decimeter resolution UltraCam-L imagery.* International Journal of Applied Earth Observation and Geoinformation, 2012. **15**: p. 70-78.
134. Duro, D.C., S.E. Franklin, and M.G. Dubé, *Multi-scale object-based image analysis and feature selection of multi-sensor earth observation imagery using random forests.* International Journal of Remote Sensing, 2012. **33**(14): p. 4502-4526.
135. Swain, P.H., *Fundamentals of pattern recognition in remote sensing.* Remote sensing: The quantitative approach, 1978: p. 136-188.
136. Huang, C., L. Davis, and J. Townshend, *An assessment of support vector machines for land cover classification.* International Journal of remote sensing, 2002. **23**(4): p. 725-749.
137. Li, T., C. Zhang, and M. Ogihara, *A comparative study of feature selection and multiclass classification methods for tissue classification based on gene expression.* Bioinformatics, 2004. **20**(15): p. 2429-37.
138. Breiman, L., *Random forests.* Machine learning, 2001. **45**(1): p. 5-32.
139. Brieman, L., et al., *Classification and regression tree analysis*. 1984, Boca Raton, FL: CRC Press.
140. Breiman, L., *Random forests.* UC Berkeley TR567, 1999.
141. Swain, P.H. and H. Hauska, *The decision tree classifier: Design and potential.* IEEE Transactions on Geoscience Electronics, 1977. **15**(3): p. 142-147.
142. Breiman, L., *Bagging predictors.* Machine Learning, 1996. **24**(2): p. 123-140.
143. Segal, M.R., *Machine learning benchmarks and random forest regression.* 2004.
144. Hastie, T., R. Tibshirani, and J. Friedman, *Random forests*, in *The elements of statistical learning*. 2009, Springer. p. 587-604.
145. Breiman, L. and A. Cutler, *Random forests-classification description.* Department of Statistics, Berkeley, 2007. **2**.
146. Duro, D.C., S.E. Franklin, and M.G. Dubé, *A comparison of pixel-based and object-based image analysis with selected machine learning algorithms for the classification of agricultural landscapes using SPOT-5 HRG imagery.* Remote sensing of environment, 2012. **118**: p. 259-272.
147. Kuhn, M., *Caret: classification and regression training.* Astrophysics Source Code Library, 2015.
148. Vapnik, V., *The nature of statistical learning theory*. 2013: Springer science & business media.
149. Yu, L., et al., *Towards automatic lithological classification from remote sensing data using support vector machines.* Computers & Geosciences, 2012. **45**: p. 229-239.
150. Boser, B.E., I.M. Guyon, and V.N. Vapnik. *A training algorithm for optimal margin classifiers*. in *Proceedings of the fifth annual workshop on Computational learning theory*. 1992.
151. Gunn, S.R., *Support vector machines for classification and regression.* ISIS technical report, 1998. **14**(1): p. 5-16.

152. Kuhn, M., *The caret package.* R Foundation for Statistical Computing, Vienna, Austria. URL https://cran. r-project. org/package= caret, 2012.
153. Kavzoglu, T. and I. Colkesen, *A kernel functions analysis for support vector machines for land cover classification.* International Journal of Applied Earth Observation and Geoinformation, 2009. **11**(5): p. 352-359.
154. Hsu, C.-W., C.-C. Chang, and C.-J. Lin, *A practical guide to support vector classification*. 2003, Taipei.
155. Kohavi, R. *A study of cross-validation and bootstrap for accuracy estimation and model selection*. in *Ijcai*. 1995. Montreal, Canada.
156. Fitzpatrick-Lins, K., *Comparison of sampling procedures and data analysis for a land-use and land-cover map.* Photogrammetric Engineering and Remote Sensing, 1981. **47**(3): p. 343-351.
157. Rosenfield, G.H., K. Fitzpatrick-Lins, and H. Ling, *Sampling for thematic map accuracy testing.* Photogrammetric Engineering and Remote Sensing, 1982. **48**(1): p. 131-137.
158. Lillesand, T., R.W. Kiefer, and J. Chipman, *Remote sensing and image interpretation*. 2015: John Wiley & Sons.
159. Congalton, R.G., *A comparison of sampling schemes used in generating error matrices for assessing the accuracy of maps generated from remotely sensed data.* Photogrammetric engineering and remote sensing, 1988.
160. Macleod, R.D. and R.G. Congalton, *A quantitative comparison of change-detection algorithms for monitoring eelgrass from remotely sensed data.* Photogrammetric engineering and remote sensing, 1998. **64**(3): p. 207-216.
161. Rodriguez-Galiano, V.F., et al., *Random Forest classification of Mediterranean land cover using multi-seasonal imagery and multi-seasonal texture.* Remote Sensing of Environment, 2012. **121**: p. 93-107.
162. Adam, E., et al., *Land-use/cover classification in a heterogeneous coastal landscape using RapidEye imagery: evaluating the performance of random forest and support vector machines classifiers.* International Journal of Remote Sensing, 2014. **35**(10): p. 3440-3458.
163. Lindenmayer, D.B. and J.F. Franklin, *Conserving forest biodiversity: a comprehensive multiscaled approach*. 2002: Island press.
164. Bettinger, P., et al., *Forest management and planning*. 2016: Academic press.
165. Pu, R. and S. Landry, *A comparative analysis of high spatial resolution IKONOS and WorldView-2 imagery for mapping urban tree species.* Remote Sensing of Environment, 2012. **124**: p. 516-533.
166. Taylor, J., T. Brewer, and A. Bird, *Monitoring landscape change in the National Parks of England and Wales using aerial photo interpretation and GIS.* International Journal of Remote Sensing, 2000. **21**(13-14): p. 2737-2752.
167. Buchanan, G., et al., *Characterization of moorland vegetation and the prediction of bird abundance using remote sensing.* Journal of Biogeography, 2005. **32**(4): p. 697-707.
168. Prasad, A.M., L.R. Iverson, and A. Liaw, *Newer classification and regression tree techniques: bagging and random forests for ecological prediction.* Ecosystems, 2006. **9**(2): p. 181-199.

169. Bradter, U., et al., *Prediction of National Vegetation Classification communities in the British uplands using environmental data at multiple spatial scales, aerial images and the classifier random forest.* Journal of Applied Ecology, 2011. **48**(4): p. 1057-1065.
170. Yang, L., et al., *A new generation of the United States National Land Cover Database: Requirements, research priorities, design, and implementation strategies.* ISPRS Journal of Photogrammetry and Remote Sensing, 2018. **146**: p. 108-123.
171. Hansen, M.C., et al., *Global land cover classification at 1 km spatial resolution using a classification tree approach.* International Journal of Remote Sensing, 2010. **21**(6-7): p. 1331-1364.
172. Anderson, J.R., *A land use and land cover classification system for use with remote sensor data*. Vol. 964. 1976: US Government Printing Office.
173. Vogelmann, J.E., et al., *Completion of the 1990s National Land Cover Data Set for the conterminous United States from Landsat Thematic Mapper data and ancillary data sources.* Photogrammetric Engineering and Remote Sensing, 2001. **67**(6).
174. Schulz, K., R. Hänsch, and U. Sörgel, *Machine learning methods for remote sensing applications: an overview.* Earth resources and environmental remote sensing/GIS applications IX, 2018. **10790**: p. 1079002.
175. Juel, A., et al., *Spatial application of Random Forest models for fine-scale coastal vegetation classification using object based analysis of aerial orthophoto and DEM data.* International Journal of Applied Earth Observation and Geoinformation, 2015. **42**: p. 106-114.
176. Hogland, J., et al., *Mapping Forest Characteristics at Fine Resolution across Large Landscapes of the Southeastern United States Using NAIP Imagery and FIA Field Plot Data.* ISPRS International Journal of Geo-Information, 2018. **7**(4).
177. Monahan, W.B., et al., *A spectral three-dimensional color space model of tree crown health.* PloS one, 2022. **17**(10): p. e0272360.
178. Monahan, W., Arnspiger, Colton, Bhatt, Parth, An, Zhongming, Krist, Jr., Frank, Liu, Tao, Richard, Robert, Edson, Curtis, Froese, Robert, Steffenson, John, Lammers, Tony, & Frosh, Randy, *Data and code from: A spectral three-dimensional color space model of tree crown health*, DRYAD, Editor. 2022.
179. Survey, U.S.G. *National Hydrography, Watershed Boundary Dataset*. [cited 2021 15 September]; Available from: https://www.usgs.gov/core-science-systems/ngp/national-hydrography/watershed-boundary-dataset?qt-science_support_page_related_con=4#qt-science_support_page_related_con.
180. USDA. *2018 Michigan Image Dates*. 2018 [cited 2022 8/7/2022]; Available from: https://naip-image-dates-usdaonline.hub.arcgis.com/datasets/8abca94b0db34143b3b5cdd2c99e7fe9_0/about.
181. Adam, E., O. Mutanga, and D. Rugege, *Multispectral and hyperspectral remote sensing for identification and mapping of wetland vegetation: a review.* Wetlands Ecology and Management, 2009. **18**(3): p. 281-296.

182. Tassi, A. and M. Vizzari, *Object-oriented lulc classification in google earth engine combining snic, glcm, and machine learning algorithms.* Remote Sensing, 2020. **12**(22): p. 3776.
183. Franklin, S.E. and O.S. Ahmed, *Deciduous tree species classification using object-based analysis and machine learning with unmanned aerial vehicle multispectral data.* International Journal of Remote Sensing, 2018. **39**(15-16): p. 5236-5245.
184. Bandos, T.V., L. Bruzzone, and G. Camps-Valls, *Classification of hyperspectral images with regularized linear discriminant analysis.* IEEE Transactions on Geoscience and Remote Sensing, 2009. **47**(3): p. 862-873.
185. Clark, M.L., D.A. Roberts, and D.B. Clark, *Hyperspectral discrimination of tropical rain forest tree species at leaf to crown scales.* Remote sensing of environment, 2005. **96**(3-4): p. 375-398.
186. Mahdianpari, M., et al., *Fisher Linear Discriminant Analysis of coherency matrix for wetland classification using PolSAR imagery.* Remote Sensing of Environment, 2018. **206**: p. 300-317.
187. Gong, P., R. Pu, and B. Yu, *Conifer species recognition: An exploratory analysis of in situ hyperspectral data.* Remote sensing of Environment, 1997. **62**(2): p. 189-200.
188. Altman, D.G., *Practical statistics for medical research*. 1990: CRC press.
189. Landis, J.R. and G.G. Koch, *The measurement of observer agreement for categorical data.* biometrics, 1977: p. 159-174.
190. McHugh, M.L., *Interrater reliability: the kappa statistic.* Biochemia medica, 2012. **22**(3): p. 276-282.
191. Shang, J., et al., *Mapping spatial variability of crop growth conditions using RapidEye data in Northern Ontario, Canada.* Remote Sensing of Environment, 2015. **168**: p. 113-125.
192. Fernández-Manso, A., O. Fernández-Manso, and C. Quintano, *SENTINEL-2A red-edge spectral indices suitability for discriminating burn severity.* International journal of applied earth observation and geoinformation, 2016. **50**: p. 170-175.
193. Hill, M.J., *Vegetation index suites as indicators of vegetation state in grassland and savanna: An analysis with simulated SENTINEL 2 data for a North American transect.* Remote Sensing of Environment, 2013. **137**: p. 94-111.
194. Zhu, Y., et al., *Exploring the potential of worldview-2 red-edge band-based vegetation indices for estimation of mangrove leaf area index with machine learning algorithms.* Remote Sensing, 2017. **9**(10): p. 1060.
195. Guo, X., et al., *Estimating mangrove leaf area index based on red-edge vegetation indices: A comparison among UAV, WorldView-2 and Sentinel-2 imagery.* International Journal of Applied Earth Observation and Geoinformation, 2021. **103**: p. 102493.